論文 / 著書情報
Article / Book Information

題目(和文)	電流―電圧特性,熱起電力計測に基づく単分子接合の電子状態計測
Title(English)	Resolving electronic structures of single-molecule junctions based on current-voltage characteristics and thermopower measurement
著者(和文)	小本祐貴
Author(English)	Yuki Komoto
出典(和文)	学位:博士(理学), 学位授与機関:東京工業大学, 報告番号:乙第4170号, 授与年月日:2018年10月31日, 学位の種別:論文博士, 審査員:木口 学,大島 康裕,河内 宜之,沖本 洋一,西野 智昭
Citation(English)	Degree:Doctor (Science), Conferring organization: Tokyo Institute of Technology, Report number:乙第4170号, Conferred date:2018/10/31, Degree Type:Thesis doctor, Examiner:,,,,
学位種別(和文)	博士論文
Type(English)	Doctoral Thesis

TOKYO INSTITUTE OF TECHNOLOGY

Thesis

Resolving electronic structures of single-molecule junctions based on current-voltage characteristics and thermopower measurement

電流—電圧特性,熱起電力計測に基づく

単分子接合の電子状態計測

小本　祐貴

Yuki Komoto

Contents

1. General introduction

1.1. Single-molecule junctions

Single-molecule junction is the system which single molecule bridging between the two metal electrodes as shown in Fig.1-1. Much attention has been paid to single-molecule junctions since establishment to measurement method of single-molecule conductance[1-5]. Single-molecule junction has many distinctive characteristics.

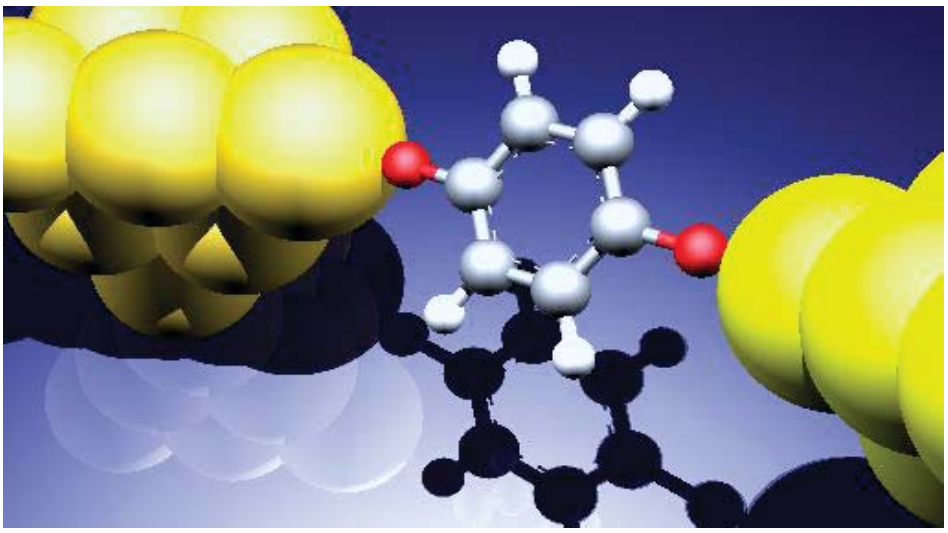

Fig.1-1 . Schematic image of single-molecule junction. Single molecule binds to two metal electrodes.

First, single-molecule junction is an ultra-small system in electronic circuits. The attempt to develop molecular device have been paid to attention since molecular diode was proposed by Aviram and Ratner[6]. Single-molecule junctions were consisted of single-molecule. The scale of single-molecule junction is nanometer or sub-nanometer scale. Single-molecule junction is smaller than the scale of current semiconductor process. The development of the electronic devices caused the miniaturization and high integration of semiconductor process. The limit of miniaturization is inevitable because of molecular or atomic size. Therefore, bottom up approach is desired for development method of devices. If single-molecule has a function of electronic components, we can utilize single-molecule junctions for devices. One of the most important challenge in the field of single-molecule junctions is development of practical molecular devices.

Second, single-molecule junction has two metal-molecule interfaces as shown in Fig.1-1 . Unique behaviors are observed at surface. The properties of molecules at surface are different from bulk or isolated molecules as represented by catalysis of chemical reactions. It is expected that more distinctive features appear in the single-molecule junctions due to their two surfaces. Single-molecule junction has attention from basic field.

Furthermore, measurement of single-molecule junctions is specific method in the aspect from the number of target molecules. The ordinally measurement methods such as spectroscopy measure the ensemble of molecules which number is in order of Avogadro number. The behaviors of single molecules are observable in single-molecule junctions. This characteristic is noted from application field as well as basic research. In single-molecule junction, we can capture the molecular information from single molecule. Fig.1-2(a) shows schematic view of DNA sequencer with single-molecule junctions[7-9]. Fig.1-2(b) shows tunneling current through nanogap formed in RNA solution. The current depends on the base between two metal electrodes. The bases of DNA are readable because the current through DNA is depend on its bases. Single molecule measurement realizes rapid, low-cost measurements.

Single-molecule junctions have many attractive features and are investigated from both basic and applicational aspects.

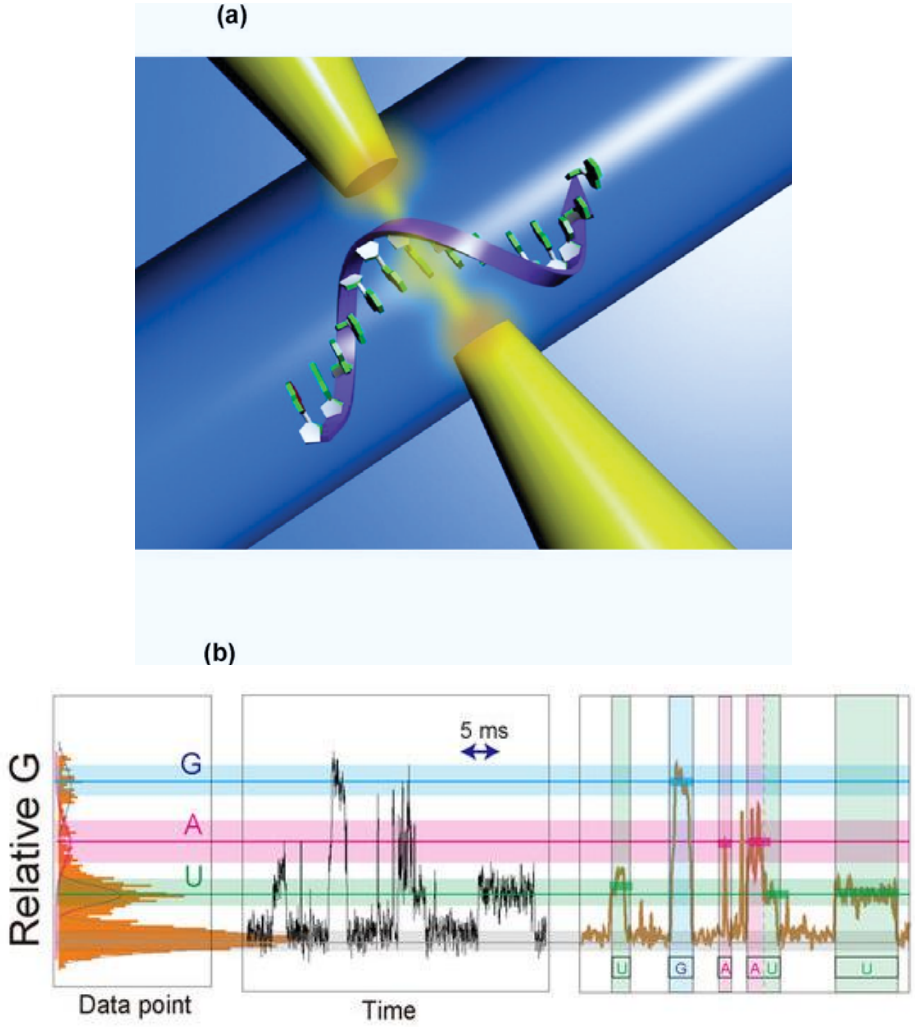

Fig.1-2 . (a)Schematirc image of DNA sequencer with single-molecule junction. Single base molecules on a DNA molecule in a solution are identified via a tunnelling current that passes between nanoelectrodes. (b) Typical relative conductance (G) histogram, raw and smoothed conductance-time profiles of randomly fragmented sequences from a 1.0 μM solution of UGAGGUA with 100 mM phosphate buffer. The figures are from Ref.[8] with permission by the author.

1.2. Fabrication method and conductance measurement of single-molecule junctions

1.2.1. Mechanically Controllable Break Junction (MCBJ)

Mechanically Controllable Break Junction (MCBJ) method was developed to observe the conductive properties of metallic atomic junctions[10-12]. The schematic image of the setup is shown in Fig.1-3. Reed *et al*. succeeded to measure single-molecule conductance in 1997[13]. In this study, 1,4-benzenedithiol (BDT) single-molecule junctions are fabricated with MCBJ

method. Fabrication of single-molecule junctions with MCBJ method is described as below. A notched gold wire is mounted on an elastic substrate. The elastic substrate is strained and gold wire are pulled to cut by pushing with piezo from backside. After breaking gold wire, nanogap was formed. Single-molecule junction was fabricated when a molecule bridge between the nanogap incidentally.

The substrates fabricated with lithography are frequently used for MCBJ research. The concept to form single-molecule junction is same to the substrate at first[14]. MCBJ substrate fabricated with lithography technique enable to form stable single-molecule junction.

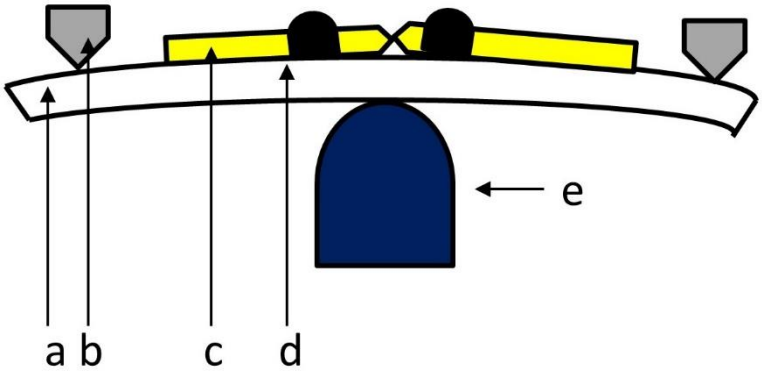

Fig.1-3 A schematic of the MCBJ with (a) the bending beam, (b) the counter supports, (c) the notched gold wire, (d) the glue contacts, and (e) the piezo element.

1.2.2. Scanning Tunneling Microscope-Break Junction (STM-BJ)

Scanning Tunneling Microscope-Break Junction (STM-BJ) method was developed in 2003 by Xu and Tao.[15]. They measured the single-molecule conductance of 4,4'-bipyridine using STM. The STM-BJ method is a Break Junction method using STM. The STM tip is brought into contact with the metal substrate to form a metal nanocontact. Thereafter, the tip is withdrawn and the metal bond is broken. Similar to the MCBJ method, conductance of a single-molecule junction is measured when a molecule bridge to a nanogap. This method is easy to obtain statistically sufficient experimental results. MCBJ setup take advantage to STM-BJ method in stability of the single-molecule junction. However, STM-BJ is easy to perform single-molecule conductance measurement because STM is commercially available. Therefore, research on single molecule conductance measurement widely spread by the STM-BJ method[16-21].

1.2.3. Principle of break junction method

Fig.1.4 represents schematic image of conductance change in BJ method and schematic view of changes of molecular junction corresponding with the conductance trace.

First, a metallic contact is formed by bringing two metal electrodes into contact. In this case, corresponding to 1 in Fig.1.4, the conductance is saturated. Next, the two electrodes are pulled apart at a constant speed. At this time, a metal single-atomic junction is formed. This corresponds to 2 in Fig.1-4 and this single-atomic junction is confirmed by a conductance quantum ($1G_0$).

By further separating the two electrodes, the metal single-atomic junction breaks. Then, a nanogap formed between the two electrodes. An abrupt decrease in conductance is observed. If molecules crosslink into this gap, the conductance of the single molecule is measured. Since the electrodes are further withdrawn, the number of bridging molecules becomes 1, and single-molecule conductance can be measured at this time. In Fig.1-4, corresponding to 3, the conductance of a single molecule is measured and a plateau is observed in the conductance trace. By further separating the two electrodes, the single molecular junction breaks. Corresponding to 4 in Fig.1-4 , a decrease in conductance is seen. Repeat this process to statistically determine the conductance of the molecule.

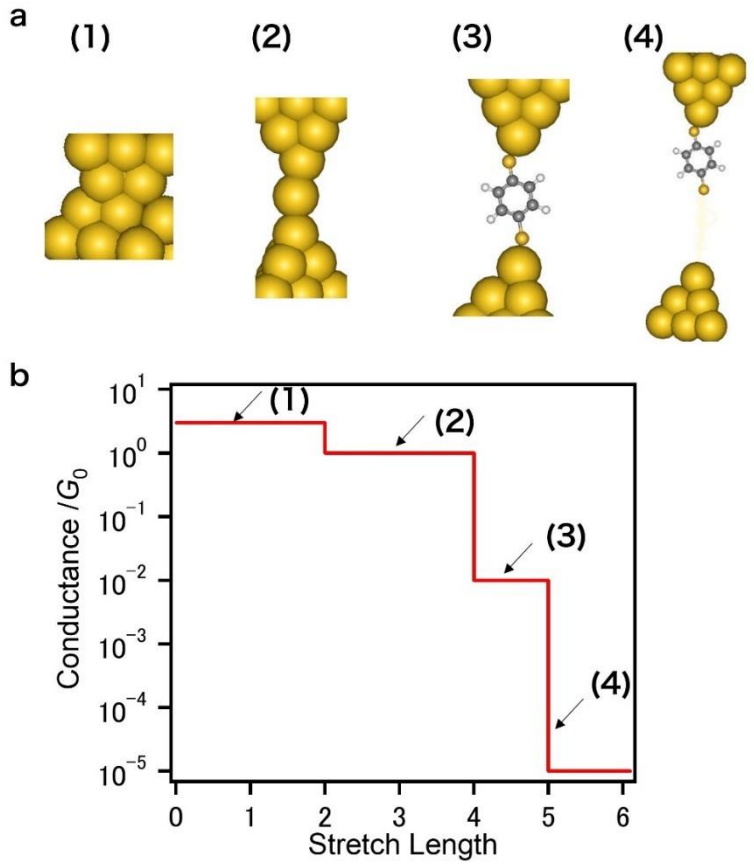

Fig.1-4 (a) Schematic image of rupture process in BJ method. (b) schematic view of conductance trace of BJ method. (1) First, metallic wire becomes narrow. (2) single-atomic junction formed before breaking metal wire. Forming single atomic junction is confirmed the plateau at 1 G_0. (3) Single-molecule junction formed incidentally. A plateau appears in conductance traces. (4) Single-molecule junction break by further stretch. The conductance abrupt decrease to 0.

1.3. Molecular electronics

As mentioned above, Single-molecule junctions are investigated for development of molecular devices. Molecular diodes[22-30], transistors[31, 32] and switches[33-36] have been reported.

1.3.1. Molecular diodes

First research of molecular device is single-molecule rectifier reported by Aviram and Ratner in 1974[6]. Aviram and Ratner proposed molecular diode in Fig.1-5 theoretically. This molecule is consisted from accepter part of tetracyanoquinodimethane (TCNQ) and doner part of Tetrathiafulvalene (TTF) and spacer of saturated carbons to separate delocalization of TCNQ and TTF. Energy levels are different between donor site and acceptor site. When the bias voltage applied to electrode binds to the donor, electrons injected into the molecule from electrode

easily, because the energy difference between the acceptor and the donor is small. As a result, large current passes. On the other hand, when a bias is applied in the opposite direction, the energy difference between the electrode and the donor molecular orbital becomes large, so that the current hardly flows. Therefore, it was expected that the conductance of the molecule shown in Fig.1-5 was different between direction from the acceptor to the donor and direction from the donor to the acceptor.

More than 40 years have passed since the theoretical prediction of the rectifying property of this molecule. However, this molecule has not been synthesized yet. The rectifying property of this molecule has not been confirmed[22-30]. However, it is possible to form single-molecule junctions and to evaluate conduction with the development of experimental techniques[13, 37].

Molecules with expected rectifying properties are expected to be used as diodes in single-molecule. High integration is expected for molecular devices in which such a molecule plays a role in current circuits. To realize a molecular device that operates only one functional molecule in a circuit, it is required to study the physical properties including the conductance of single molecules.

The development of measurement method of single-molecule junction enables to realize the molecular rectification. Experimentally, some previous research reported single-molecule diodes. Many of molecular junctions reported as molecular rectifier have asymmetric molecular backbones. Some studies have reported of molecular diode is originated from difference of anchoring groups[26, 30].

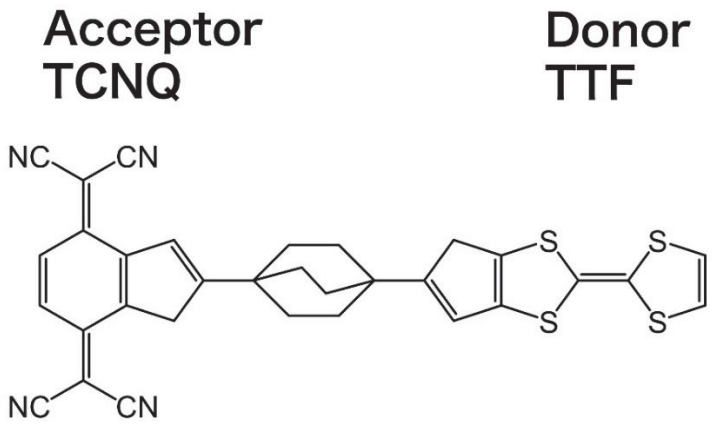

Fig.1-5 Molecule with a function of single-molecule diode proposed by Aviram and Ratner in Ref.[6].

1.3.2. Molecular transistors

Fig.1-6 shows schematic view of molecular transistor[32]. It was confirmed that the current increased by applying the gate voltage. This represents the possibility that a single molecule can be used as a transistor. Transistors are extremely important in the industry. If a single molecular junction has a function as a transistor and is put to practical use, it greatly contributes to high integration. It is expected to miniaturize the element and improve the calculation capability.

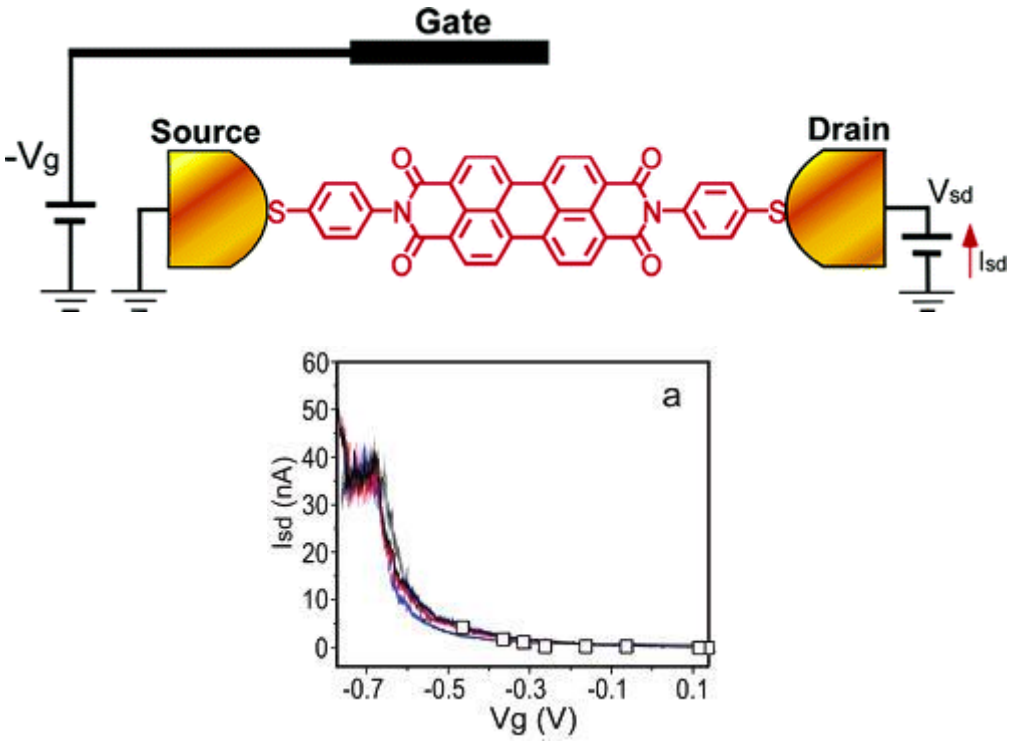

Fig.1-6 (top)Schematic of a single molecule transistor with an electrochemical gate (Ag wire reference electrode in 0.1 M $NaClO_4$). The gate and the source-drain bias voltages are controlled with a bipotentiostat (a Pt counter electrode not shown for clarity). (a) Source-drain current (*I*sd) versus gate voltage (*V*g) for a single perylene tetracarboxylic diimide (PTCDI) molecule transistor. The open squares were obtained from the peak position of the conductance histograms. The solid lines were obtained by directly recording the source-drain current while sweeping the gate voltage. From Ref.[32] Xu B, Xiao X, Yang X, Zang L and Tao N 2005 Large gate modulation in the current of a room temperature single molecule transistor *J. Am. Chem. Soc.* **127** 2386 Copyright (2005) American Chemical Society.

1.3.3. Molecular switches

A molecular junction of diarylethene which is famous as photochromic molecule work as

switch[34, 35, 38]. The conductance of the molecular junction decreased to 1000 times smaller by visible light irradiation. Molecular switches induced by mechanical force also have been reported[33].

In these molecular devices, the electronic structures of single-molecule junction are important idea to tune conductive properties of molecular junctions. For example, in molecular switch induced by light irradiation, the photochromic molecule changes structures from closed from to open form by light irradiation[34]. Decreasing of the conductance is caused by delocalization of π-conjugation broken with opening of the ring. In molecular transistor, the conductance changes with changes of conduction level by applying gate voltage. The understanding of electronic structures of single-molecule junctions is important to develop molecular devices.

1.4. Influence of interfaces of single-molecule junctions

In typical molecular junctions, the single-molecule junction is connected to metal electrodes by an anchoring group in the molecule. Thiol group (-SH)[39-44] and amino group (-NH_2)[41, 45] are frequently used as anchoring groups. Cyanide groups (-CN)[46] and iodo groups (-I)[47] and others have also been used.

The thiol group is the most typical anchoring group of single-molecule junctions. Because of strong interaction between gold and sulpher, it is possible to easily bond with gold electrode. Benzenedithiol which used in single-molecule junction reported firstly also have thiol groups[13]. However, thiol groups have various bonding modes for gold[48]. Multiple conductance states are observed in the conductance measurements. The peak of the conductance histogram is broad[44]. It is a problem that the conductance cannot be determined with high accuracy. Tao's group suggested that the conduction states of thiol groups are due to the difference between hollow and on-top structures[40].

Venkataraman's group studied amino anchoring group[41]. They reported that a single-molecule junction with an amino group as an anchor shows a sharp peak in the conductance histogram than thiol group and cyanide group. Fig.1-7 shows the conductance histogram and trace of the benzene derivatives with various anchor groups.

A thiol group is bonded with electron pairs of a thiol group by forming π bond which is anisotropic with the electrode in addition to the σ bond between gold and thiol. The conductance is influenced by the bridging structure. Therefore, a molecule having a thiol group as an anchoring shows multiple conduction states. On the other hand, in a molecule having amino

groups as an anchoring group, since a lone electron pair of an amino group coordinates isotropically to a gold electrode. A difference in geometric structure between the electrode and the molecule does not affect to conductance too much. Therefore, molecular junctions bonded by amino anchoring group show well-defined conductance.

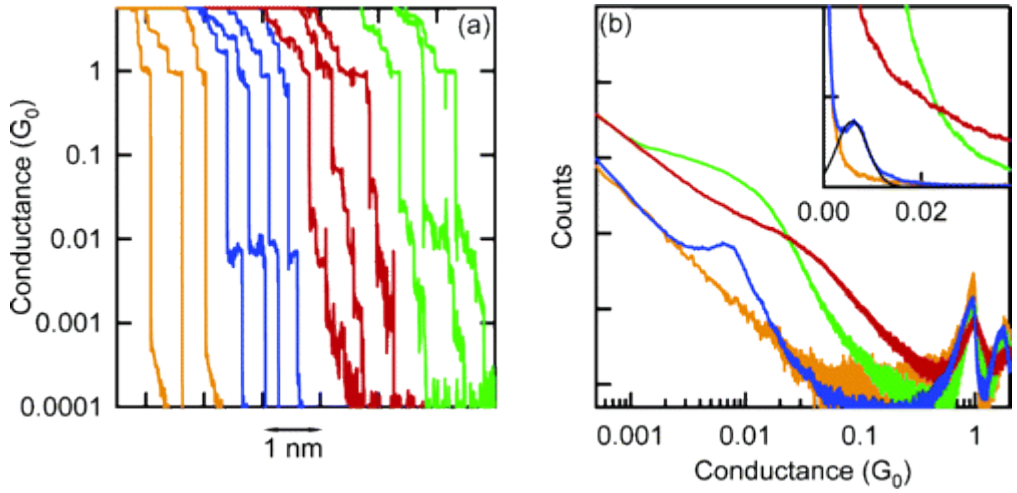

Fig.1-7 (a) Sample conductance traces measured without molecules (yellow) and with 1,4-benzenediamine (blue), 1,4-benzenedithiol (red), and 1,4-benzenediisonitrile (green) shown on a semilog plot. All data were measured at 25 mV bias, although no bias dependence was found up to 250 mV. (b) Conductance histograms constructed from over 3000 traces measured in the presence of 1,4-benzenediamine (blue), 1,4-benzenedithiol (red), and 1,4-benzenediisonitrile (green) shown on a log-log plot. The control histogram of Au without molecules is also shown (yellow). Histograms are normalized by the number of traces used to construct the histograms. Inset: same data on a linear plot showing a Gaussian fit to the peak (black curve). Bin size is 10^{-4} G_0. From Ref.[41]

Venkataraman L, Klare J E, Tam I W, Nuckolls C, Hybertsen M S and Steigerwald M L 2006 Single-molecule circuits with well-defined molecular conductance *Nano lett.* **6** 458. Copyright (2006) American Chemical Society

1.5. Influence of molecular backbone

Not only interface but also the conformational change of the molecular backbone also influences the conductance.

Fujihira *et al*. measured the conductance of Au-1,6-hexanedithiol single-molecule junction using STM in ultrahigh vacuum[49]. In the experiment, the conductance change in the stretching processes measured, and a conductance trace was obtained. The conductance traces showing single-molecule conductance indicate a feature that the single-molecule conductance increase with the elongation of the distance between the tip-substrate. It was suggested that the

origin of the increase in the conductance of a single molecule junction during the tip-substrate elongation process is attributable to the change of the alkyl chain structure of 1,6-hexanedithiolate from gauche to the trans structure.

Li *et al*. measured the conductance of gold-alkanedithiol junctions with STM-BJ[40]. The conductance trace of the gold-alkanedithiol junction showed multiple plateaus. Conductance histogram showed multiple peaks. Multiple conduction states of single-molecule junction of Au-alkanedithiol were obtained. Fig.1-8 shows the conductance histograms and traces of Au-octanedithiol junctions.

They carried DFT calculation and proposed a structural model for multiple conduction states as shown in Fig.1-9.The difference in the states of L and M results from the conformation of the molecular backbone. In the lowest conductivity L, the alkane has a gauche structure. M is all trans structure. The gauche effect, which reduces the conductance of conformation with gauche structure, is caused by the difference in potential barrier. In addition to the change of potential barriers, it was suggested that the gauche isomer decreases conductance due to different couplings caused by molecule-electrode geometries.

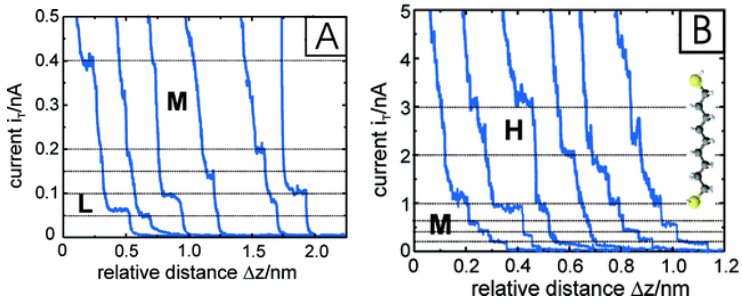

Fig.1-8 (A)Current−distance retraction curves recorded with a gold STM tip (low-current channel with a preamplifier limit of 1 nA) for 0.1 mM 1,9-nonanedithiol in 1,3,5-trimethylbenzene on Au(111), at E_{bias} = 0.10 V. The setpoint current before disabling the feedback was chosen at i_0 = 100 pA. The pulling rate was 4 nm s^{-1}. (B) Same conditions as in (A), except that the preamplifier limit was chosen at 10 nA. The dotted lines represent characteristic regions of the low, mid, and high currents. From Li X, He J, Hihath J, Xu B, Lindsay S M and Tao N 2006 Conductance of single alkanedithiols: conduction mechanism and effect of molecule− electrode contacts *J. Am. Chem. Soc.*. **128** 2135 Copyright (2006) American Chemical Society

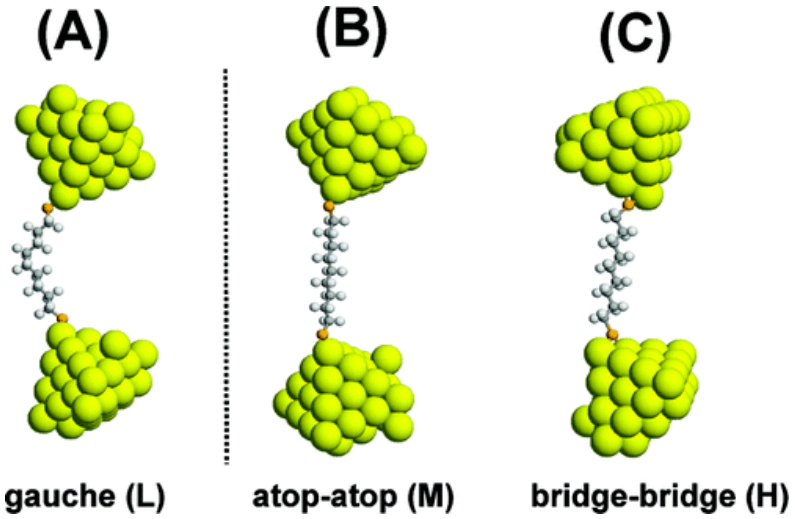

Fig.1-9 Three typical arrangements of a single alkanedithiol molecule bridged between Au electrodes as used for the conductance calculations. (A) 1,9-Nonanedithiol (ND) with one gauche defect and both terminal sulfur atoms coordinated in the atop position (low, L). (B) ND in all-trans conformation and in atop−atop coordination (medium, M). (C) All-trans ND in a bridge−bridge coordination (high, H). From Li X, He J, Hihath J, Xu B, Lindsay S M and Tao N 2006 Conductance of single alkanedithiols: conduction mechanism and effect of molecule− electrode contacts *J. Am. Chem. Soc.*. **128** 2135 Copyright (2006) American Chemical Society

1.6. Purpose of this study

In previous sections, I mentioned that electronic structures of single-molecule junctions are important to control the conduction properties of junctions, and single-molecule junction is easily affected by the conformation of metal-molecule interfaces and molecular backbones. However, many previous studies report only single-molecule conductance at fixed bias voltage. These measurements only reveal single-molecule conductance and cannot clarify the electronic structures, geometries of metal-molecule interface, and conformation of single-molecule junction. The results of theoretical calculations are compared to only conductance to determine the structures. The assignment of the structures of single-molecule junction with only conductance is low-validity. The structures of single molecule junction have been clear in spite of its importance.

In this study, I performed experiments of *I-V* measurements and thermopower measurements with two purposes described as below.

First purpose is establishment of method to measure the electronic structures of

single-molecule junctions. The conductance of single-molecule junction is determined by their electronic structures. However, the method to determine the electronic structure have not been established. Establishment of method to determine the electronic structure gives higher validity of single-molecule measurement and policies to develop molecular devices.

Second purpose is characterization of metal-molecule geometries of single-molecule junction. Especially I focused Au-BDT molecule interfaces connected to electrodes via bonding with thiol groups. As mentioned above, thiol group is most typical anchoring group in the field of single-molecule junctions. Single-molecule conductance depends on the difference of the interface structures. For practical use of single-molecule junctions, it is necessary to determine contact geometries.

2. Theoretical background

The current through single-molecule junctions is understood as resonant tunneling current via molecular orbital of bridging molecules. In long molecular junctions, the current mechanism become hopping mechanism from tunneling mechanism. Main targets of my study are single-molecule junctions of small molecules such as BDT and bipyridine. Therefore, in this chapter, I introduce two tunneling model of single-molecule junctions, Simmons model and Breit-Wigner model.

2.1. Landauer's theory

I introduce Landauer approach to describe the charge transport in one-dimentional nanojunctions before two models of transmission, Simmons model and Breit-Wigner model[1,50]. In consideration of a one-dimensional potential barrier, a sample is connected by two macroscopic electrodes in an experiment on a typical nano-scale transport phenomenon. Bias voltage is applied by the two electrodes and current flows through the potential. The electrodes behave as ideal electron reservoirs according to thermodynamically defined temperature and chemical potential. The tunneling current is described as scattering problem with the transmission and reflection probabilities in the sample. We think that this potential barrier corresponds to molecular orbitals of single-molecule junctions and elastic scattering occurs. Here, it is assumed that the electrons in the electrode are in a thermal equilibrium state with the temperature of the electrode. We consider plane wave $(1/\sqrt{L})\exp(ikx)$, electron reflected with probability r, and transmitted with probability T. The current density J_k of electrons with wave number k is calculated with considering flux,

$$\boldsymbol{J_{\mathrm{k}}} = \frac{\hbar}{\boldsymbol{2mi}}\left[\boldsymbol{\psi}^{*}(\boldsymbol{x})\frac{\mathrm{d}\boldsymbol{\psi}}{\mathrm{d}\boldsymbol{x}} - \boldsymbol{\psi}(\boldsymbol{x})\frac{\mathrm{d}\boldsymbol{\psi}^{*}}{\mathrm{d}\boldsymbol{x}}\right] = \frac{\boldsymbol{e}}{\boldsymbol{L}}\boldsymbol{v}(\boldsymbol{k})\boldsymbol{T}(\boldsymbol{k}). \quad (\mathbf{1})$$

Here,

$$\boldsymbol{v}(\boldsymbol{k}) = \frac{\hbar\boldsymbol{k}}{\boldsymbol{m}} \quad (\mathbf{2})$$

means group velocity and $\hbar$, m means Plank constant and electron mass. Many electrons contribute current. Therefore, it is necessary for calculation of current through single-molecule junction to summate of k. $f_{\mathrm{L}}(k)[1\text{-}f_{\mathrm{R}}(k)]$ is multiplied to current density to take into consideration

of Pauli's principle of each orbital of the electrodes. Here, $f_{L,R}(k)$ represents the Fermi-Dirac distribution of left or right metal electrodes. Chemical potential in Fermi-Dirac distribution $f(k)$ shift with the bias voltage. Current density from occupied states of left electrode to unoccupied states of right electrode is calculated as

$$J_{\mathrm{L}\to\mathrm{R}} = \frac{e}{L}\sum_{k} v(k)T(k)f_{\mathrm{L}}(k)[1 - f_{\mathrm{R}}(k)]. \tag{3}$$

Summation in Eq.(3) is converted to integration.

$$J_{\mathrm{L}\to\mathrm{R}} = \frac{e}{2\pi}\int \mathrm{d}k v(k)T(k)f_{\mathrm{L}}(k)[1 - f_{\mathrm{R}}(k)] \tag{4}$$

is obtained. Using the relation between energy and wave number,

$$E = \frac{\hbar^2 k^2}{2m} \tag{5}$$

current density is described as

$$J_{\mathrm{L}\to\mathrm{R}} = \frac{e}{h}\int \mathrm{d}E T(k)f_{\mathrm{L}}(k)[1 - f_{\mathrm{R}}(k)]. \tag{6}$$

The current density from right electrode to left electrode is described as same way.

$$J_{\mathrm{R}\to\mathrm{L}} = \frac{e}{h}\int \mathrm{d}E T(k)f_{\mathrm{R}}(k)[1 - f_{\mathrm{L}}(k)]. \tag{7}$$

The current in the cuicuit is

$$I(V) = J_{\mathrm{L}\to\mathrm{R}} - J_{\mathrm{R}\to\mathrm{L}}. \tag{8}$$

Substitute Eq.6 and Eq.7, to Eq8,

$$I(V) = \frac{2e}{h}\int \mathrm{d}E T(k)[f_{\mathrm{L}}(k) - f_{\mathrm{R}}(k)] \tag{9}$$

is obtained. Fermi-Dirac distribution is 1 when the electron energy is below chemical potential and 0, otherwise. The current is described with transmission within bias window in the single-molecule junction. Detail explanation of transmission is described in nest section.

In completely transmitted case, that is, when $T = 1$, Eq(9). become

$$I = \frac{2e^2}{h}V \tag{10}$$

under the condition which temperature is zero.

$$G_0 = \frac{2e^2}{h} \tag{11}$$

is defined as a conductance quantum. Conductance quantum means conductance without scatter in one conduction channel. Single atomic junctions of Gold shows conductance of 1 G_0.

2.2. Simmons model

In previous section, I mentioned the current of the single-molecule junction is determined by transmission. Here, I introduce two models to describe transmission of single-molecule junctions.

First model is Simmons model. Simmons proposed the model for the current through thin semiconductor film between two metal electrodes[51]. This model is also utilized for single-molecule junctions. Current equation in the Simmons model is described as below.

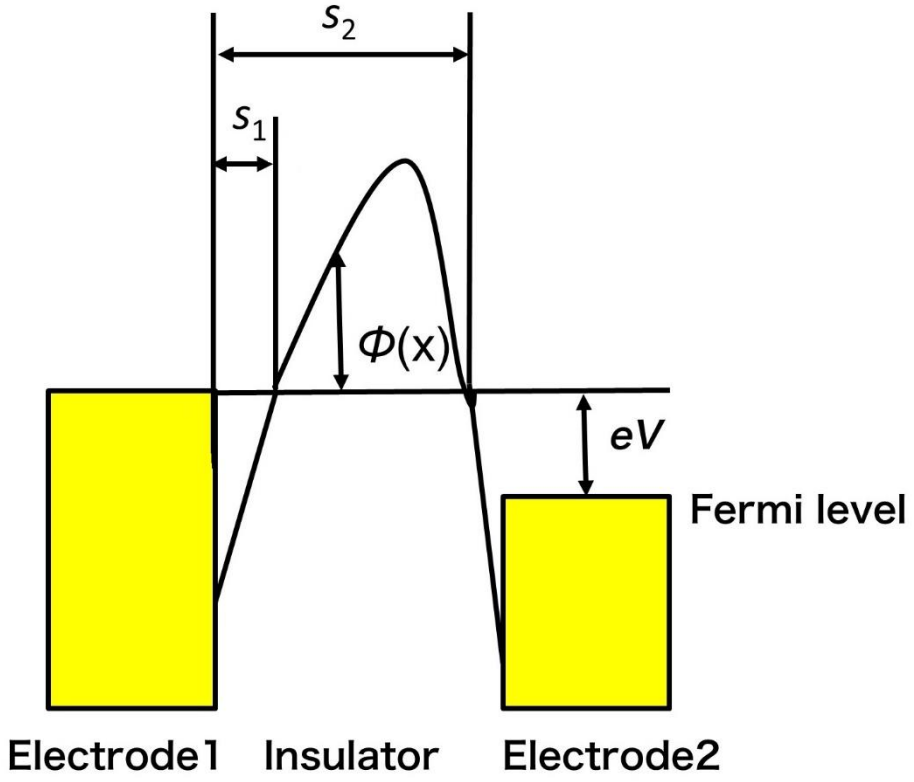

Fig.2-1 Schematic view of the general potential in Simmons model.

In Simmons model, electrons tunneling through one-dimensional potential. The transmission is calculated with WKB approximation. In one-dimensional barrier, Electrons transport with X direction and pass the potential barrier in range from $x = s_1$ to $x = s_2$. The probability which the electrons with energy of Ex tunnel through the potential given V(x) is represented by

$$D(E_x) = \exp\left\{-\frac{4\pi}{h}\int_{s_1}^{s_2} \mathrm{d}x\sqrt{2m(V(x)-E_x)}\right\} \tag{12}$$

from well-known WKB approximation. The number of electrons transporting from electrode 1 to electrode 2, N_1 is given by Eq.13.

$$N_1 = \int \mathrm{d}v_x v_x n\,(v_x) D(E_x) = \frac{1}{m}\int dE_x n\,(v_x) D(E_x). \tag{13}$$

Here,v_x means velocity of electrons. $N(v_x)\mathrm{d}v_x$ means the number of electrons with the velosity within the range between v_x and $v_x + \mathrm{d}v_x$ per unit volume. Assuming isotropic velocity distribution of electron in the electrodes, the number of electron with the velocity of v, is

$$n(v)dv_x dv_y dv_z = \left(\frac{2m^4}{h^3}\right) f(E) dv_x dv_y dv_z. \tag{14}$$

Here, $f(E)$ is Fermi-Dirac distribution. Eq.14 is convert to cylindrical coordinate, and substituted to Eq.(13) , number of electron from electrode 1 to electrode 2,N_1 is described as below.

$$N_1 = \frac{4\pi m^2}{h^3}\int_0^{E_m} D(E_x) dE_x \int_0^{\infty} f(E) dE_r. \tag{15}$$

Similarly, number of electron from electrode 2 to electrode 1, N_2 is described as Eq.16

$$N_2 = \frac{4\pi m^2}{h^3}\int_0^{E_m} D(E_x) dE_x \int_0^{\infty} f(E+eV) dE_r \tag{16}$$

The number of effective electrons number, N=N_1-N_2 is calculated as below.

$$N = \int_0^{E_m} D\,(E_x) dE_x \times \left\{\frac{4\pi m^2}{h^3}\int_0^{\infty} [f(E) - f(E+eV)]\, dE_r\right\} \tag{17}$$

Current J is described as Eq.18

$$J = \xi \int_0^{E_m} D\,(E_x) dE_x. \tag{18}$$

Here,

$$\xi = e\left\{\frac{4\pi m^2}{h^3}\int_0^{\infty} [f(E) - f(E+eV)]\, dE_r\right\}. \tag{19}$$

Potential is defined as $V(x)=\eta+\varphi(x)$, Transmission is approximated as

$$D(E_x) \cong \exp\left(-A\sqrt{\eta + \phi - E_x}\right). \tag{20}$$

Here,

$$\mathrm{A} = \frac{4\pi\Delta s\sqrt{2m}}{h}, \tag{21}$$

φ represents mean of barrier height. Assuming the low temperature limit, simplification of Fermi-Dirac distribution to 1 or 0 is substituted to Eq.19

$$\xi = \begin{cases} \dfrac{4\pi me}{h^3}(eV) & 0 < E_x < \eta - eV \\ \dfrac{4\pi me}{h^3}(\eta - E_x) & \eta - eV < E_x < \eta \\ 0 & \eta < E_x \end{cases} \tag{22}$$

is obtained. Using Eq.18 and Eq.19, Eq.20 is described as below.

$$J = \frac{4\pi me}{h^3}\left\{ eV\int_0^{\eta - eV} \exp\left(-A\sqrt{\eta + \phi - E_x}\right) dE_x \right.$$
$$- \phi\int_{\eta - eV}^{\eta} \exp(-A\sqrt{\eta + \phi - E_x})dE_x$$
$$\left. + \int_{\eta - eV}^{\eta} (\eta + \phi - E_x)\exp(-A\sqrt{\eta + \phi - E_x})dE_x \right\} \tag{23}$$

Integration of the first term is calculated and we ignore small order. We obtain

$$\frac{8\pi me^2 V}{h^3 A}\sqrt{\phi + eV}\exp\left(-A\sqrt{\phi + eV}\right). \tag{24}$$

The second term is also calculated,

$$\frac{8\pi me}{h^3 A^2}\phi\left\{\left(A\sqrt{\phi} + 1\right)\exp(-A\sqrt{\phi}) - \left(A\sqrt{\phi + eV} + 1\right)\exp(-A\sqrt{\phi + eV})\right\} \tag{25}$$

is obtained. The third term is described as below.

$$\frac{8\pi me^2}{h^3 A}\left\{\phi^{\frac{3}{2}}\exp\left(-A\phi^{\frac{1}{2}}\right) - (\phi + eV)^{\frac{3}{2}}\exp\left(-A(\phi + eV)^{\frac{1}{2}}\right)\right\}$$
$$+ \frac{24\pi me^2}{h^3 A^2}\left\{\phi\exp\left(-A\phi^{\frac{1}{2}}\right) - (\phi + eV)\exp\left(-A(\phi + eV)^{\frac{1}{2}}\right)\right\}. \tag{26}$$

From Eq.24,Eq.25 and Eq.26 , The current is described as below.

$$J = \frac{e}{2\pi h(\Delta s)^2}\left\{\phi\exp(-A\sqrt{\phi}) - (\phi + eV)\exp(-A\sqrt{\phi + eV})\right\}. \tag{27}$$

From here, consider the potential shape as rectangular potential as shown in Fig.2-2

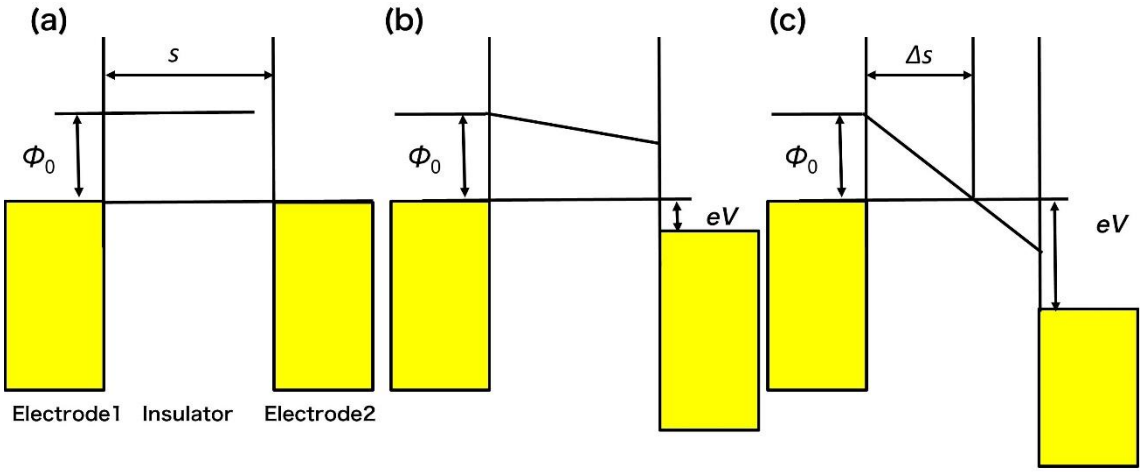

Fig.2-2 Schematic potential barrier approximated to be homogenous potential in insulator thin film as trapezoidal barrier under bias voltage applied (a) when bias voltage is not applied, (b) when small bias voltage is applied, and (c) when large bias voltage is applied.

This barrier is described as a potential barrier which the electric field gradient increase with bias voltage. We derive the equation of the current density when the bias voltage is small and when bias voltage is large. The behavior of the electron transmission due to the voltage is well shown in the potential of Fig.2-2 . That is, when the bias voltage is small, the potential can be approximated as a rectangle and the distance that electrons pass through due to the tunnel effect is constant. On the other hand, when the bias voltage is large, the potential is a triangular barrier. Electrons transport from the electrode 1 to the electrode 2 within the region where the potential barrier is higher than the electron energy, the tunnel distance becomes shorter as the voltage becomes larger. Based on this model, we obtain the expression of current density by approximation in individual cases.

When bias voltage is small ($eV<\varphi_0$)

When bias voltage is small, the barrier height is approximated to φ_0-$eV/2$, the distance electron through the potential $\Delta s = s$ (constant). From Eq.27, current is described as Eq.28 .

$$J = \frac{e}{2\pi hs^2}\left\{\left(\varphi - \frac{eV}{2}\right) exp\left(-\frac{4\pi s}{h}\sqrt{2m\left(\varphi - \frac{eV}{2}\right)}\right)\right.$$
$$\left. - \left(\varphi + \frac{eV}{2}\right) exp\left(-\frac{4\pi s}{h}\sqrt{2m\left(\varphi + \frac{eV}{2}\right)}\right)\right\}. \quad (28)$$

When bias voltage is large ($eV>\varphi_0$)

When bias voltage is large, field emission occurs. In this situation, the potential height is approximated to φ_0 , and Δs is approximated to $s\varphi/eV$. Current density is described as

$$J = \left(\frac{2e^3V^2}{8\pi hs^2\varphi_0}\right)\left\{\exp\left(-\frac{4\pi s}{eV}\sqrt{m{\varphi_0}^3}\right)\right.$$
$$\left. - \left(1 + \frac{2eV}{\varphi_0}\right)\exp\left(-\frac{4\pi s}{eV}\sqrt{m{\varphi_0}^3\left(1 + \frac{2eV}{\varphi_0}\right)}\right)\right\}. \quad (29)$$

Transport from electrode 2 to electrode 1 is transport to occupied states. And transport from electrode 1 to electrode 2 is transport to unoccupied states. Hence, we can ignore the second term of Eq.29 . When bias voltage is large, the equation of current,

$$J = \left(\frac{2e^3V^2}{8\pi hs^2\varphi_0}\right)\exp\left(-\frac{4\pi s}{eV}\sqrt{m{\varphi_0}^3}\right) \quad (30)$$

is obtained. We obtained equation of current when bias voltage is small and large.

When the applied bias voltage equal to the potential height, field emission contributes to conduction. As a result, the length of the potential barrier through which electrons pass becomes shorter as the voltage increase. The rate of increase in current increases. Transition Voltage Spectroscopy (TVS) is the method to determine the height of the potential barrier base on change the conduction mechanism from simple tunneling to field emission[52].

In TVS analysis, a graph with $\ln(I\text{-}V^2)$ on the vertical axis and $1/V$ on the horizontal axis called Fowler-Nordheim (FN) plot is plotted. The minimum in the graph is the transition voltage (TV). As shown in Eq.30 , When the voltage is large, $\ln(I\text{-}V^2)$ is a line with negative slope with respect to $1/V$. On the other hand, when the voltage is low, $\ln(I\text{-}V^2)$ increases with $1/V$. $\ln(I\text{-}V^2)$ have minimum at a certain voltage in the FN plot. The transition voltage is the voltage at which field

emission begins to occur and the expression corresponding to the voltage of the Simmons model changes. The height of the potential barrier can be determined as the transition voltage.

TVS is used for analysis of *I-V* characteristics of molecular junctions[39, 53]. The HOMO or LUMO level is assumed to the potential barrier or transition voltage. In single-molecule junction, it is difficult to consider that the electron is emitted into vacuum in the molecule. Hence, this model is too simple to consider the current in the single-molecule junction. However, it is easy to analyze *I-V* curves and determine energy level. A previous report suggest that the transition voltage is not indicate molecular level considered in Breit-Wigner model explained in next section[54]. But this paper also reported the transition voltage is related with molecular orbital level.

2.3. Breit-Wigner model

In Simmons model described in previous section, only potential height and and gap length are taken into consideration. In particular, the height of potential barrier is focused in TVS analysis. Energy alignment is important parameter to characterize conduction in single-molecule junctions. Couplings between molecule and electrode are also important factors for conduction of single-molecule junctions. The coupling between molecule and left or right electrode is setted as Γ_L,Γ_R, the transmission through single-molecule junction is described as Breit-Wigner formula[1, 55],

$$\tau(E) = \frac{4\Gamma_L\Gamma_R}{(\Gamma_L + \Gamma_R)^2 + (\mathrm{E} - \varepsilon)^2} . \tag{31}$$

In ε is energy level of molecular orbital, E represents energy of electron. Here, I derived Eq.31 and explain the physical meaning of couplings. We consider double barriers, barrier 1 and barrier 2 in Fig.2-3 , barrier 1,2 represent barrier between electrodes and molecule.

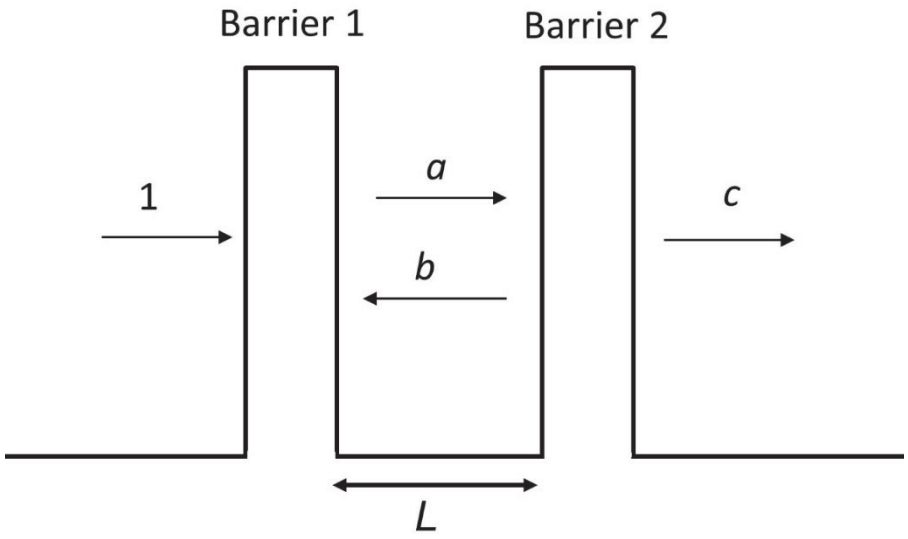

Fig.2-3 Schematic potential in double barrier model of Breit-Wigner model

Let t_i, r_i be to transmission and reflection amplitude at barrier i. We consider transmission of double barriers τ, from transmission and reflection at two barriers. Let electron transport from left electrode to right. Amplitudes in Fig.2-3 are described as below.

$$a = t_1 + r_1 b, \tag{32}$$

$$b = a r_2 \exp(i\varphi), \tag{33}$$

$$c = a t_2 \exp\left(\frac{i\varphi}{2}\right). \tag{34}$$

Here, $\varphi=2kL$ is phase shift which electron with wavenumber of k transport the range between of two barriers of 2L. Eliminating a and b from Eq.32,Eq.33 and Eq.34 ,

$$c = \frac{t_1 t_2 \exp(\frac{i\varphi}{2})}{1 - r_1 r_2 \exp(i\varphi)} \tag{35}$$

is obtained. Total transmission of two barriers τ is ratio of squares of the amplitudes of incident wave and transmitted wave. The transmission is denoted as

$$\tau = |c|^2 = \frac{|t_1|^2 |t_2|^2}{1 + |r_1|^2 |r_2|^2 + 2|r_1||r_2|\cos\theta}. \tag{36}$$

Here, $\theta=2kL+\varphi r_1+\varphi r_2$. When $\cos\theta$ = 1, It is called resonance, the transmission of junctions becomes maximum.

When the transmission of each potential barriers is small, that is, when the approximations of

$|t_1|^2, |t_2|^2 << 1$ and $|r_1|^2, |r_2|^2 \simeq 1$, are reasonable, reflection rate $|r_i|^2$ is expanded with $|t_i|^2$.

$$|r_i|^2 = 1 - \frac{|t_i|^2}{2} + \frac{|t_i|^2}{4} \tag{37}$$

is obtained. Consider transmission of electron which wavenumber is slightly different from resonance with δk. Expanding cosθ with δk, transmission is described as Eq.38,

$$\tau = \frac{4|t_1|^2|t_2|^2}{(|t_1|^2 + |t_2|^2)^2 + (2L\delta k)^2}. \tag{38}$$

In one-dimensional quantum well, small wavenumber shift δk is related with energy shift $\delta\varepsilon$ as,

$$2L\delta k = \frac{2\pi}{\Delta\varepsilon}\delta\varepsilon. \tag{39}$$

Substitute Eq.39 to Eq.38

$$\tau(\delta\varepsilon) = \frac{4\Gamma_1\Gamma_2}{(\Gamma_1 + \Gamma_2)^2 + (\delta\varepsilon)^2} \tag{40}$$

is obtained. Here,

$$\Gamma_i = \frac{\Delta\varepsilon}{2\pi}|t_i|^2. \tag{41}$$

Eq.31 is obtained by rewriting energy of Eq.41 . From Eq.31, coupling is parameter to promote with transmission of single barrier between electrode and molecule.

The transmission of Eq.31 is a Lorentzian shape with HWHM of $\Gamma = \Gamma_L + \Gamma_R$. From uncertainty principle, exponential decay with time is obtained by Fourier transform of Lorentzian. Coupling which is energy width of transmission correspond to a lifetime of bound state in the double barriers.

3. Principles of measurement methods of electronic structures of single-molecule junctions

The current of single-molecule junctions is determined by electronic structures. In this chapter, I describe the principle and some previous reports of *I-V* measurements and thermopower measurements as determination methods of electronic structure of single-molecule junctions.

3.1. Principle of *I-V* measurement

The electronic structures of single-molecule junctions are determined with *I-V* measurements.

Let origin of energy set the average potential of both electrodes. The current of single-molecular junction is denoted as Eq.9. Assuming the low temperature limit, Fermi-Dirac distribution is approximated as

$$f(E) = \begin{cases} 1, & E \leqq \dfrac{eV}{2} \\ 0, & E > \dfrac{eV}{2} \end{cases} . \tag{42}$$

From Eq.9 and Eq.31, the current is described as Eq.43.

$$I(V) = \frac{8e}{h}\alpha(1-\alpha)\Gamma\left\{\arctan\left(\frac{\alpha eV - \varepsilon_0}{\Gamma}\right) + \arctan\left(\frac{(1-\alpha)eV + \varepsilon_0}{\Gamma}\right)\right\}. \tag{43}$$

Here, Γ=Γ_{L}+Γ_{R} and α is asymmetric factor of couplings described as below.

$$\alpha = \frac{\Gamma_L}{\Gamma_L + \Gamma_R}. \tag{44}$$

I-V curves are fitted with Eq.43. We can obtain electronic structure of single-molecule junctions[44, 56, 57].

When bias voltage *V* is applied, the energy level of conduction orbital is assumed to Eq.45.

$$\varepsilon = \varepsilon_0 + \frac{\Gamma_L - \Gamma_R}{\Gamma_L + \Gamma_R}\frac{eV}{2}. \tag{45}$$

Bias dependence of orbital energy with couplings is assumed that the molecular orbital of the junction shifts towards the electrode with the larger coupling. When the couplings of left and right electrodes are equal, the shift of the molecular orbital should be the average of the Fermi energy difference of the two electrodes. When the coupling of one electrode is remarkably large, the molecular orbital completely follows the electrode with large coupling. This corresponds to the situation where the molecule is adsorbed only on the substrate and the STM tip is far from

molecule. At this situation, the energy level of the molecule completely follows the substrate and is not affected by the tip. By considering the limit of the couplings, the molecular orbital energy of Eq.45 is derived.

At finite temperature, the value of Fermi-Dirac distribution become in range between 0 and 1. However, the shift of Fermi-Dirac distribution is enough small to ignore. Hence, the *I-V* curves are fitted with Eq.46 in this study.

Considering the number of bridging molecules *n*, the current of multiple-molecule junctions is described as below.

$$I(V) = n\frac{8e}{h}\alpha(1-\alpha)\Gamma\left\{\arctan\left(\frac{\alpha eV-\varepsilon_0}{\Gamma}\right)+\arctan\left(\frac{(1-\alpha)eV+\varepsilon_0}{\Gamma}\right)\right\}. \tag{46}$$

3.2. Principle of thermopower measurement

Paulsson and Datta proposed thermoelectric effect in molecular electronics theoretically[58]. Thermopower of molecular junction is also determined by the transmission. Thermopower measurement gives us electronic structure of single-molecular junction.

The electrical transport through single-molecule junction are described as Eq.9 . A difference between the Fermi-Dirac distributions due to a temperature difference will drive a thermoelectric current. The transmission of molecular junctions is differentiable which allows us to use the Sommerfield expansion.

$$I(V) = \frac{2e^2}{h}\tau(E_F)V + \frac{2e}{h}\frac{\pi^2 k_B^2 T}{3e}\frac{\partial\tau(E)}{\partial E}\bigg|_{E=E_F}\Delta T \tag{47}$$

Here, *T* represents the average temperature of two electrodes. The origin of *E* is defined as Fermi energy of electrode. The second term of thermoelectric current. Usually, the thermoelectric current is enough small because the shift of Fermi-Dirac distribution is small.

From Eq.47 , the voltage at $I = 0$ is written in Eq.48 .

$$\Delta V = \frac{\pi^2 k_B^2 T}{3e}\frac{\partial \ln\tau(E)}{\partial E}\bigg|_{E=E_F}\Delta T \tag{48}$$

and Seebeck coefficient is defined as

$$S = -\frac{\pi^2 k_B^2 T}{3e}\frac{\partial \ln\tau(E)}{\partial E}\bigg|_{E=E_F}. \tag{49}$$

This voltage is thermoelectric voltage in single molecular junction. It is noteworthy that thermoelectric voltage is determined by not transmission but energy differential of transmission. As mentioned in previous section, fitting of *I-V* curves with Eq.43 are able to be determined the

absolute values of coupling and energy alignment. However, *I-V* characteristics cannot reveal whether the conduction orbital position is below Fermi level or over Fermi level, that is, HOMO or LUMO. Transmission of Breit-Wigner model in Eq.31 is even function of the energy position. It means that the carriers are not distinguishable, hole and electron transport similarly through molecular junctions. On the other hand, thermopower is described as energy differential of transmission at Fermi level. If HOMO is conduction orbital, the energy differential of transmission at Fermi level is negative. and *vice versa*. Thermopower measurement reveals the conduction orbital level.

4. Determination of electronic structures of single-molecule junctions with Current-Voltage measurements

In this chapter, I measured the electronic structures of 1,4-benzenediamine (BDA), 1,4-butanediamine (C4DA), 4,4'-bipyridine, 1,4-benzenedithiol (BDT). It is known that BDT shows multiple conductance states due to different molecular adsorption sites on the Au surface namely on-top, hollow, and bridge. I determined the electronic structures of single-molecule junctions. Compared *I-V* histograms of BDA and C4DA, BDA consisted with rigid structure shows sharper distribution than C4DA which have a flexible molecular backbone. *I-V* histogram of BDT which has same rigid backbone to BDA indicates three conductance states. From the comparison with the result of theoretical calculation, the contact geometries are assigned as on-top, hollow, and bridge structures for low, medium, high conductance states, respectively.

4.1. Introduction

Single-molecule conductance is determined by an electronic structure of single-molecule junction. Determination of electronic structures of the single-molecule junctions is necessary to understand charge transport through single-molecule junctions. However, method to determine electronic structure have not been established yet[39]. In this study, I performed the *I-V* measurement of BDA, C4DA, bipyridine, BDA single-molecule junctions with the aim to establish a method to determine the electronic structures.

Some groups reported *I-V* measurements previously[13, 14, 39, 57, 59, 60] such as that *I-V* characteristics of Au-BDT single-molecule junction is reported in the first report of single-molecule junction by Reed *et al*.[13]. However, unlike single-molecule conductance measured by BJ method[37], it is not frequently that the *I-V* characteristics are measured statistically[13, 59, 56, 60], and most of them are not able to statistically determine the electronic structure of the single-molecule junction[13, 39, 61].

Venkataraman's group measured the *I-V* characteristics of the molecules using STM in 2007 and obtained over 1000 *I-V* curves[61]. However, in this study, they have only performed the *I-V* measurement and calculated the average *I-V* curve. Detailed parameters of the electronic state of the single molecule junction have not been determined.

Guo *et al*. statistically measured *I-V* characteristics of alkanedithiol and biphenyldithiol using STM. Fig.4-1 shows the *I-V* histogram of octanedithiol[39]. Analytical methods in this study are making *I-V* 2D histogram, finding value of transition voltage for each *I-V* curves, and making 2D histograms indicating the relationship between conductance and transition voltage.

In 2D histogram of biphenyldithiol, a single distribution of *I-V* curves was observed, and the transition voltage of TVS was found to be 0.7 V. In the measurement of alkanedithiol, three distributions were observed in the *I-V* two dimensional histogram, and it was clarified that three conduction states exist. The transition voltage in the TVS measurement was obtained for each state. The transition voltages agree each other between two high conductance states. From this, they postulated that the difference in this conduction state is due to contact resistance.

Tao's group also measured *I-V* characteristics of Au-BDT single molecule junctions using STM under ultra-high vacuum at liquid helium temperature[60] . Multiple states of *I-V* characteristics were measured during the bond breakage process and the transition voltage in the TVS measurement of each *I-V* curve was reported. Fig.4-2 represents the *I-V* curves and Fowler-Nordheim plot of the BDT junctions. An increase of conductance was observed in the

rupture process. From the *I-V* characteristic, it was reported that the transition voltage decreases with the increase of conductance. From this result, they considered that the BDT formed a structure distorted by the STM tip in the breaking process, and the orbital energy level contribute to the conductance change BDT single-molecule junctions. In this study, statistically the parameters of the electronic structures of BDT single-molecule junction have not been determined.

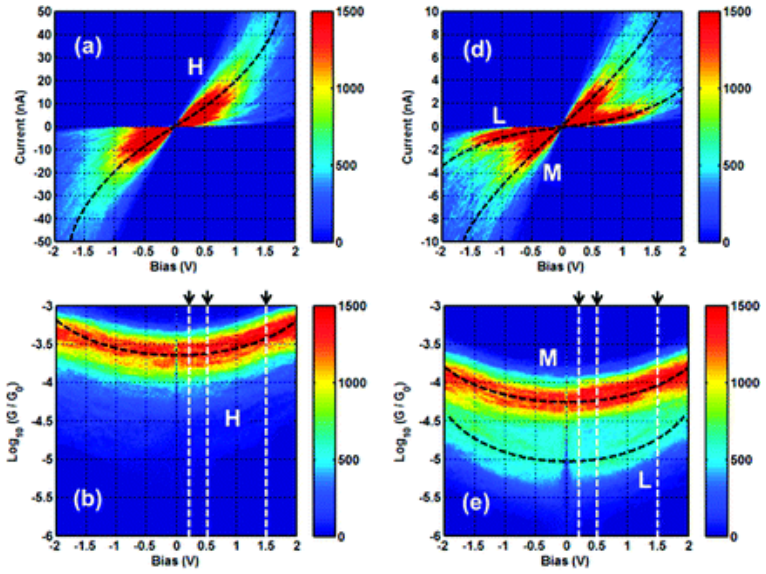

Fig.4-1 *I-V* and G–V histograms for octanedithiol. (a) *I-V* histogram for H-junctions consisting of 2151 curves. (b) G–V histogram for H-junctions. (c) 1-D conductance histogram at different bias voltages for H-junctions. (d) *I-V* histogram for M- and L-junctions consisting of 1661 curves. From (Guo S, Hihath J, Diez-Perez I and Tao N 2011 Measurement and statistical analysis of single-molecule current-voltage characteristics, transition voltage spectroscopy, and tunneling barrier height *J. Am. Chem. Soc.* **133** 19189) Copyright (2011) American Chemical Society.

One of the problems of such *I-V* measurement is that the electronic structures of single-molecule junctions are not completely determined. Many previous studies do not determine the parameters of electronic structures by measuring the *I-V* curves[13, 39, 60-62]. The previous researches reported TVS also determine only orbital energy[39, 60]. However, as mentioned above, not only orbital energy but also the coupling between molecule and metal electrodes contribute to charge transport through single-molecule junctions. In this research,

experiments and analyzes were carried out with the aim of obtaining both the coupling between electrodes and molecules and the orbital energy.

Bruot *et al*. succeeded in measuring *I-V* of multiple conduction states of a Au-alkanedithiol single-molecule junction[60]. They mentioned the conduction state is due to contact resistance on the basis of TVS analysis of *I-V* curves of Au-alkanedithiol single-molecule junctions. However, it has not yet been clarified whether the contact resistance named by them is due to the geometry of the interface. This is because molecules indicating multiple conduction states in this paper are alkane dithiols having a flexible alkane molecular backbone[49, 63]. As described in the influence of the molecular backbone on the single-molecule junction, it is known that molecules having an alkane backbone exhibit different conductance due to the conformational isomers of the alkane. Therefore, in the measurement using a molecule having an alkane backbone, whether multiple conduction states are due to difference of the alkane backbone, or geometry of the metal electrode-molecule interface even when multiple conduction states are observed. It is a very difficult problem to distinguish between either.

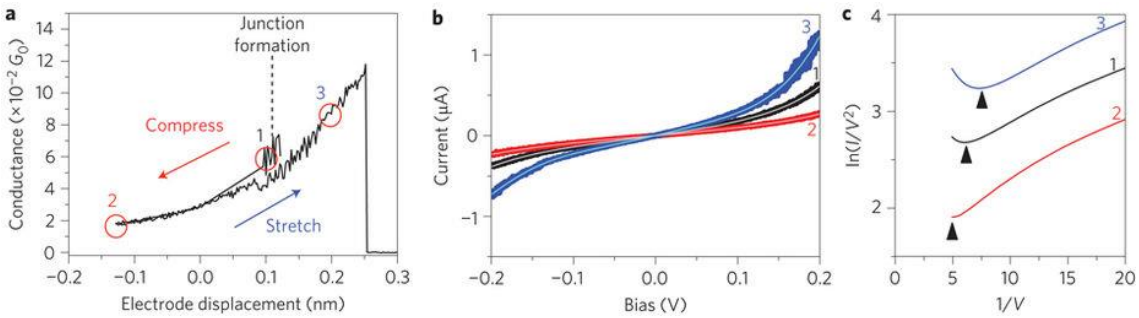

Fig.4-2 Exploring the energy levels of a molecular junction. a, Plot of conductance versus electrode displacement of a BDT junction at 4.2 K. The conductance decreases when the junction is compressed, and then increases to a relatively high value when the junction is stretched. b, Plots of current I versus bias voltage V at the three positions indicated in a. Thin lines are fits to the data. c, Plots of ln(I-V^2) versus 1/V for three different values of the displacement (based on fits to the *I-V* curves in b). The height of the barrier that electrons have to tunnel through is determined by the transition voltage, which is the voltage corresponding to the minimum of each plot (indicated by arrows). The height of the barrier decreases as the molecule is stretched. From (Bruot C, Hihath J and Tao N 2011 Mechanically controlled molecular orbital alignment in single molecule junctions *Nat. Nanotechnol.* **7** 35) Copyright (2011) Nature Publishing Group.

4.2. Experimental

4.2.1. Sample preparation

BDA, C4DA, bipyridine and BDT were purchased from TCI Japan (Fig.4-3) and were used without further purification. The Au(111) substrate was prepared by thermal deposition of gold on mica at elevated temperature under high vacuum[64]. The sample for the *I-V* measurement was prepared by dipping the Au substrate into a 1 mM ethanol solution containing the target molecules. After evaporation of the solution, the substrate surface was washed with ethanol for BDA, C4DA and BDT substrate.

For bipyridine, the substrate is used without washing with ethanol. As mentioned in Chapter 1, the metal electrode-molecule interface has a large influence on single- molecule conductance. In order to clarify the influence of the electrode-molecule interface on the electronic state of the molecular junction, the anchoring group is desired to show multiple conduction states[48, 59], but in the molecular junction having a rigid sp^2 or sp^3 backbone. Furthermore, statistical *I-V* measurement is necessary to eliminate the possibility of incidentally current change. However, such research has not been reported yet. The influence of the interface on the electronic state has also not been clarified yet.

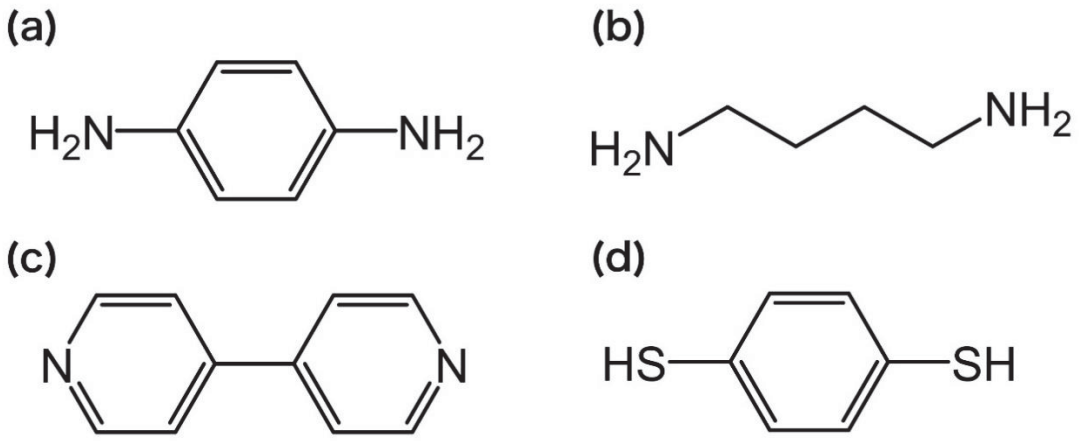

Fig.4-3 molecular structures of (a)1,4-benzenediamine (BDA), (b)1,4-butanediamine (C4DA), (c)4,4'-bipyridine, and (d) 1,4-benzenedithiol (BDT)

4.2.2. *I-V* measurement of molecular junctions

In this study, I used a commercially available STM (Nanoscope V, Bruker, Santa Barbara, CA) operating at ambient conditions. Two current amplifiers, 1 μA/V and 10 nA/V, were used to

access wide molecular conductance ranges from 10^{-5} to 10 G_0. STM tips were prepared by mechanically cutting an Au wire (Nilaco, diameter ≈ 0.3 mm, purity >99%). The *I-V* curves of the single-molecule junction were obtained by the following procedure (Fig.4-4). Firstly, an Au point contact (~10 G_0) was made between the STM tip and the sample surface. Secondly, the tip was withdrawn by 10 nm at a speed of 38 nm/s to break the Au contact and to make a nanogap between the Au electrodes, forming the molecular junction during current monitoring at a fixed bias voltage of 20 mV. Thirdly, the tip position was fixed and one *I-V* curve was recorded by scanning the bias voltage from 20 to 1000, –1000 mV, and back to 20 mV within a time period of 2.5~25 ms at constant tip-sample separation. Finally, the junction was broken by pulling the STM tip away from the substrate. To capture possible structural variation of the junction structures, I cycled the molecular junction making and breaking process and reformed the junction-structure after obtaining each *I-V* curve. This *I-V* measurement-scheme was performed though a signal access module III (Bruker, Santa Barbara, CA) using an external piezo driver (E-665 LVPZT-Amplifier, Physik Instrumente) and a data-acquisition-device with LabVIEW2014 (USB-6363, National Instruments). More than 1,000 *I-V* curves for the molecular junctions were collected for each molecule. The *I-V* curves of molecular junction were obtained by automatically removing *I-V* curves corresponding to Au-metallic junctions and vacuum gap formation. For the *I-V* measurement using the 1 μA/V (10 nA/V) current amplifier, *I-V* curves with <100 nA (<5 nA) current at the bias of 1.0 V was classified as vacuum tunneling, while *I-V* curves with <10,000 nA (<100 nA) current at the bias of 0.2 V was classified as charge transport through an Au-metallic contact.

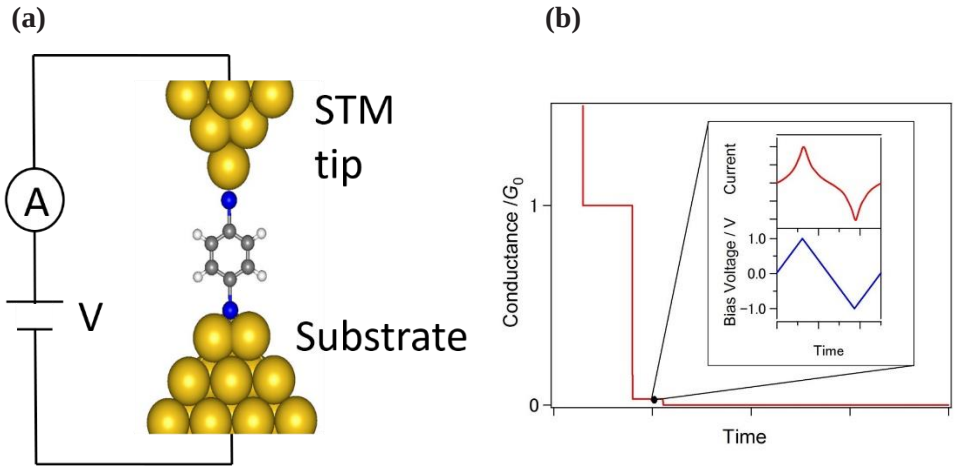

Fig.4-4 (a) Schematic illustration of STM-BJ setup. White, grey, yellow, and orange balls correspond to H, C, S, and Au atoms, respectively. (b) Schematic illustration for conductance (current) change as a function of time in one cycle of the *I*-*V* measurement. After making the metal contact, the contact was stretched at bias voltage of 20 mV. When the current drops below 2 μA, the Au tip position was fixed. Then the bias voltage was scanned from 20 mV to 1000 mV, –1000 mV, and back to 20 mV to measure the *I*-*V* curve of the single-molecule junction (see inset). Finally, the Au tip is pulled further away from the surface to break the molecular junction.

4.2.3. Theoretical calculations

Theoretical calculations were carried out by Associate Prof. Tomofumi Tada (Tokyo Institute of Technology) and Dr. Hisao Nakamura (National Institute of Advanced Industrial Science and Technology).

NEGF-DFT calculation was carried out to determine the transmission of Au-BDT single-molecule junction[65-67]. The detail is described in Ref.[68]

4.3. Results and Discussion

4.3.1. Scan rate dependency of *I*-*V* measurement of BDA

I-*V* measurement of BDA molecular junctions were performed with STM-BJ methods for various rate of bias sweep. Typical *I*-*V* curves are shown in Fig.4-5(a)-(c) for the sweep rate of 4Hz, 40Hz, and 400Hz, respectively. The *I*-*V* curve in Fig.4-5(a) were measured under the condition with the sweep rate of 4Hz. *I*-*V* curves of single-molecule junctions have been measured under the similar sweep rate in some previous reports. *I*-*V* curves measured by slow

sweep show large fluctuation and discontinuous jump and drop of current. These abrupt current changes are caused by structural changes of molecular junction including electrode structures. Conductance of single-molecule junction is easily influenced by the structures. It is desirable that *I*-*V* characteristics measurements were performed while the junctions remain one constant structures. Therefore, faster sweep rate than 4Hz is proper. *I*-*V* curves of 40 Hz, 400 Hz in Fig.4-5(b) and Fig.4-5(c) show law noise features. Fig.4-5(d-f) shows (d*I*/d*V*)/*I*-*V* plot for the BDA. This is parameter for evaluating fluctuating of *I*-*V* curves at large bias voltage. *I*-*V* curves at scan rate of 4 Hz shows larger fluctuation. Probability of forming molecular junctions also depends on sweep rates. Appropriate *I*-*V* curves of molecular junction are obtained of 10 % of total rupture processes measured under the conditions with 40 Hz and 400 Hz sweep rate, whereas *I*-*V* curves of molecular junctions are measurable less than 1% in case of sweep rate of 4 Hz. The lifetimes of single-molecule junctions depend on the mechanical stabilities of the setup. STM-BJ method does not have high stabilities. Current-time (*I*-*t*) method is a method of conductance measurement method with STM without tip withdrawing. The current of *I*-*t* method rises less than 100 ms[69]. It suggests that sweep rate of 4Hz (250ms) is not proper condition for measurement of *I*-*V* characteristics of single-molecule junctions.

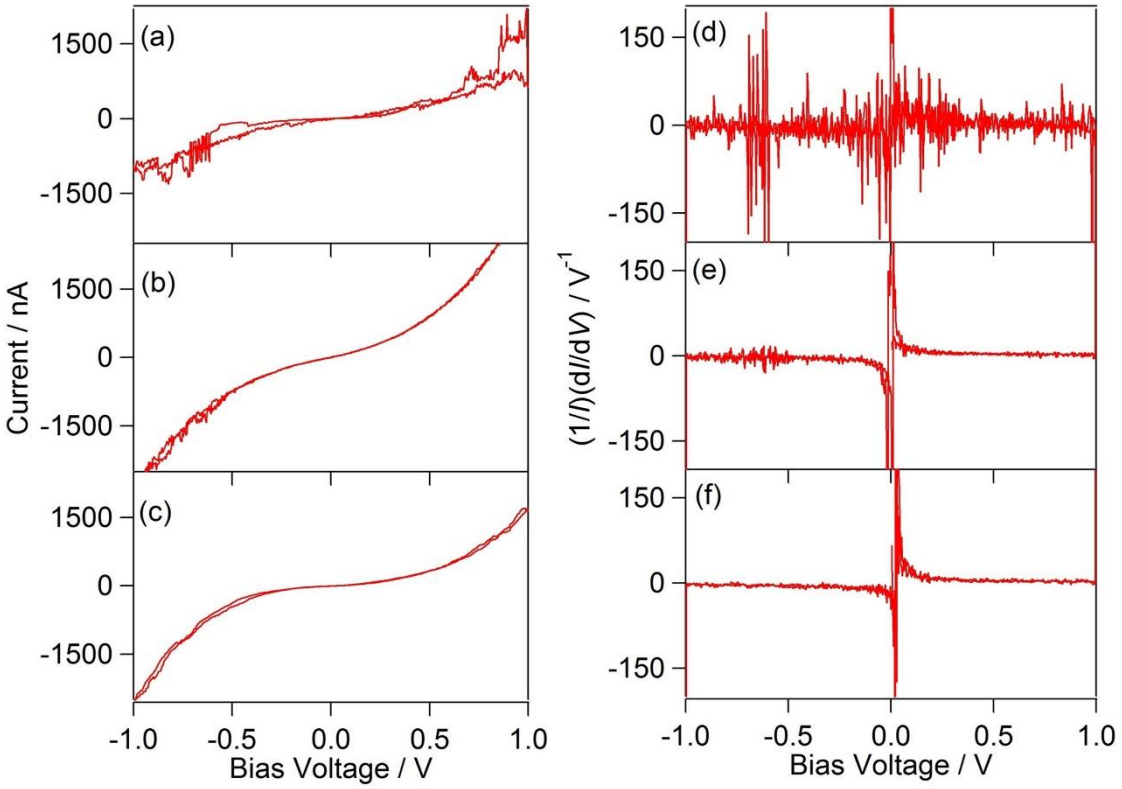

Fig.4-5. Examples of *I-V* curve and normalized (dI/dV)/*I-V* plot for the BDA molecular junction measured for both forward and backward bias voltage scans. The scan rate is (a,d) 4 Hz, (b,e) 40 Hz, and (c,f) 400 Hz. In (d)-(f), data in the lower bias range is not plotted due to inaccuracy in the bias voltage.

4.3.2. *I-V* characteristics of BDA

More than 1000 *I-V* curves are recorded. Fig.4-6 represents a histogram of BDA molecular junctions constituted from more than 1000 *I-V* curves. It is well known that BDA molecule binding to gold electrodes with amino groups show small dispersion peak in the conductance histogram of the conductance measurement with STM-BJ methods under constant bias voltage[41]. The narrow distribution of *I-V* curves in Fig.4-6 agrees with previous results of STM-BJ conductance measurements. Two distributions are observed in Fig. 4-6. Fig. 4-7 shows a conductance histogram at 0.3V to distinguish the two states. A peak top position of the histogram is 13 mG_0. This conductance is correspond with the peak top conductance of the histogram obtained by STM-BJ measurement under constant bias voltage of 20 mV (Fig.4-8)[47]. This conductance correspondence between two methods is evidence that the *I-V*

curves obtained *I-V* measurement method by are originated from BDA molecular junctions. Main peak and small shoulder peak are observed in the current histogram of *I-V* curves at 0.3V. Many researches reported integer multiple steps is observed in the conductance trace in ordinal conductance measurements with BJ methods. It is considered that decreasing of the number of bridging molecules appear as integer multiple steps. Based on peak positions in the Fig.4-9, the *I-V* curves which current are within the two ranges are separated and averaged into two averaged *I-V* curves. Two averaged *I-V* curved are indicated in Fig.4-10. Two current ranges are setting as from 240 to 370 nA and from 370 to 600 nA at 0.3V to separate two states. In averaged *I-V* curves or individual *I-V* curve, the current increase with bias voltage in low bias voltage region linearly and increase non-linearly in high bias voltage region. It suggests that the charge transport mechanism become resonance tunneling mechanism at high bias voltage range from non-resonance mechanism. The current is described as Eq.46 with using Breit-Wigner model transmission (Eq.31). The averaged *I-V* curves were fitted with Eq.46 for quantitative analysis of electronic structures of molecular junctions. For low conductance averaged *I-V* curve, It is determined by fitting with Eq.46 that the coupling Γ ($=\Gamma_L+\Gamma_R$) is 85 meV, and energy alignment ε_0 is 0.68 eV ant the asymmetry factor α= 0.53. the asymmetry factor is defined as Γ_L/Γ and become 0.5 in case of symmetric coupling. Here, the origin of ε_0 is set as Fermi level of Au electrode. For high conductance *I-V* curves, the averaged *I-V* curve was fitted with Eq.46 with the assumption of the number bridging molecule n=1 and 2. The electronic structures are determined to be Γ is 105 meV, ε_0 is 0.70 eV for n = 1 and Γ is 75 meV, ε_0 is 0.71 eV.. The obtained set of Γ and ε_0 is closely similar to that found for the low conductance state. High conductance state is inferred to be originated from BDA double molecular junctions. Previous researches report BDA single molecular junction displays a single conductance state formed by a preferential metal-molecule contact geometry[41, 45]. The number of bridging molecules n seem to be arbitrary. However, many previous single molecular conductance-studies reported that the most typical number is 1, the maximum number of n is typically less than n = 3 or 4 in the conductance histograms, and formation probability of the multiple molecular junctions are low. For the BDA molecular junctions, the single conductance state and the corresponding set of Γ and ε_0 values were obtained by fitting the averaged *I-V* characteristics within a reasonable choice of *n*, which indicates that the single BDA junction displays a single conductance state with a preferential metal-molecule contact configuration. The observation of *I-V* curves of

double molecular junction agrees with the results of a separate STM-BJ conductance measurement. In a STM-BJ experiment at a constant bias voltage of 20 mV, formation of the double BDA molecular junction with n = 2 were observed, as shown in Fig.4-9.

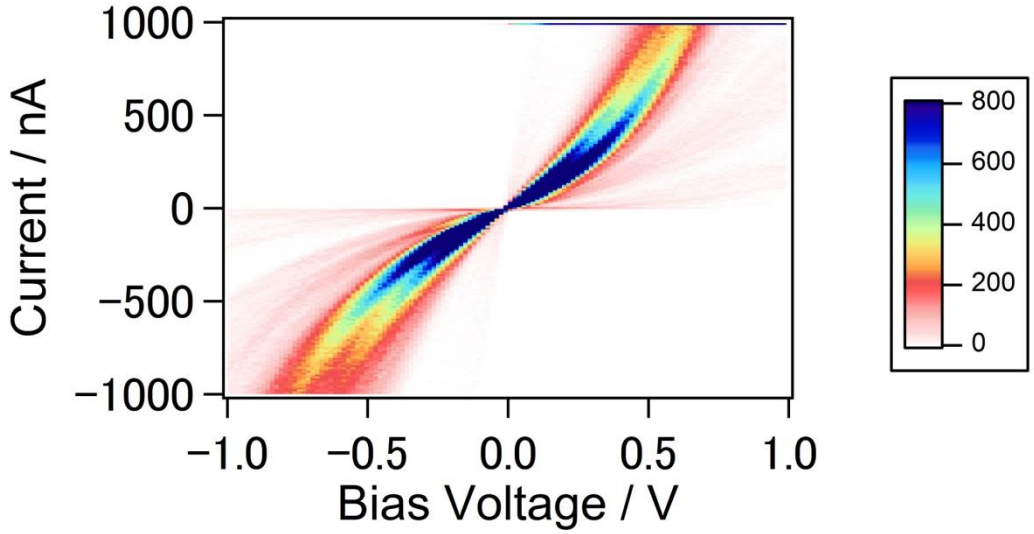

Fig.4-6 Two dimensional (2D) *I-V* histogram of the BDA molecular junction, constructed from 1000 *I-V* curves. Bin size is 0.016 V × 10 nA.

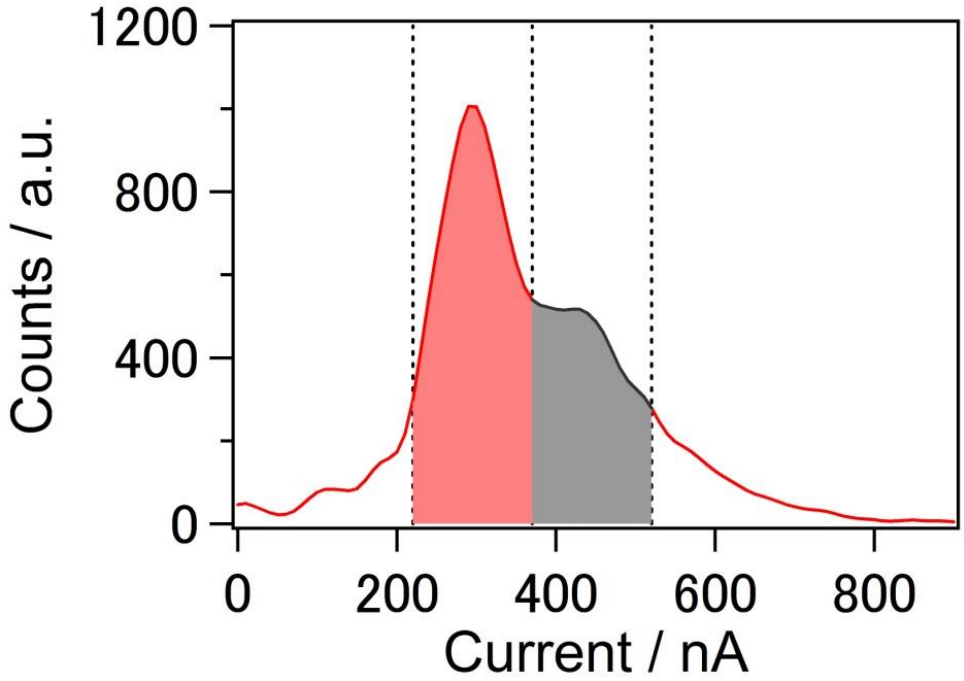

Fig.4-7 Current histogram of BDA molecular junction at the bias voltage of 0.3 V. Bin size is 10 nA.

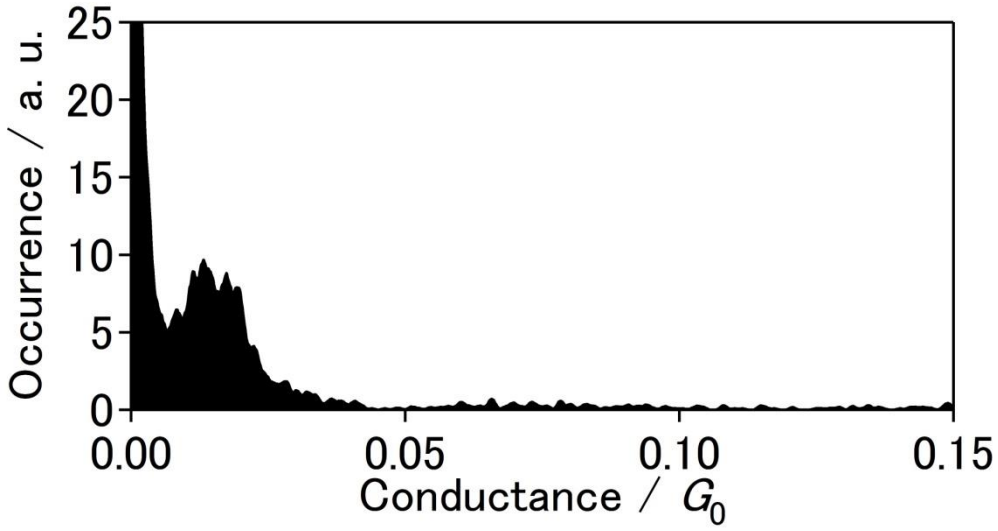

Fig.4-8 Conductance histogram of the BDA junctions with double molecular junction formations. A peak appeared at 13 mG_0

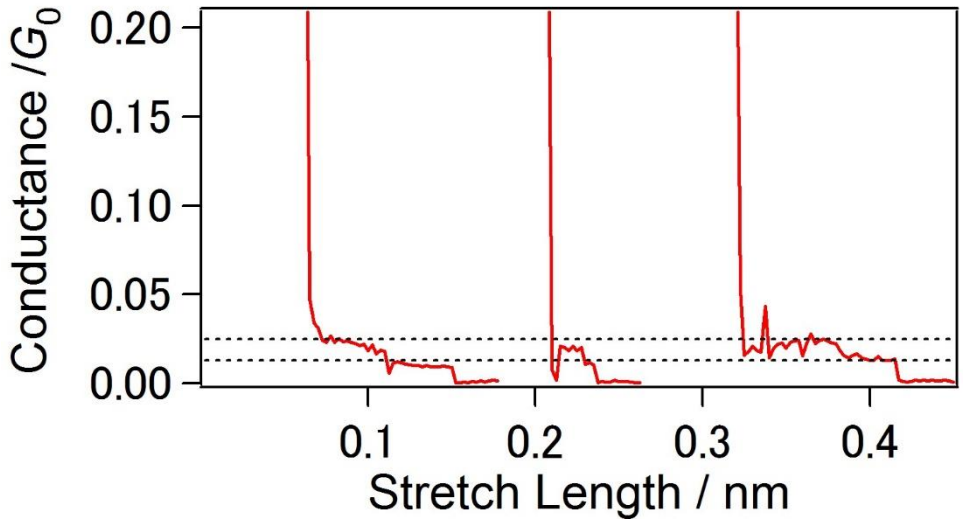

Fig.4-9 Conductance traces of the BDA junctions with double molecular junction formations. Black dotted lines represent the molecular conductance for the single (13 m G_0) and double (26 m G_0) junction-formation. Bias voltage was 20 mV. Tip velocity was 50 nm/s. The conductance measurement was carried out under tetraglyme solution

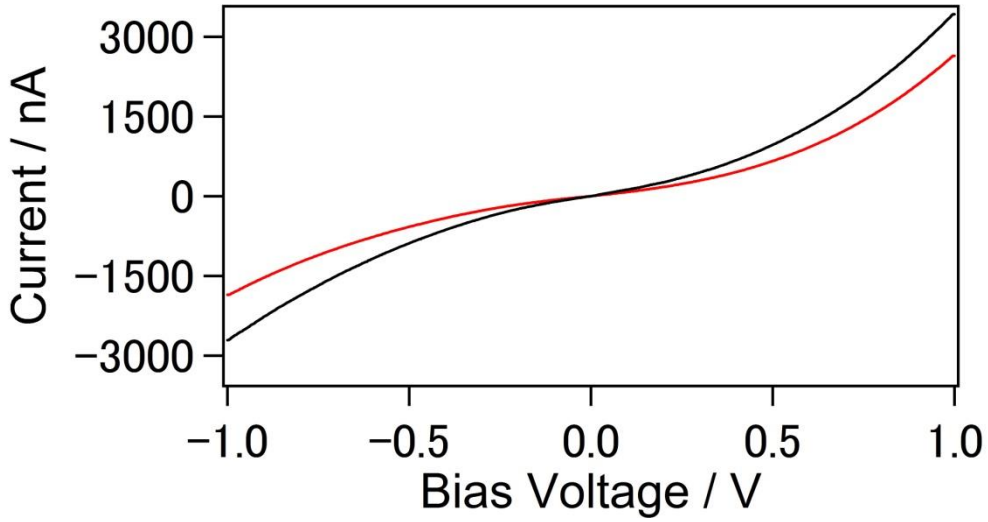

Fig.4-10 Averaged *I-V* curves within the current windows of 20~370 nA and 370~520 nA at 0.3 V. The two windows correspond to the red and black colored areas in Fig.4.7

4.3.3. *I-V* characteristics of C4DA

In previous section, I have reported *I-V* characteristics of BDA molecular junctions. BDA has rigid phenylene backbone. In this section, I focused on alkanediamine, 1,4-butanediamine (C4DA), which has the same amino anchoring group with BDA, but has a flexible alkane backbone. Alkane molecular junctions shows different conductance due to difference of backbone structures. It is reported by a previous study of STM-BJ conductance measurement that the gauche conformation shows lower conductance than trans conformation[49, 63]. I performed same *I-V* measurements for C4DA. Fig. represents typical *I-V* curves of C4DA molecular junctions. The *I-V* curves shows significant fluctuation of current. Compared to BDA, C4DA has large fluctuation. The difference between BDA and C4DA is only molecular backbone. BDA include rigid sp^2 flame and C4DA has flexible sp^3 structure. The current fluctuation is due to conformational change of molecular backbone. A 2D *I-V* histogram of C4DA molecular junctions. The histograms show several distributions. *I-V* curves of C4DA varies broadly than BDA. This large distribution of *I-V* curves can be explained that C4DA molecular junction exhibits diverse structures due to its flexible alkane backbone. Here, I mention one of the distributions, whose current ranged between 15 and 25 nA at 0.3V. This current range was set on the basis of the literature conductance measured by STM-BJ

conductance measurements in previous report. The averaged *I-V* curve are obtained by similar way to BDA. The averaged *I-V* curve are shown in Fig.4-11. as dotted black line. The significant difference between averaged *I-V* curves of BDA and C4DA is a shape of the *I-V* curves. On contrast that BDA shows non-linear behavior, the averaged *I-V* curve of C4DA is linear characteristics.

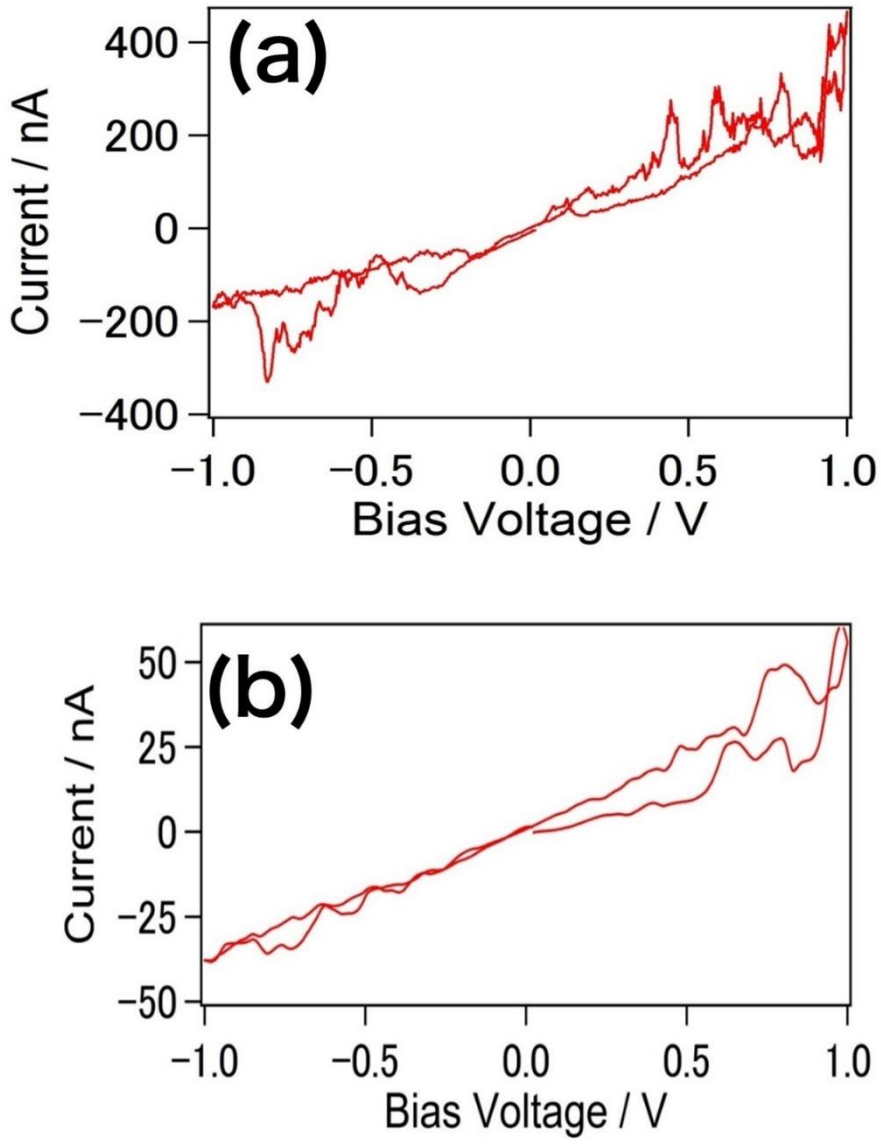

Fig.4-11 Examples of *I-V* curves for the C4DA molecular junction measured for both forward and backward bias voltage scans with (a) 1 μA/V amplifier and (b) 10 nA/V amplifier. scan rate was 400 Hz.

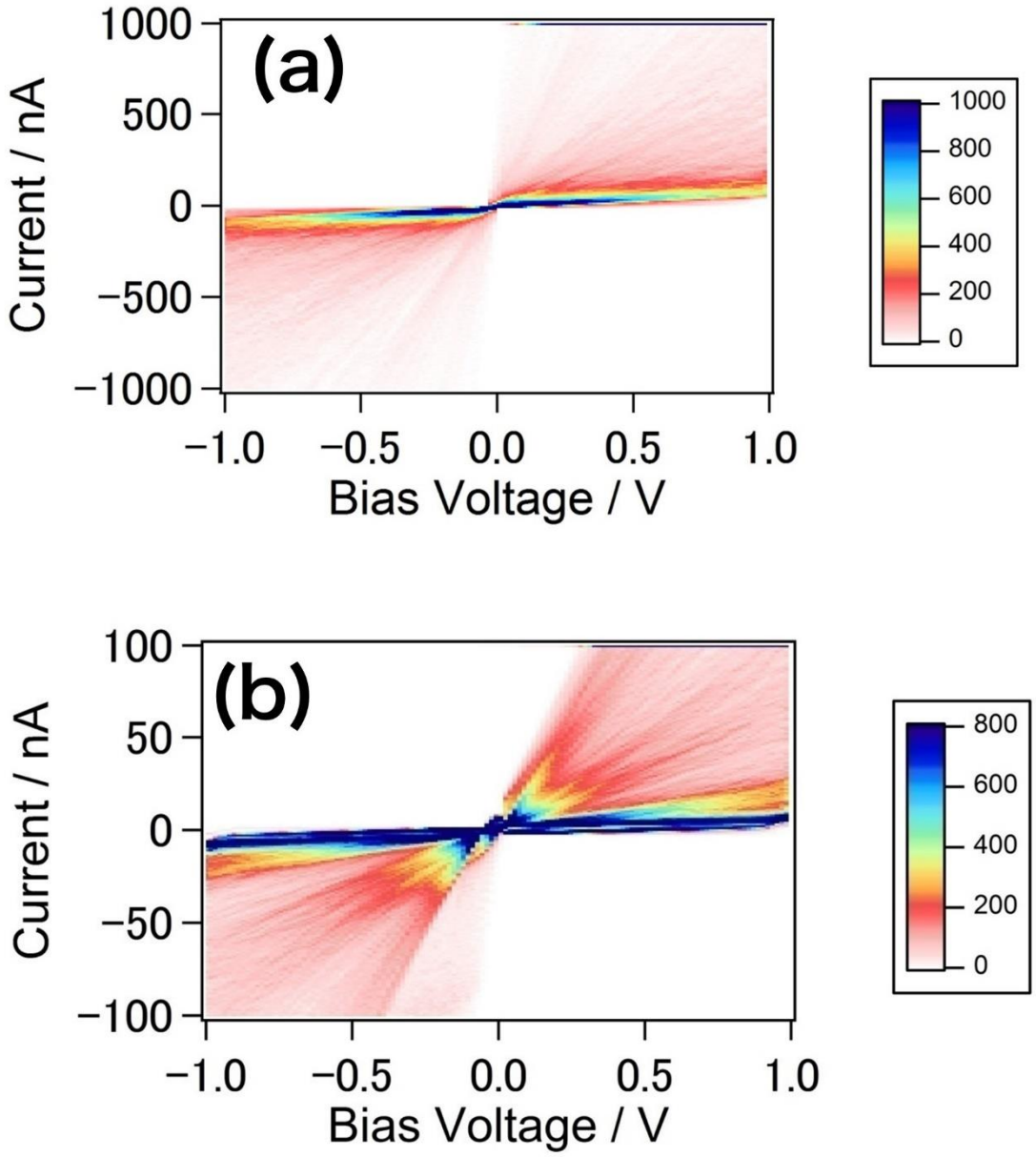

Fig.4-12 (a) 2D *I-V* histogram of the C4DA molecular junctions constructed from 1,000 *I-V* curves. The current regime was 0–800 nA. (b) Magnified view of (a) in the current regime between 0 and 100 nA. Bin sizes are (a) 0.016 V × 10 nA and (b) 0.016 V × 1 nA.

This linear behavior is able to be explained by large energy difference with both conduction model of Breit-Wigner resonant tunneling model and Simmons' model. In Breit-Wigner model, the transmission of molecular junction is described as Lorentzian curve. The transmission

become maximum when the energy of electron is corresponding to the energy level of molecular orbital. When the coupling is constant, and the energy of electron *E* is enough smaller than energy level of bridging molecule, energy differentiate of the transmission dτ/d*E* is also small. dτ/d*E* is represented as Eq.31 in Breit-Wigner model.

$$\frac{\mathrm{d}\tau(E)}{\mathrm{d}E} = \frac{-8\Gamma_L\Gamma_R(\mathrm{E}-\varepsilon)}{\{(\Gamma_L+\Gamma_R)^2+(\mathrm{E}-\varepsilon)^2\}^2} \tag{50}$$

The energy difference of electron and conduction orbital getting larger, the absolute value of dτ/d*E* decrease to 0. Hence, when the ε_0 is enough large, the shape of *I-V* curves is linear.

In Simmons model, when the bias voltage is enough small than energy barrier, the current density is approximated as

$$J = \frac{3e^2\sqrt{2m\varphi_0}}{2\pi hsh^2}\exp\left(-\frac{4\pi s}{h}\sqrt{2m\varphi_0}\right)V. \tag{51}$$

In low bias voltage range, the current is proportional with bias voltage. The linear behavior of *I-V* curves is interpreted by large energy difference.

The electronic structure of averaged C4DA junction was determined by fitting with Eq.43 to quantitative analysis. Here, the bridging molecular number n was assumed to be one. From the fitting, the electronic structure was determined to be $\Gamma = 48$ meV and $\varepsilon_0 = 1.7$ eV. The obtained energy difference ε_0 of 1.7 eV is significant larger than the ε_0 of 0.7 V obtained for the BDA molecular junctions. Observed large energy difference of 1.7 eV is caused larger HOMO-LUMO gap of alkane molecule. This *I-V* measurement method can capture molecular dependent of *I-V* characteristics in a qualitative property.

Focused on the coupling, the coupling of C4DA (48 meV) is much smaller than BDA (75 meV) despite both molecules have same amino anchoring groups. The coupling depends on not only the local binding group geometry but also electronic properties of molecular backbones such as orbital delocalization. The amino anchoring group in BDA binds to a sp^2 carbon atom of benzene and the lone pair in the nitrogen atom is delocalized into the π-electron system of the phenylene ring. It is guessed that the electronic interaction between the anchoring groups and molecular backbone cause the larger coupling for BDA. On the other hand, the amino anchoring group is directly bonding with sp^3 alkane backbone. The lone pair of the nitrogen of C4DA cannot delocalize into molecular backbone. Thus, the coupling of C4DA is smaller than BDA. The interaction was demonstrated in rupture force measurements with AFM of C4DA and BDA molecular junctions[70].

Several conductance states are observed *I-V* histogram of C4DA. Tao's group reported the origin of multi states of alkanedithiol is contact resistance rather than energy difference between conduction orbital and Fermi level by TVS analysis[39]. In rectangle potential model, the tunneling conductance is described below by using of WKB approximation,

$$G = G_c \exp(-\beta l) \tag{51}$$

Here, l means length of barrier. Tao's group called inverse of *G*c as contact resistance. In this model, β is constant and l is variable. the conductance is *G*c in the limit of l = 0. Therefore, *G*c is called contact resistance. However, the structural changes of molecular backbone can affect to *G*c. It is not clear that the contact resistance is due to only contact geometry between molecule and electrode. It is well known from theoretical and experimental aspects that the conductance of alkane molecular junction decreases by gauche structures. The *I-V* measurement of flexible molecular junctions cannot clarify how contact part of electrode-molecule interfaces affect contact resistance.

4.3.4. *I-V* characteristics of bipyridine

To insure reliability of the *I-V* measurement method, *I-V* characteristics of bipyridine were also examined. Fig.4-13 represents *I-V* histogram of bipyridine molecular junction. Two clear distributions are observed in Fig.4-13. The magenta line and black line indicate the conductance reported previously. The current (Fig.4-14) obtained by *I-V* measurement are good agreement with previous STM-BJ conductance measurement [71]. It is considered that high conductance state is due to π-plane binding to the electrodes and low conductance sate is due to the lone-pair binding. From the fitting results, the coupling and energy difference are determined to be $\Gamma = 22$ meV and $\varepsilon_0 = 0.95$ eV for high conductance state and $\Gamma = 9.1$ meV and $\varepsilon_0 = 0.76$ eV for low conductance state. Venkaraman's group reported the electronic structurtes of bipyridine with thermopower measurement[72]. They reported $\varepsilon_0 = 1.5$ eV and 1.2 for high and low conductance state. It agrees qualitatively in the view that high conductance state is far from Fermi level of Au electrodes. The difference between this method and their thermopower measurement seemed to due to under estimation of Seebeck coefficient. It is difficult to measure temperature difference between both electrodes. They overestimated temperature difference. As a result, the energy alignment they reported became larger. *I-V* characteristics of bipyridine confirmed the validity of the *I-V* method.

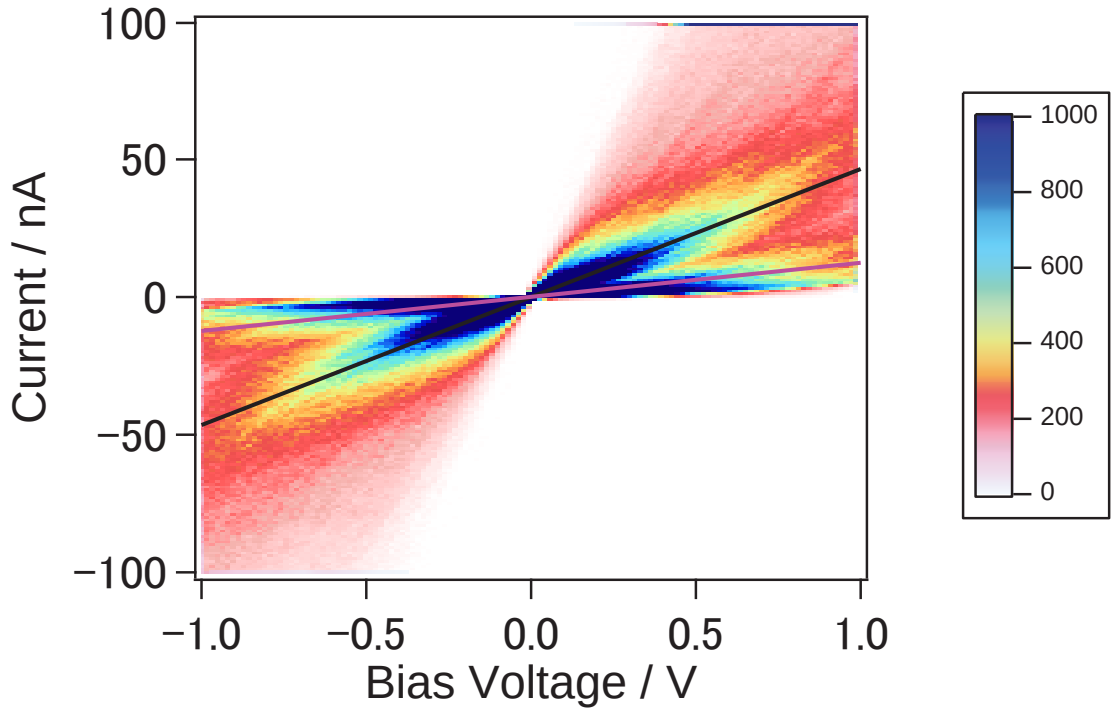

Fig.4-13 *I-V* 2D histogram of Au-bipyridine junctions. bin size is 0.016 V × 1 nA constructed from more than 3000 *I-V* curves. magenta and black line indicate 0.16 mG_0 and 0.6 mG_0 reported as single-molecule conductance of Au-bipyridine junction in Ref.[71]

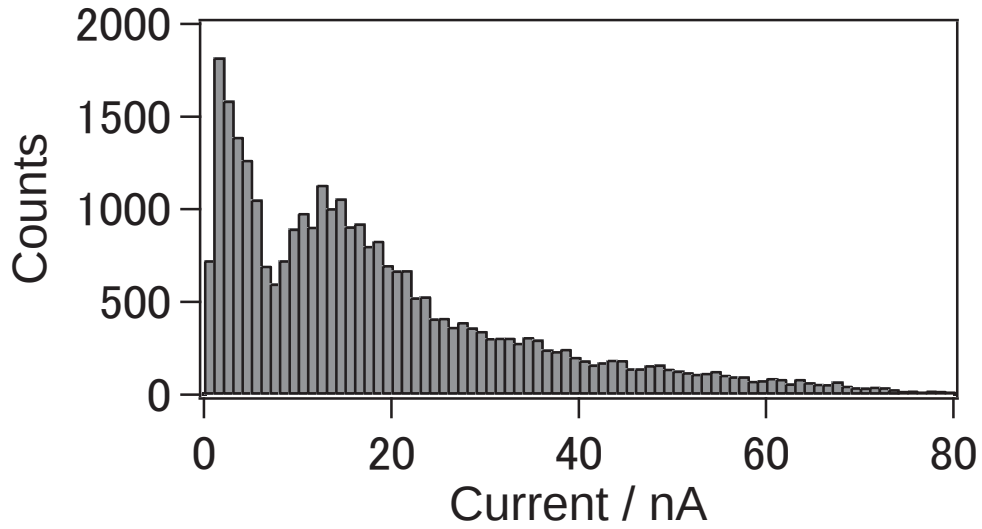

Fig.4-14 Current histogram of Au-bipyridine single-molecule junction at the bias voltage of 0.3 V. Bin size is 1 nA.

4.3.5. *I-V* characteristics of BDT

In previous sections, the validity and effectiveness of *I-V* measurement are confirmed. To

characterize metal-molecule interface of single-molecule junction, *I-V* measurement of BDT single-molecule junctions was performed. BDT is a model system of single-molecule junction since first study of molecular junction reported by Reed *et al*.. The much investigation of BDT molecular junction has been carried out previously[13, 41-44]. It is well-known that the conductance of BDT single-molecule junction varies widely[41, 44]. BDT has rigid phenylene molecular backbone and thiol anchoring groups. Previous studies reported the variety of conductance is due to contact geometry of Au-thiol group such as on-top, bridge, and hollow adsorption-structures[48, 63]. One of the most important problem in the field of molecular junction is to clarify the relationship between contact configurations and transport property reliably.

Examples of *I-V* curves of BDT molecular junction is shown in Fig.4-15. Fig.4-16 represents 2D *I-V* histograms of BDT molecular junctions in two different current range. In contrast to the BDA junctions, BDT junctions with multiple Au-S bonding geometries varies in wide current range shown in the *I-V* 2D histograms. The fitting of individual *I-V* curves determined each coupling and energy difference. The values of Γ and ε_0 are plotted in Fig.4-17 . In the 2D histograms of the values of Γ and ε_0, three conduction states (High: H, Medium: M, and Low: L) are observed. The one dimensional histogram of Γ and ε_0 are shown in Fig.4-18. From the peak top positions, the electronic structures are determined to be $\Gamma = 31$ and 126 meV and $\varepsilon_0 = 0.63$ eV for *I-V* curves in the large current regime (Fig.4-18(a,b)) and $\Gamma = 12$ meV, and $\varepsilon_0 = 0.65$ eV for *I-V* curves in the small current regime (Fig.4-18(c,d)). The individual curve-fitting revealed the existence of three preferential conductance states, L, M, and H. Three distributions observed in the histogram of electronic structure are observed 2D histograms of *I-V* curves. The histograms of current at 0.3V show some peaks at 7 nA for low conductance region, and 20, 60, and 670 nA in high conductance region, which correspond to 0.3, 0.9, 2.6, and 29 mG_0 as shown in Fig.4-19. Based on the peak-positons in the current histograms, the *I-V* curves passing within the current range of (L) 5~20, (M1) 20~40, (M2) 40~100 nA, and (H) 440~2200 nA at 0.3 V are divided into four groups to obtain statistically significant *I-V* characteristics. Each averaged *I-V* curve is plotted in Fig.4-16 as black dotted line.

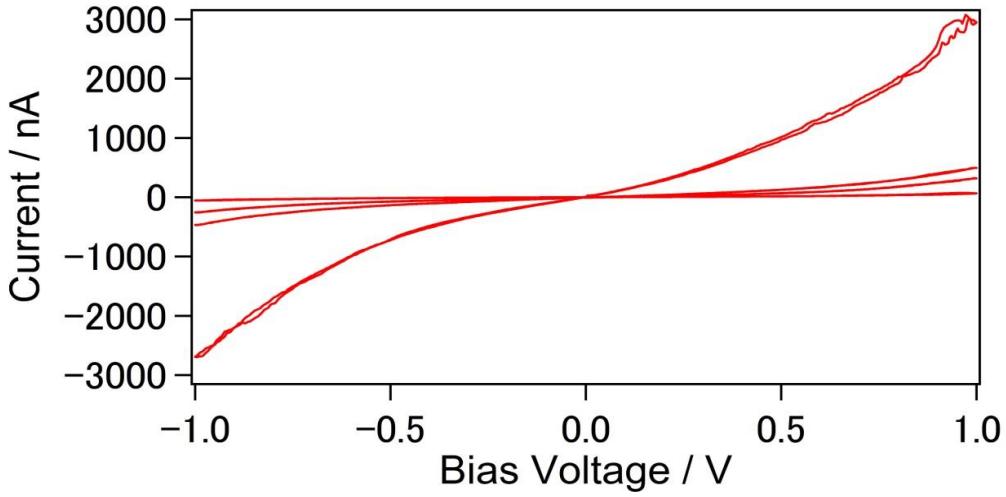

Fig.4-15 Example of *I*-*V* curves for the BDT molecular junctions measured at forward and backward bias voltage scans. Bias voltage scan rate was 400 Hz.

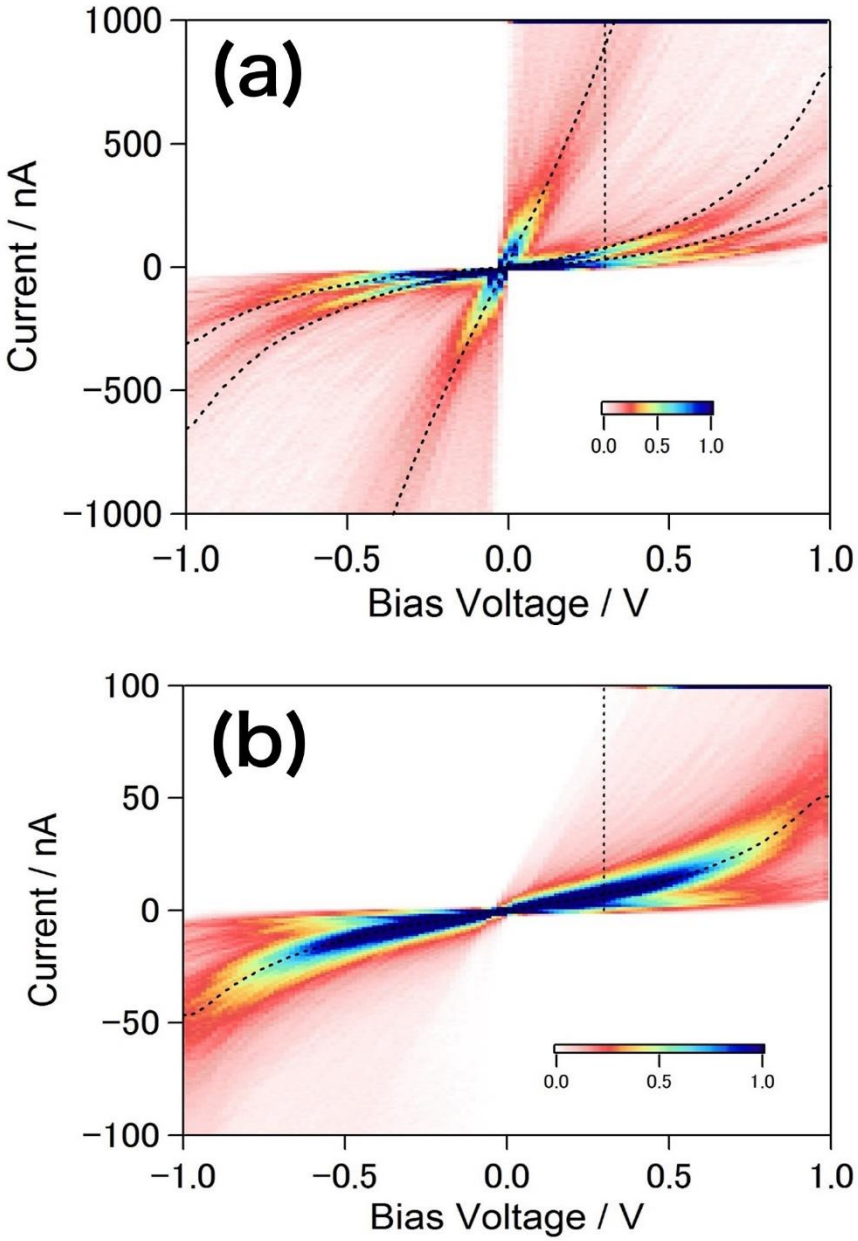

Fig.4-16 (a,b) 2D *I-V* histograms of BDT molecular junctions constructed from 1,000 *I-V* curves (Bias voltage scan rate = 400 Hz) measured by the two different current amplifiers ((a) 1 μA/V and (b) 10 nA/V) in separate experiments. Bin sizes are (a) 0.016 V × 10 nA and (b) 0.016 V × 1 nA. Dotted lines indicate bias voltage of 0.3 V. Dotted curves are the averaged *I-V* curves of the junctions within current windows of 4–11 in (b), and 0–50, 50–100, and 540–1300 nA in (a) at 0.3 V. The averaged *I-V* curves are denoted L, M1, M2, and H in order of the molecular conductance.

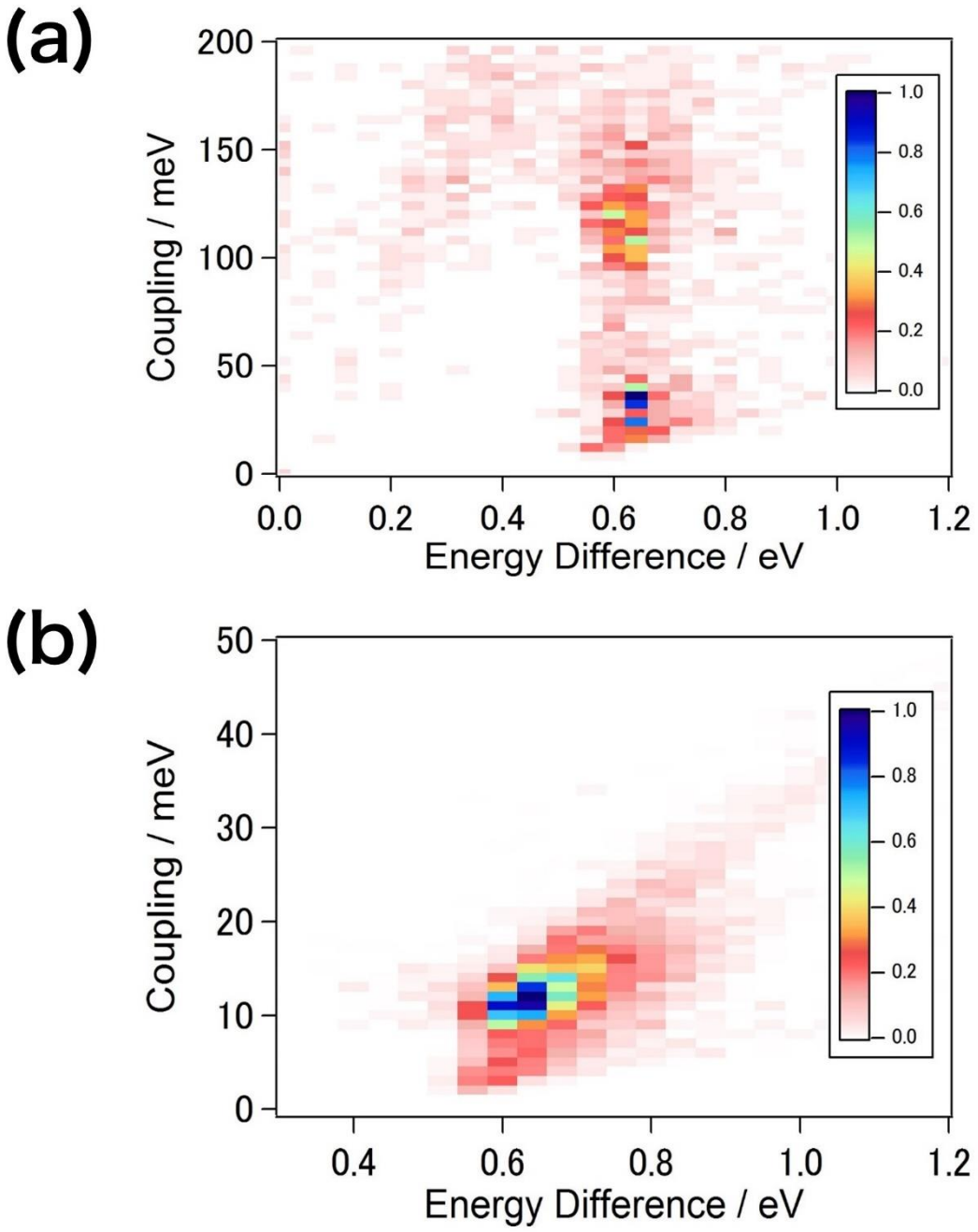

Fig.4-17 2D histograms of a set of the Γ and ε_0, which were obtained by fitting each 1,000 *I*-*V* curves using Eq.43. The bin sizes are 0.04 eV measured with (a) 1μA/V amplifier and (b) 10 nA/V amplifier.

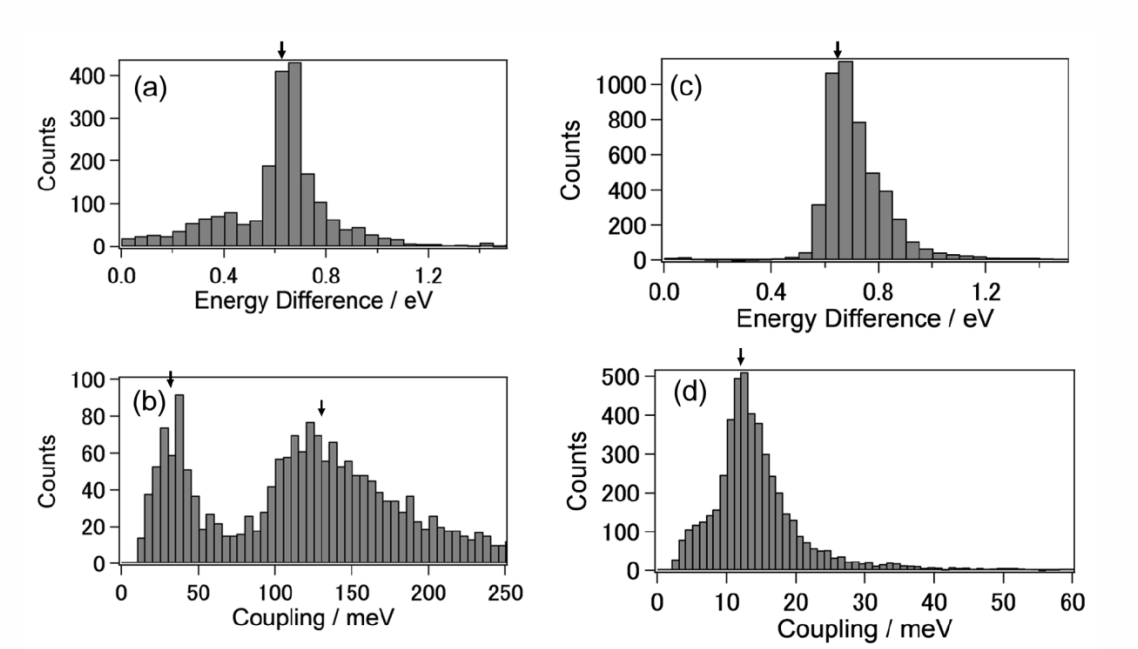

Fig.4-18 Histograms of the fitted e0 and G obtained from 1,000 of individual *I-V* curves of the BDT molecular junctions in the (a,b) large and (c,d) small conductance regime. Peak positions found by Gaussian fitting of the distributions are indicated by arrows; (a) 0.63 eV, (b) 31 meV and 126 meV, (c) 0.65 eV, and (d) 12 m eV.

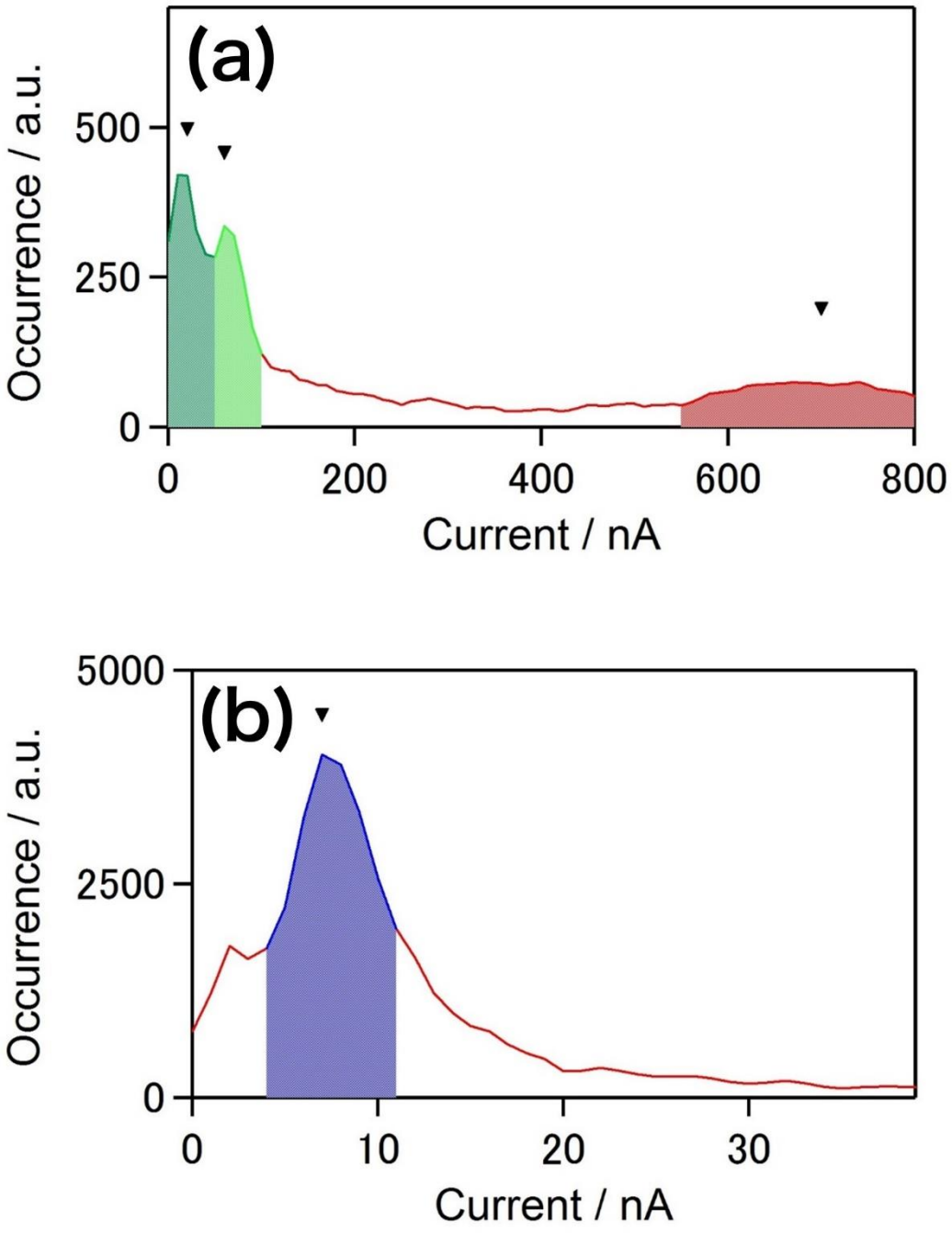

Fig.4-19　Current histograms of the BDT molecular junctions at the bias of 0.3 V with　(a) 1μA/V amplifier and (b) 10 nA/V amplifier. See the dotted line in Fig.4-16. The peak position of three states, H, M1, and M2, are indicated by arrows.

To consider the number of bridging molecules n, the statistically averaged *I-V* curves (dotted line in Fig.4-16) of M1, M2, and L were normalized on the basis of the current at 0.3 V. The

normalized *I-V* curves are shown in Fig.4-20 . The multiplication factors only permitted integers or inverse of integers are 3, 1, and 0.5 for the curves of L, M1, and M2, respectively. The normalized *I-V* curves of M1 and M2 are almost identical in the full bias voltage range. On the other hand, the normalized *I-V* curve of L state shows significant mismatch with M (M1 and M2). These results indicate that M1 and M2 belong to the same conductance state (i.e., M) with different bridging molecule number n= 1,2. It should be note here that the conductance of H is more than one order of magnitude larger than that of M, and therefore, the difference in the conductance between H and M is unlikely to be explained by the difference in the number of the bridging molecules n.

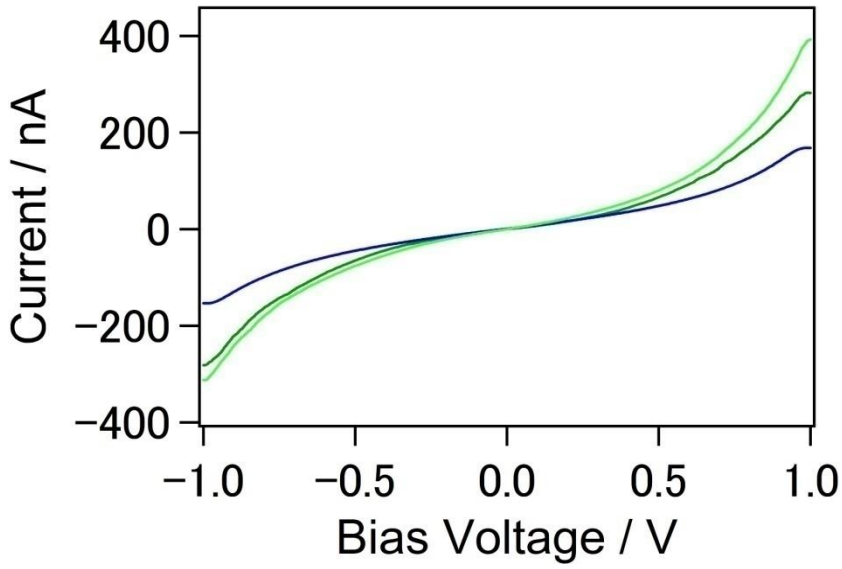

Fig.4-20 Averaged and current-normalized *I-V* curves of the BDT molecular junction at 0.3 V.

I-V measurement reveals existence of three states of BDT molecular junctions. The electronic structures of the junctions were determined to be Γ = 12 meV, ε_0 = 0.67 eV, Γ = 26 meV, ε_0 = 0.63 eV, Γ = 129 meV, ε_0 = 0.66 eV for L,M, and H, respectively by fitting averaged *I-V* curves with Eq.46 . The fitting results indicate that the coupling dominate the conduction of BDT molecular junction. A previous study reported energy difference (TVS) of BDT junctions changes between different conduction *I-V* curves with STM-BJ method under liquid He temperature[60]. It is not corresponding with the results obtained by our method. In this study, transition voltage is less than 0.2 eV, which is much lower than the results. The difference is

interpreted by the difference of the measurement conditions. In my study, *I*-*V* curves are obtained under ambient condition. On the other hand, the previous research is carried out under ultra-low temperature. BDT can be unstabilized by compression of STM tip.

I also analyzed the averaged *I*-*V* curves with transition voltage spectroscopy as previous report[60, 39, 52]. Fig.4-21 represents Fowler-Nordheim (FN) plot of BDT averaged *I*-*V* curves. The minimum of FN plot is transition voltage which correspond the barrier height in the one-dimensional rectangle potential model. Transition voltage is 0.81, 0.71 and 0.76 eV for H, M, and L state, respectively. Only slightly difference from the ε_0 by fitting with Breit-Wigner model are observed. No significant difference of conduction orbital level is observed with TVS analysis. TVS analysis also support the conductance of BDT single-molecule junction mainly depends on the coupling.

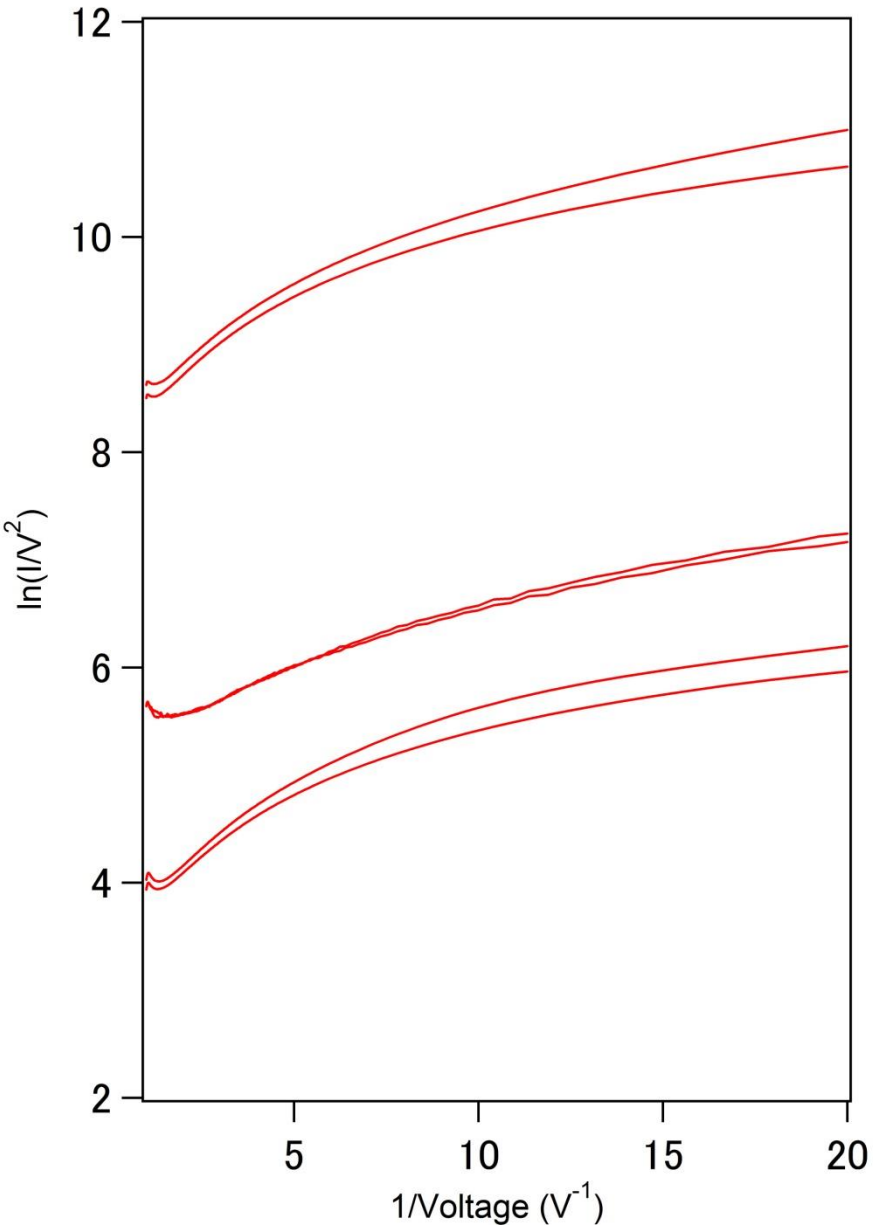

Fig.4-21 Transition voltage spectroscopy. Fowler-Nordheim plot of averaged *I*-*V* curves of Au-BDT H, M, and L state. The minimum is 0.81, 0.71 and 0.76 eV for H, M, and L state.

Thus, *I*-*V* measurement reveal the electronic structures of BDT junctions and capture the difference of conduction states clearly caused by their adsorption geometries.

4.3.6. Comparison with theoretical calculation

Contact configurations of three conduction states are assigned by means of comparison with theoretical calculation. The three possible anchoring positions, i.e., hollow, bridge, and on-top,

to the Au electrodes and determined the conformations of each junction model are calculated. The structural model is shown in Fig.4-22,4-23,4-24. The conductance of hollow and on-top configuration is 24, 9 mG_0, respectively. All of the bridge conformations have high conductance, e.g., (i) bridge, 0.22 G_0; (ii) bridge-top, 0.32 G_0; and (ii) bridge tilt, 0.27 G_0, respectively. On-top configuration has smallest conductance of 9 mG_0. Conductance of hollow structure is calculated as 24 mG_0 The conductance of the bridge family is much higher than hollow or on-top structures. The calculated *I-V* curves of on-top, hollow, and bridge configurations are plotted in Fig.4-25. The calculation results also show three distinct conductance regimes for BDT, and they can be assigned by anchoring sites, i.e., H is bridge, M is hollow, and L is on-top, respectively. The most conductive bridge type configuration, bridge-top was as the H state chosen in below discussion.

Here, I discuss the relationship of the coupling between theoretically calculated values and experimentally obtained values. The projected molecular orbital (PMO) was defined by diagonalizing the molecular projected Hamiltonian (MPSH) and identify the conductive MO, whose energy ε_a should be close to E_F and whose coupling strength to electronic state of the electrodes, γ, is sufficiently large. The value of γ is the imaginary part of the normalized self-energy to MPSH and was obtained for each PMO. Generally, the conductive MO is not the conduction channel state. Thus (ε_a, γ) is not equal to (ε_0, Γ), as defined by Eq.31 . However, identifying conducting MO's is useful to check validity of the analysis with Eq.31 . In addition, (ε_a,γ) is a good approximation that allows discussion of the tendency of γ. The calculated values ε_H, ε_M, and ε_L are −0.75, −1.09, and −0.47 eV, respectively. Since the conductive MO energies of the three states are of the same order, analysis of the relationship between the contact configuration and Γ, as evaluated by *I-V* curves using Eq.43 , is reasonable. The relative coupling strength and are 64 and 50. The correlation of conductance and Γ agree reasonably with that of conductance and γ.

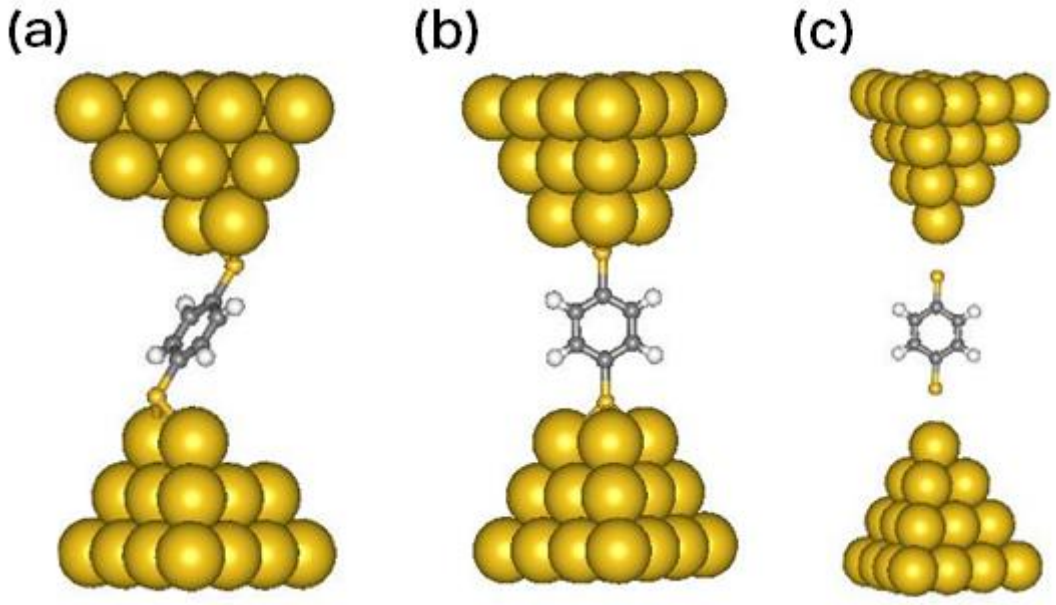

Fig.4-22 Schematic structures of (a) bridge, (b)hollow, (c) on-top adsorption configuration of Au-BDT single-molecule junctions.

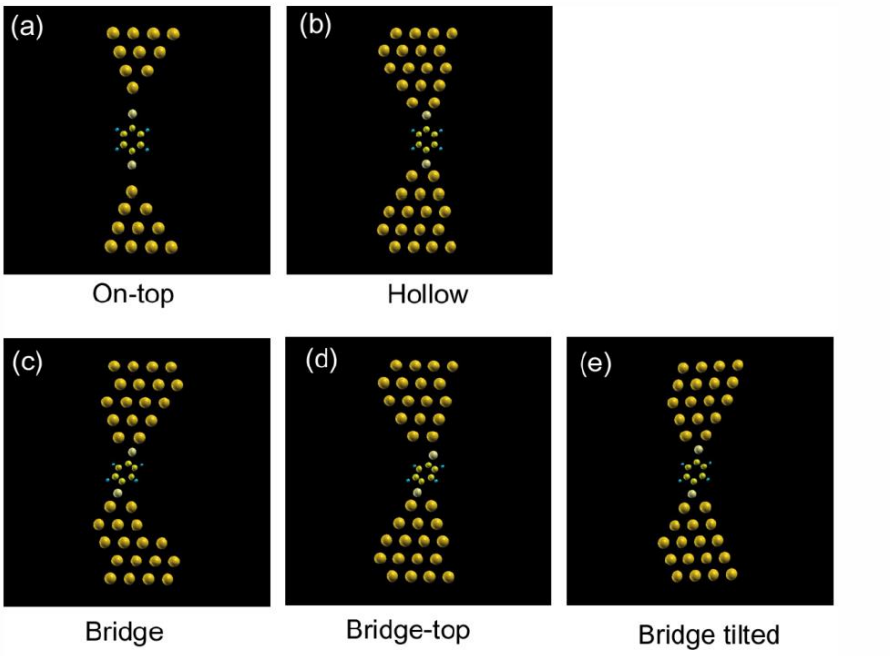

Fig.4-23 Structural models of (a) on-top, (b) hollow, (c) bridge, (d) bridge-top, and (e) bridge tilted configurations used for the DFT-transport calculations. Blue, yellow, pale yellow, and orange balls correspond to H, C, S, and Au atoms, respectively.

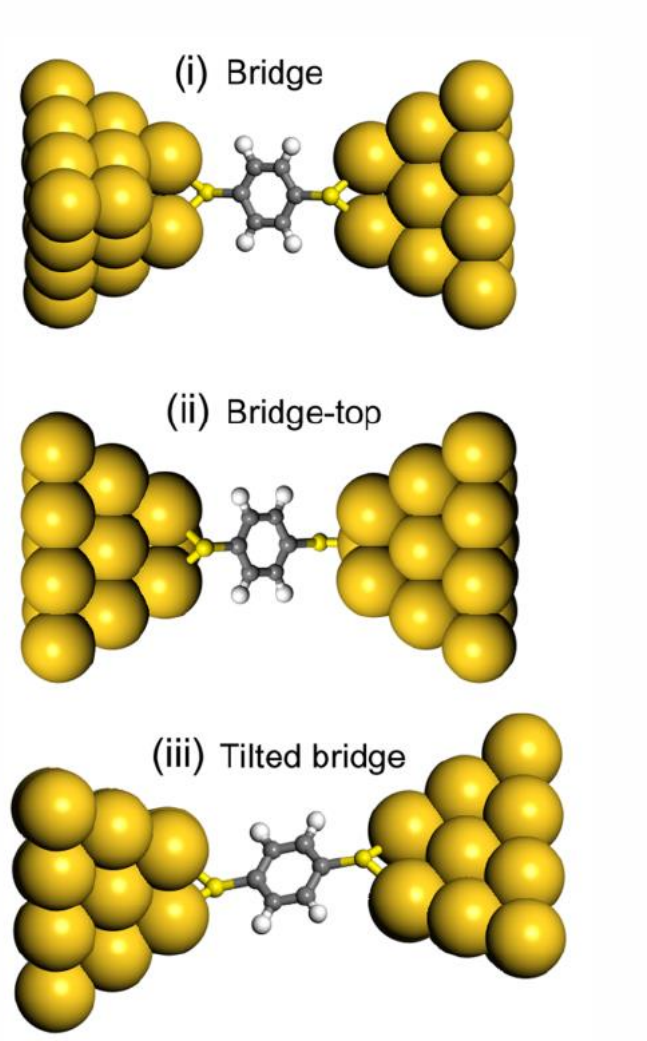

Fig.4-24 Schematic illustration of the bridge type configurations of the BDT molecular junctions; (i) bridge, (ii) bridge-top, and (iii) tilted bridge. White, grey, yellow, and orange balls represent H, C, S, and Au atoms.

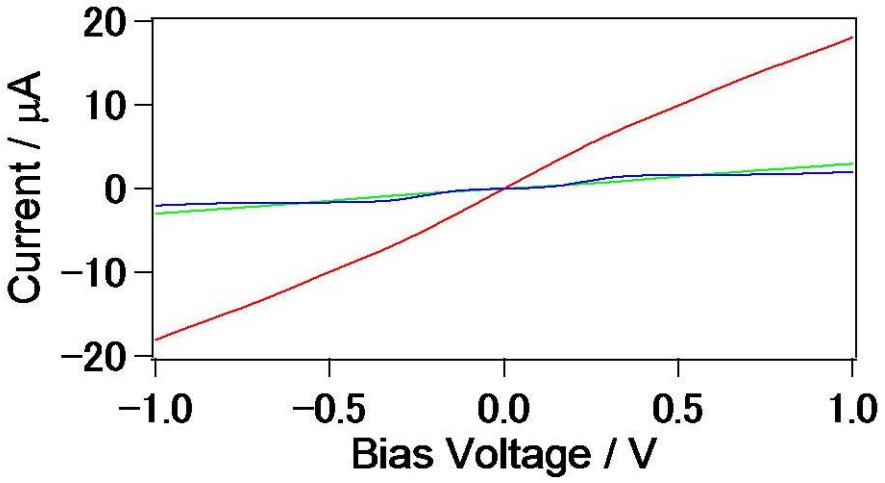

Fig.4-25 Theoretical *I-V* curves of BDT junctions for the bridge, hollow, and on-top adsorption-configurations, which are represented by red, green, and blue lines, respectively.

4.4. Conclusions

In this chapter, I investigate the *I-V* characteristics of BDA, C4DA, bipyridine, and BDT single-molecule junctions. The electronic structures are determined by fitting observed *I-V* curves with Breit-Wigner transmission model. Their *I-V* characteristics has good agreement with conduction feature reported previously. Although BDA displays single narrow distribution in the *I-V* histogram, BDT varies three distributions caused by contact geometries. I assigned the contact configuration by comparison with theoretical calculation. The structures were determined as bridge, hollow, on-top for high, medium, low conductance states.

5. Thermopower measurements of single-molecule junctions

It is insufficient only with single-molecular conductance in order to determine the electronic structure of a single molecule junction. Measurements the electronic structure of a single molecule junction improve reliability of determining the electronic structure of a single molecule junction.

In the previous chapter, the junction structure was determined by comparing the calculated energy difference between the main conduction orbital and the gold electrodes, and the coupling with DFT calculation results. The conduction orbital used for comparing the theoretical calculations is HOMO. However, *I-V* measurements do not inform any experimental evidence that the conduction orbital is HOMO. In this chapter, thermopower measurement of single-molecule junction is carried out to determine the electronic structure of a single molecule junction. I performed the experiment of thermopower measurement with an aim of establishment of the electronic state measurement method of a single molecule junction.

In the experiment, the thermoelectric voltage of BDT single-molecule junction and bipyridine single-molecule junction investigated previous chapter was measured. Their main conduction orbitals were determined. The conduction orbital of single molecule junction was determined to be HOMO for BDT, and LUMO for bipyridine.

5.1. Introduction

In the previous chapter, the energy difference and the coupling between the main conduction orbital and the gold electrode were determined by measuring the *I-V* characteristic. However, it is insufficient to measure only *I-V* characteristics to determine the electronic structure completely. This is because *I-V* measurement does not clarify main conduction orbital of a single molecule junction, that is, the career transport via HOMO or LUMO. When HOMO is main conduction orbital, the career is a hole. In case that it is LUMO, the career is electron. Holes and electrons conduct in the same way and exhibit the indistinguishable *I-V* characteristics if the energy difference from coupling conduction orbital and Fermi level and coupling are same. Poulsen and Datta proposed theoretically that thermopower measurements can identify the conduction orbital[73]. The electronic structure of the single molecule junction can be determined by combining the *I-V* characteristic measurements and the thermopower measurement[72, 74, 68].

The current of a single molecule junction with temperature difference is represented by the Eq.52

$$I = \frac{2e}{h}\int \mathrm{d}E\left\{\tau(E)\left(f_{\mathrm{Hot}}(E) - f_{\mathrm{Cold}}(E)\right)\right\}. \tag{52}$$

Consider the case where there is a temperature difference between both electrodes. The Fermi-Dirac distribution function of the electrode shows a slight temperature dependency. Therefore, an effective bias voltage is applied to the single-molecule junction. The voltage which the current becomes 0 is expressed by the Eq.53

$$\begin{aligned}\Delta V &= \frac{\pi^2 k_{\mathrm{B}}^2 T}{3e}\frac{\partial \ln\tau(E)}{\partial E}\bigg|_{E=E_{\mathrm{F}}} \Delta T, \\ &= -S\Delta T.\end{aligned} \tag{53}$$

In Eq.53, thermoelectric voltage is proportional with energy differential of logarithm of transmission at Fermi level. When conduction orbital is below Fermi level of electrode, the energy differential of transmission is negative value. the orbital is larger than Fermi level, the energy differential is positive. This is a principle of determination of conduction orbital with a thermopower measurement.

Experimentally, thermopower of molecular junction is reported by Reddy *et al.*[74]. They measured the bias voltage with temperature difference during forming molecular junction with voltage amplifier. They used STM to form junction. The thermopower of single-molecule

junction have been measured by several groups using with STM and MCBJ[75-80]. Other method to measure thermoelectric voltage is observing current shift with temperature difference as reported Ref.[72, 75] . Much attention has paid to thermopower measurements. one of the purpose of thermopower measurements of single-molecule junction is determination of electronic structures[74, 78, 81, 82]. Thermopower of single-molecule junction is also investigated for large thermopower[83]. For instance, one-dimensional materials show van Hove singularity[84, 85]. Considering Eq.52, thermoelectric voltage diverge in a characteristic system of single-molecule junction, large thermoelectric voltage is expected. Figure of merit of single-molecule junctions has not been measured yet because of difficulty of measurement small heat quantities through molecular junction. Recently, heat transport in nanoscale have been also measured[86, 87]. Thermopower measurement of molecular junction is important for electronic structures measurement and developing of thermoelectric devices.

In this chapter, I investigated the conduction orbital of single-molecule junction of BDT, bipyridine by using with thermopower measurements. The electronic structures of single-molecule junctions were determined completely with *I-V* measurements and thermopower measurements.

5.2. Experimental

5.2.1. Sample preparation

The substrate and tip were prepared as described in Chapter 4.

5.2.2. Thermopower measurement

Thermopower measurements were performed with the setup in Fig.5-1. In this setup, the temperature of the Au substrate is controllable with Peltier module. Glass plate was inserted between Peltier module and STM sample stage to prevent from heating or cooling of sample stage. The temperature of Au substrate and room temperature is monitored with Pt 1000 thermometer mounted on the substrate. The temperature of Au substrate keep constant under PID control of temperature controller. Considering the temperature of tip is room temperature, temperature difference of two electrodes was defined as temperature difference between the temperature of Au substrate and room temperature. The experiments were performed with the temperature difference from -6 K to 20 K. Here, positive temperature difference means substrate heating.

Thermopower was obtained from *I-V* dependence in small bias voltage range between ±1 mV with the condition that Au substrate is heating or cooling. *I-V* was record by same method mentioned in Chapter 4. High resolution DAQ (NI-4461) was used instead of NI USB-6363 to observe small bias voltage shifts.

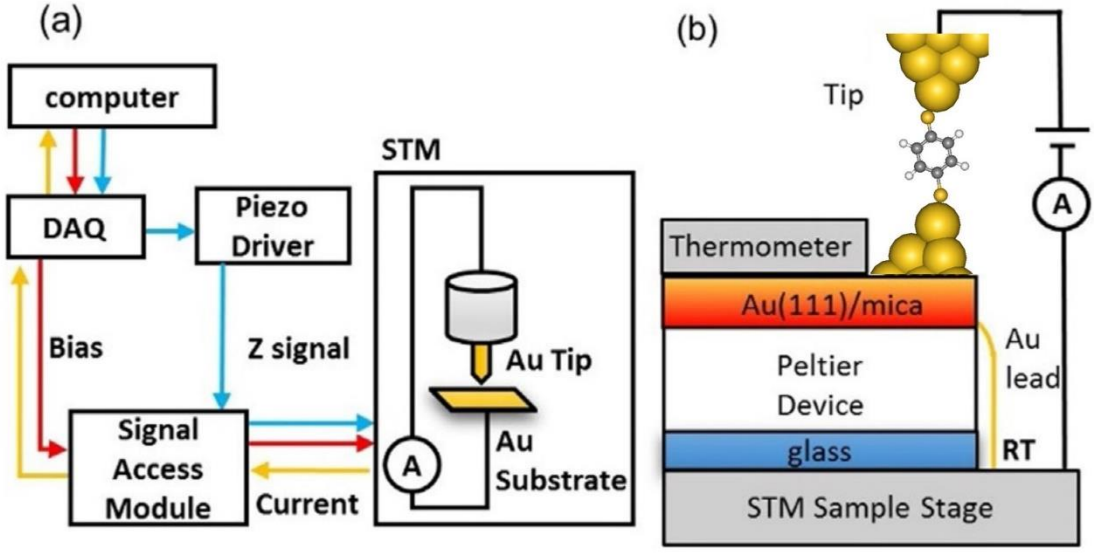

Fig.5-1. The setup of thermopower measurement on molecular junctions with STM-BJ. (a) Experimental setup for the combined *I-V* and thermoelectric measurements for the single-molecule junction. (b) Schematic illustration of the experimental setup for the thermoelectric measurement.

5.3. Results and Discussion

5.3.1. Thermopower measurement of BDT junctions

Example of *I-V* curves measured in range between ±1mV are shown in Fig.5-2. Black and red points show *I-V* characteristics measured under ΔT = 0 and 20 K, respectively. The two lines in Fig.5-2 means linear fit of data points. The bias voltage point which current is 0 is defined as voltage offset. The voltage offset of red line measured under ΔT = 20 K shows negative shift from black line without temperature difference. This voltage shift means thermoelectric voltage caused by temperature gradient in the circuit.

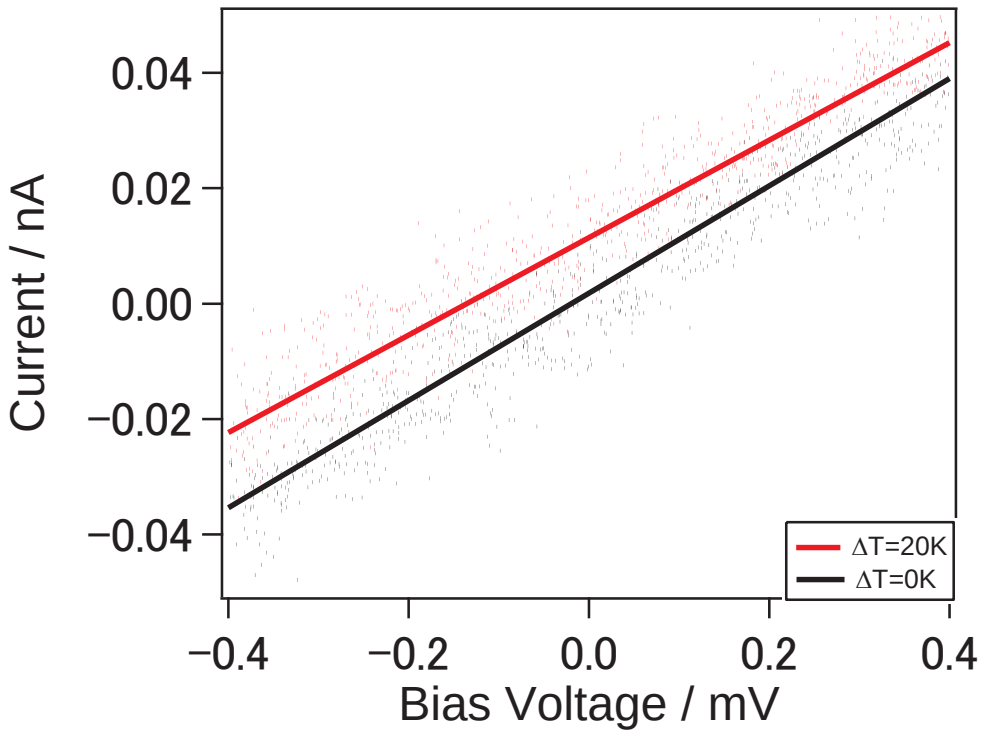

Fig.5-2 Example of the *I*-*V* characteristics of the BDT single-molecule junction at a temperature difference of (red) 20 K and (black) 0K.

It is uncertain to determine thermopower by comparing only one *I*-*V* curve. Fig5-3. represents the histograms of the voltage offset at each temperature to statistically calculate the thermoelectric voltage. From the Fig.5-3, it is confirmed that the voltage offset is shifted in the negative direction. This bias voltage shift is inferred that the thermoelectric voltage is generated. It suggests that the charge transports via HOMO of BDT single-molecule junctions. In the Fig.5-3, the width of histogram of the voltage offset under ΔT = 20 K is the largest. The broadening indicates the structural changes of molecular junction occur more frequently due to heating up of the junction or the larger temperature difference between the two electrodes.

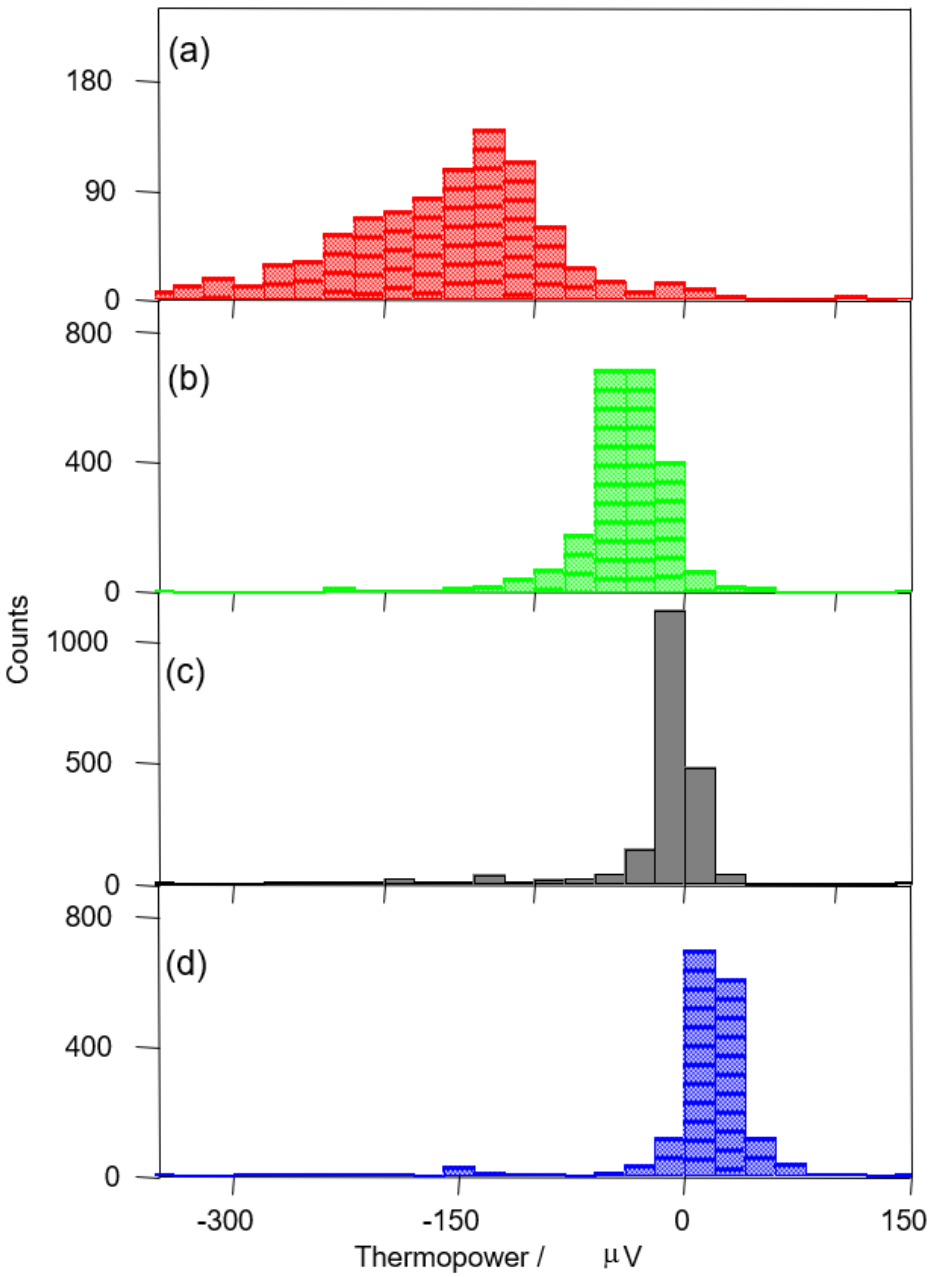

Fig.5-3 Distribution of the thermoelectric voltage of the BDT single-molecule junction at temperature differences of (a) +20 K (b) 10 K, (c) 0 K, and (d)-6 K. The STM tip was kept at ambient temperature. Thermoelectric voltage is defined as voltage offset.

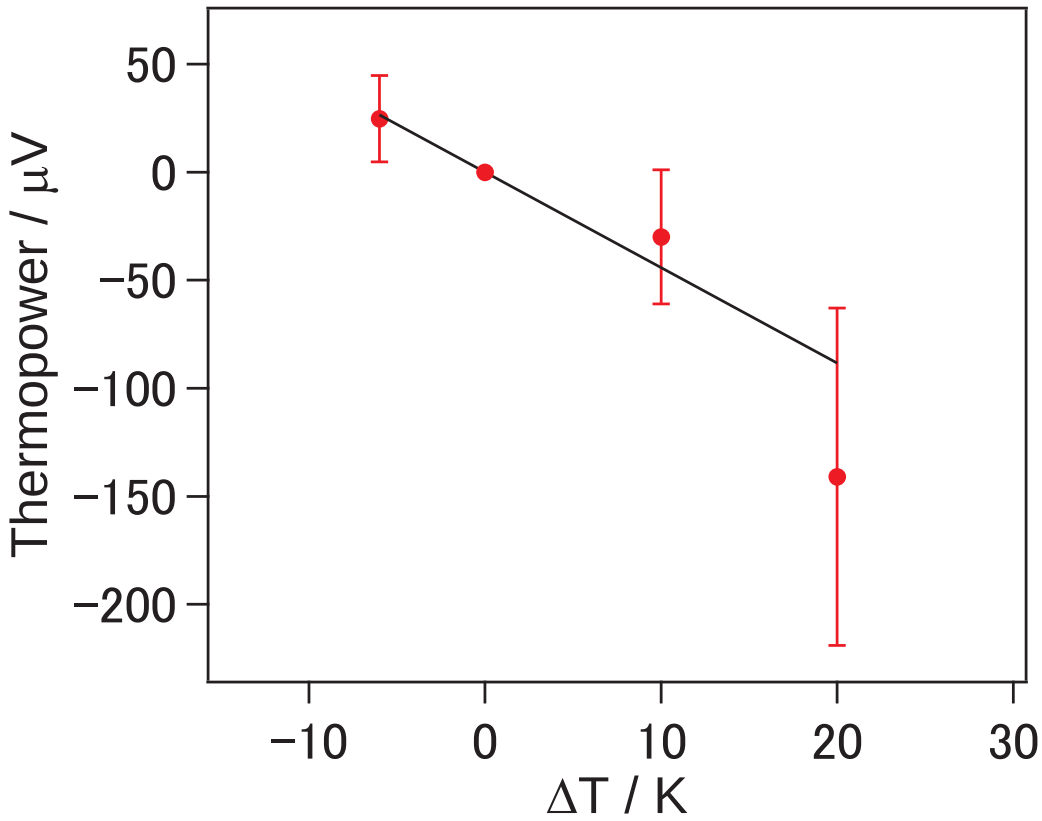

Fig.5-4 Plot of the peak values of thermoelectric voltage in the histograms as a function of the temperature difference of BDT single-molecule junction.

Seebeck coefficient were determined to evaluate thermopower quantitatively. Voltage offset are determined at each temperature difference from gaussian fitting of each histogram. Voltage offset dependence of temperature offset are plotted in Fig.5-4 . The slope of the line in Fig.5-4 . means Seebeck coefficient of the whole of the circuit. The slope of the line in Fig.5-4 is -4.4μV/K. Thermoelectric voltage caused by temperature difference. Observed thermoelectric voltage of the circuit is described as Eq.54 .

$$\Delta V = (S_{mol} - S_{Au})\Delta T \tag{54}$$

Seebeck coefficient of lead caused in Au lead from molecular junction to an amplifier of STM. This Seebeck coefficient is assumed to equal with bulk gold. Seebeck coefficient is determined by subtracting Seebeck coefficient of bulk gold from Seebeck coefficient of the circuit. Seebeck coefficient of BDT single-molecule junctions is 2.5 μV/K. This value is smaller than previous reported Seebeck coefficient of BDT junctions[74]. This difference is should be due

to overheating of tip. Seebeck coefficient of BDT junction is positive. The signature of Seebeck coefficient corresponds with signature of charge carrier. Main carrier through BDT junction is hole. Thermopower measurement reveals that conduction orbital of BDT single-molecule junction is HOMO. The HOMO level from theoretical calculation is compared with electronic structure determined by experiment in previous chapter. It agrees with the results of thermopower measurement. Combined the *I-V* measurements and thermopower measurements, I revealed the electronic structures of BDT single-molecule junctions as shown in Fig.5-5.

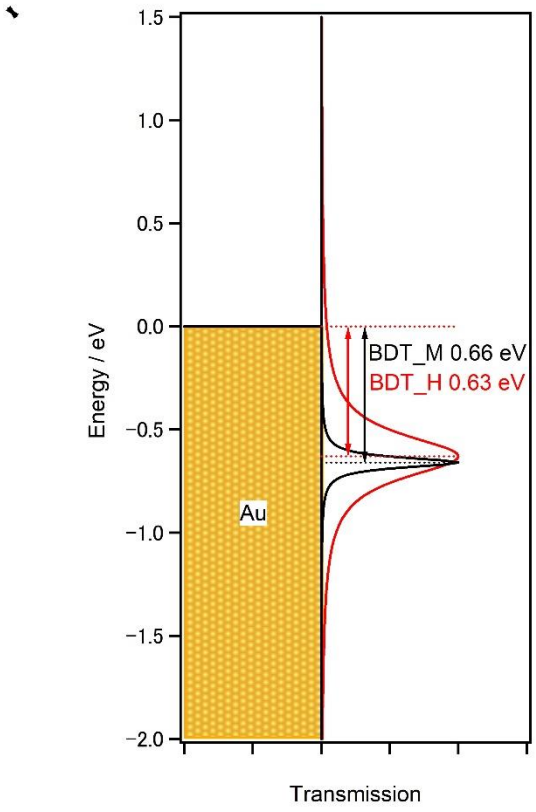

Fig.5-5 Energy level diagram of the (red) H and (black) M states of the BDT single-molecule junctions.

5.3.2. Thermopower measurement of bipyridine

Thermopower measurement of bipyridine junction also were performed. Voltage offset histograms are shown in Fig.5-6. In Contrast to BDT junctions, positive shift of voltage offset with temperature increase was observed. Thermoelectric voltage of bipyridine is plotted in

Fig.5-7. From the slope in Fig.5-7, Seebeck coefficient of bipyridine junction is determined to be -4.9 μV/K. Hence, conduction orbital of bipyridine is LUMO. This result agrees with previous report[72]. The signature of Seebeck coefficient is different from BDT. Results of bipyridine insure the validity of thermopower measurement[72].

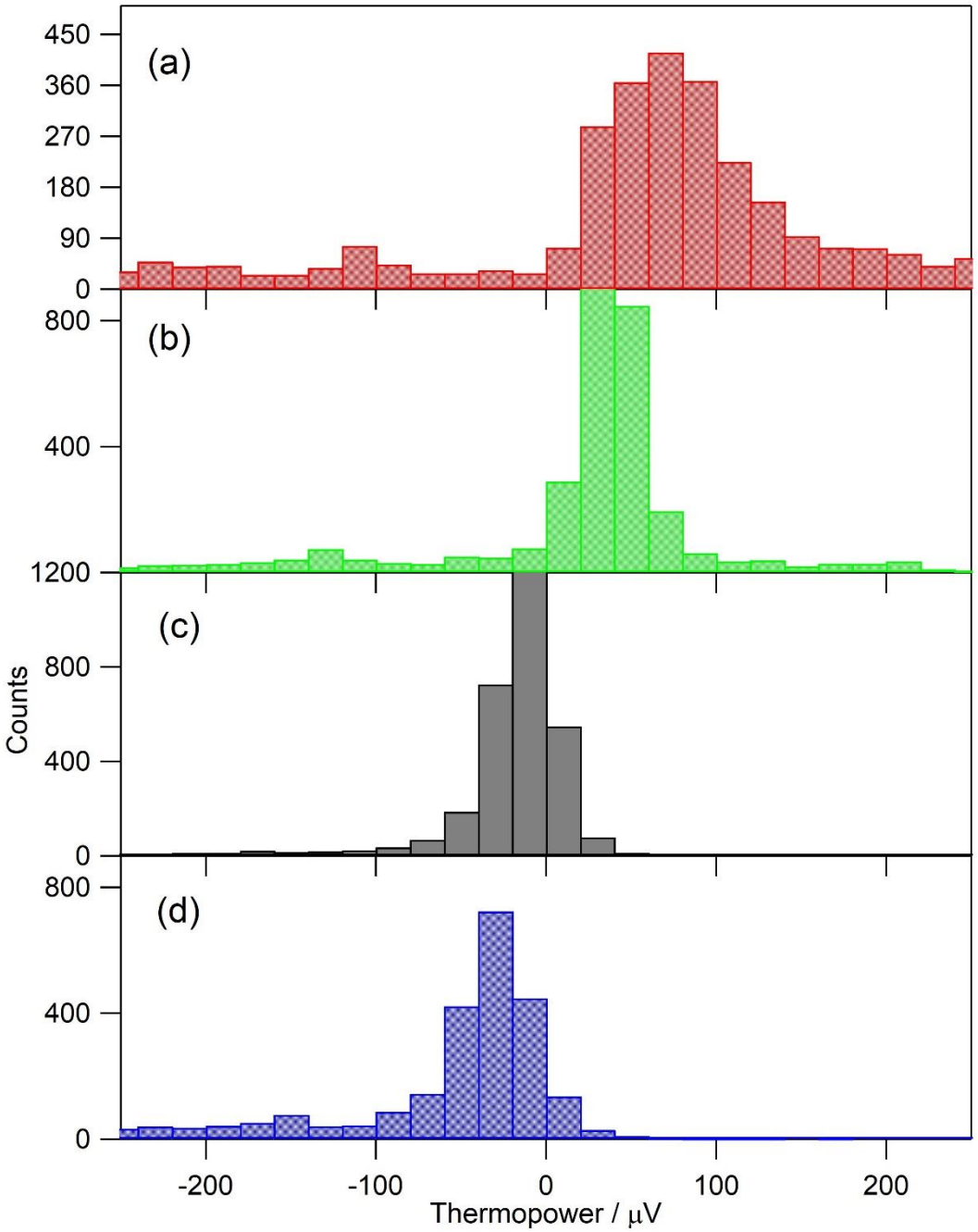

Fig.5-6 Distribution of the thermoelectric voltage of the bipyridine of molecular junctions at temperature differences of (a) +20 K (b) 10 K, (c) 0 K, and (d)-5 K. The STM tip was kept at ambient temperature.

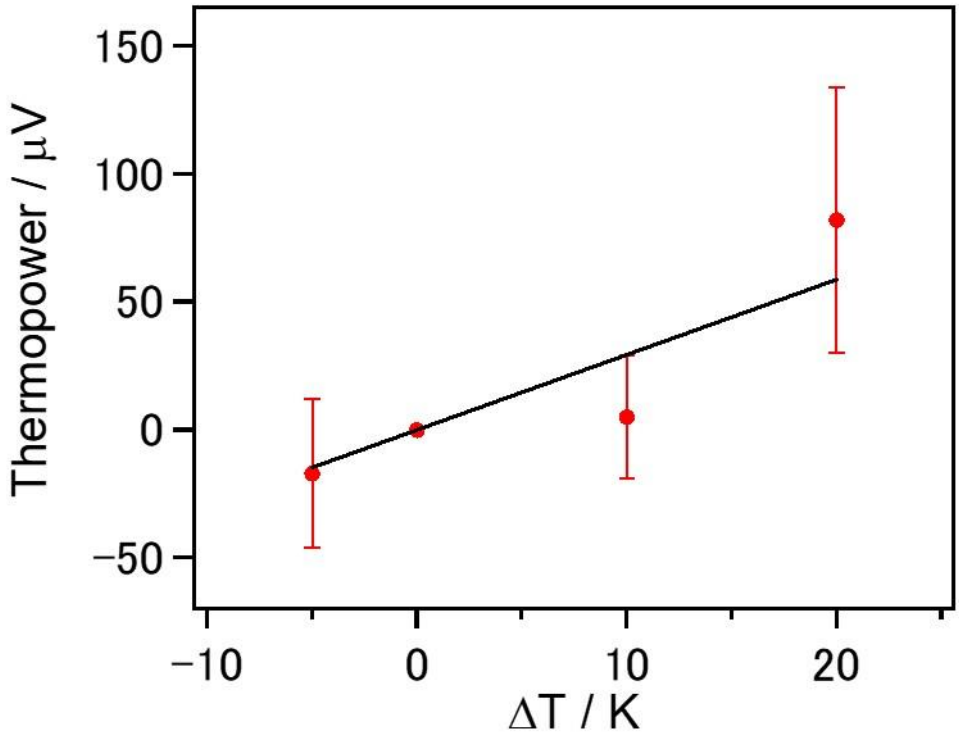

Fig.5-7 Plot of the peak values of thermoelectric voltage in the histograms as a function of the temperature difference of bipyridine molecular junction.

5.3.3. Comparison with *I-V* measurements

Both of *I-V* measurements and thermopower measurements are methods to measure electronic structure, transmission of single-molecule junctions. It is expected that common electronic structure is observed from thermopower and *I-V* measurements of same molecular junction. In *I-V* measurement in previous chapter, three different conduction structures were observed. Whereas, only single distribution of voltage offsets was observed in thermopower measurement. Voltage offset histogram for high conductance state and medium conductance state are shown in Fig.5-8 and Fig.5-9, respectively. Voltage offsets of both state are plotted in Fig.5-10. From Fig.5-10, Seebeck coefficients of BDT junctions do not exhibit significant difference between conductance states. Apparently, observed single distribution of thermoelectric voltage is inconsistent with *I-V* measurements.

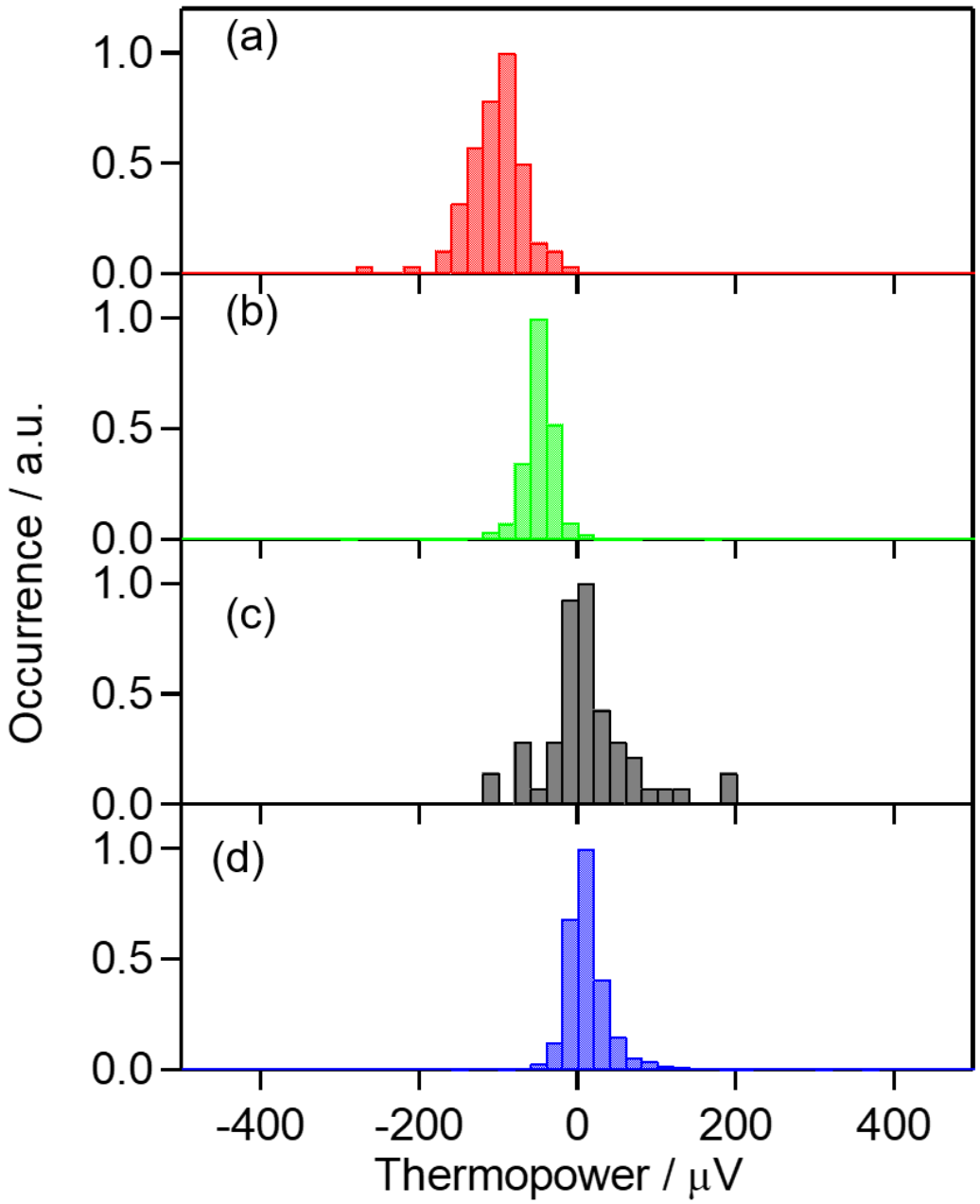

Fig.5-8 Distribution of the thermoelectric voltage of the BDT High conductance state at temperature differences of (a) +20 K (b) 10 K, (c) 0 K, and (d)-6 K. The conductance range is determined *I-V* measurement in Chapter 4.

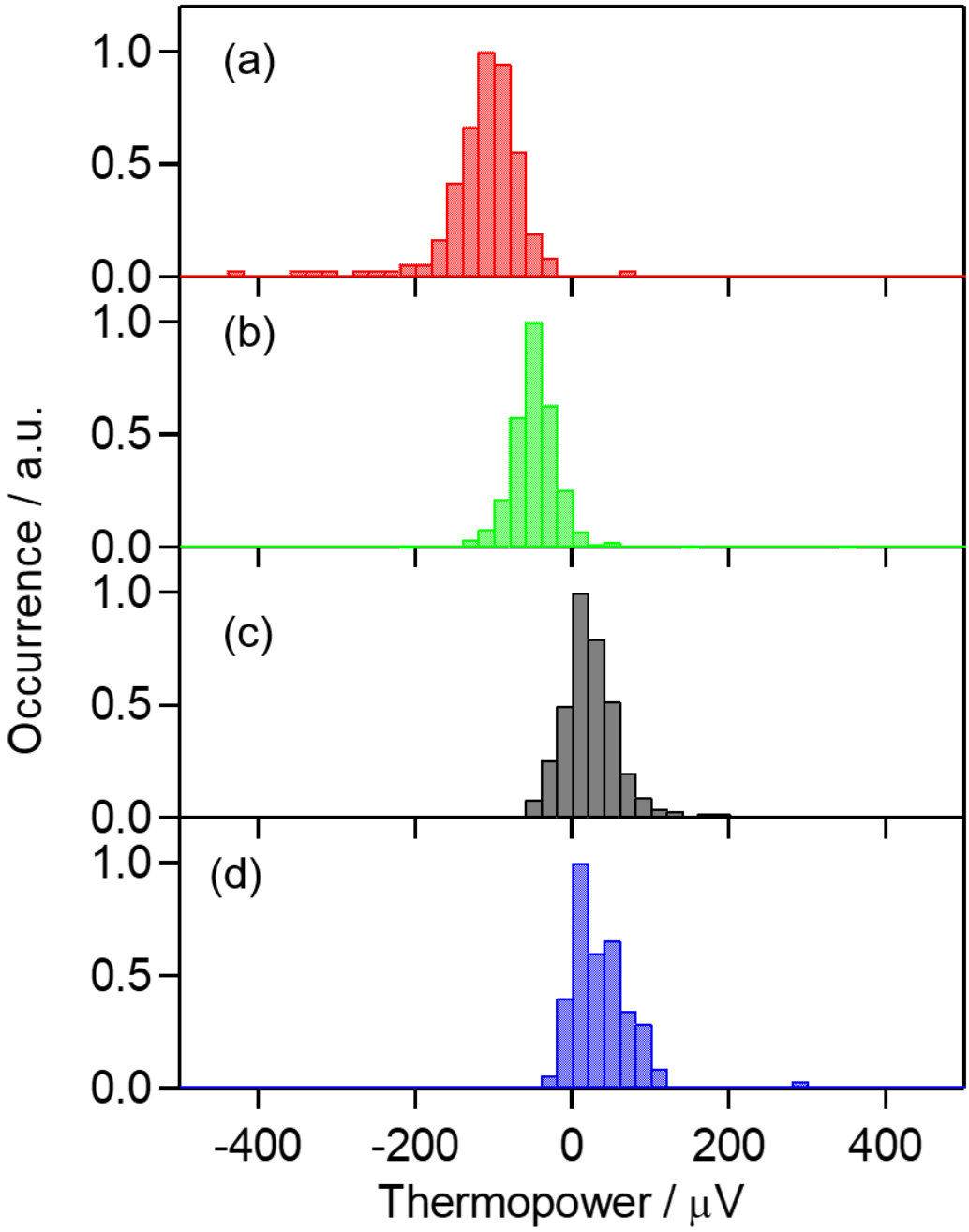

Fig.5-9 Distribution of the thermoelectric voltage of the BDT Medium conductance state at temperature differences of (a) +20 K (b) 10 K, (c) 0 K, and (d)-6 K. The conductance range is determined *I-V* measurement in Chapter 4.

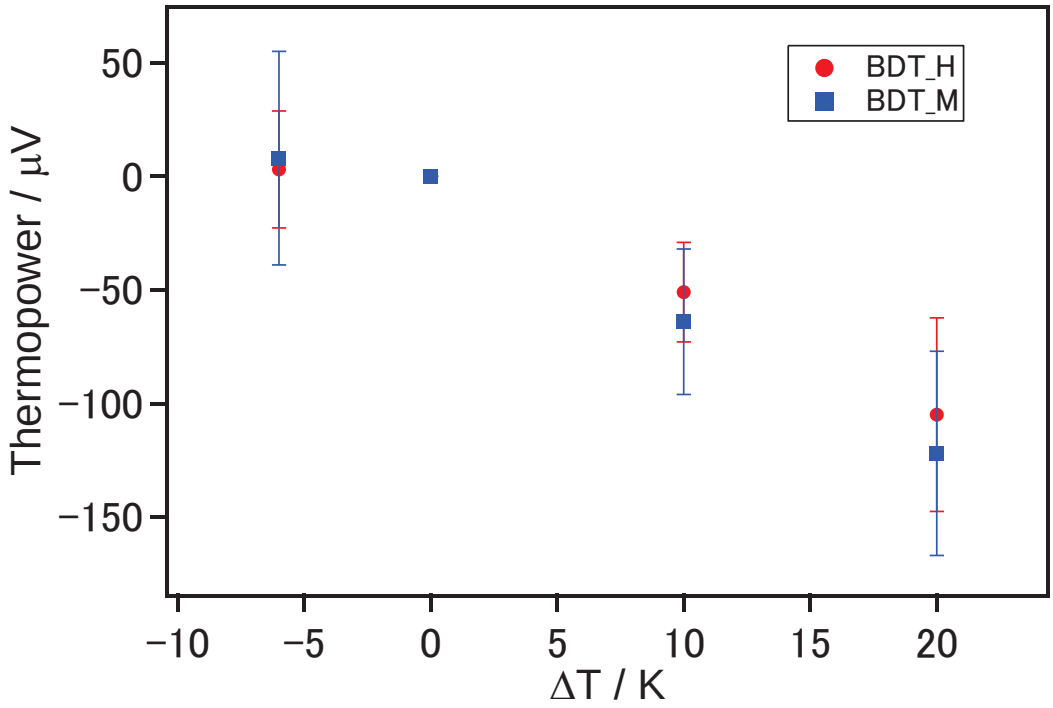

Fig.5-10 Plot of the peak values of thermoelectric voltage in the histograms as a function of the temperature difference of High and Medium states of BDT single-molecule junctions.

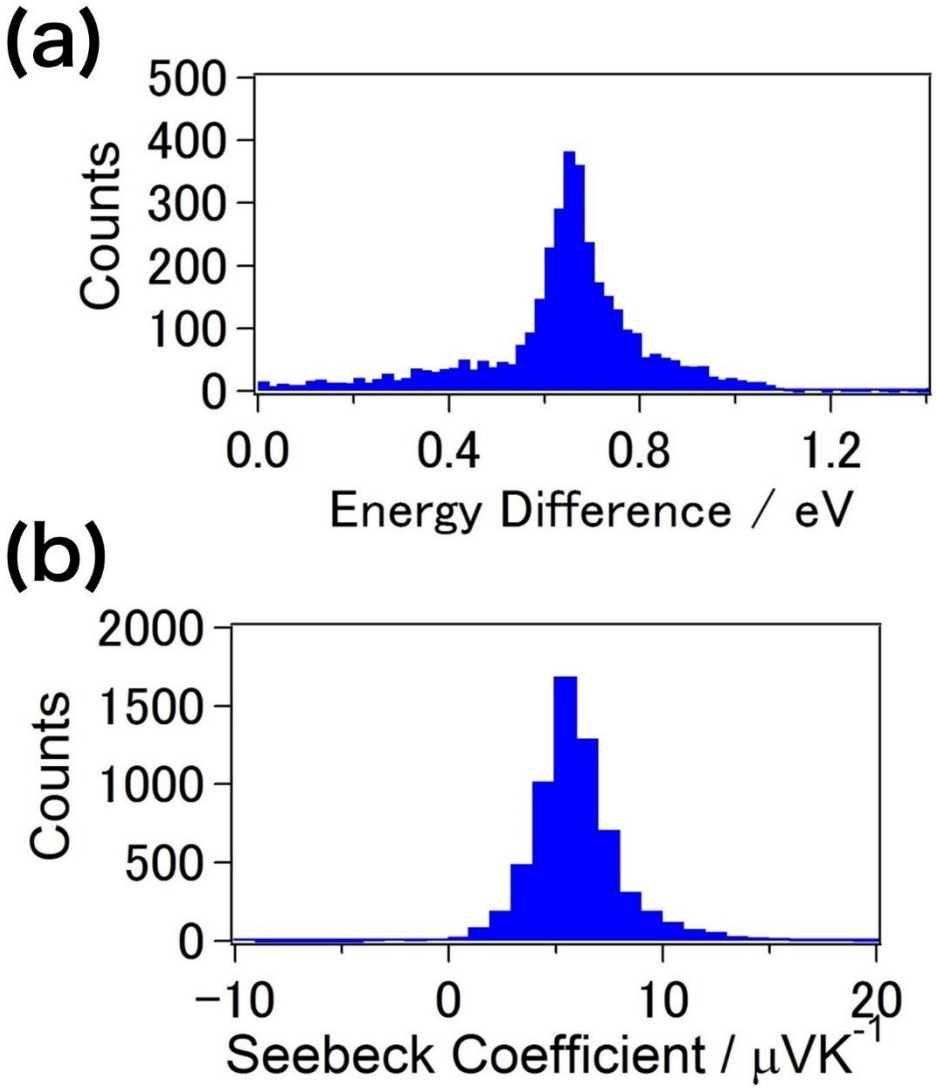

Fig.5-11 Comparison between energy difference and Seebeck coefficient of Au-BDT junctions. (a) Histogram of energy difference of conduction level. Energy difference is determined by fitting of *I-V* curves with Breit-Wigner model. *I-V* curves are measured in Chapter 4. (b) Histogram of Seebeck coefficient. Seebeck coefficient is defined by dividing voltage offset by temperature difference for each *I-V* curve in range ±1 mV.

Adopting Breit-Wigner model as transmission[55], Seebeck coefficient of single-molecule junctions are described as Eq.55 .

$$S = \frac{\pi^2 k_B^2 T}{3e} \frac{2\varepsilon_0}{{\varepsilon_0}^2 + \Gamma^2} \tag{55}$$

where the couplings of two electrode is assumed to be equal. From the results of *I-V* measurements, energy difference is approximately 0.7 eV for both state. The couplings differed

significantly between two states. The coupling is approximately 0.1 eV for high state. Hence, coupling difference, that is the difference of two conductance state influenced only 2% to Seebeck coefficient from Eq.55., the fluctuation of structure of single-molecule junction is inevitable in this thermopower measurement. Slightly change of Seebeck coefficient is not measurable. Single distribution of thermoelectric voltage is interpreted by the results of *I-V* measurements. Fig.5-11 represents the histograms of Seebeck coefficients of BDT junctions and energy difference between conduction orbital and Au Fermi level obtained from fitting of individual *I-V* curves. Seebeck coefficient is almost proportional with energy difference when $\varepsilon_0^2 >> \Gamma^2$. The shape of these two distributions is similar. This similarity support that Seebeck coefficient mainly depends on energy differenece.

By using of Eq.55., absolute value of Seebeck coefficient is determined based on the coupling and energy difference measured with *I-V* characteristics. Seebeck coefficient expected from *I-V* measurement is 20 μv/K for BDT and 15 μV/K for bipyridine. Experimental Seebeck coefficient is different from $S_{I\text{-}V}$. The difference between measured and estimated Seebeck coefficient can be explained by the effective temperature affected by heating of tip from substrate. Previous research reported that the temperature difference was 0.34 times smaller of setting temperature by AFM-based nanoscale thermometer[88]. In this study, the effective temperature difference is estimated with Eq.56.

$$\Delta T_{\mathrm{eff}} = c\Delta T_{\mathrm{set}}. \tag{56}$$

c is estimated approximately 0.1 for BDT and 0.3 for bipyridine. Setting temperature difference is estimated with the assumption that the difference between observed and estimated Seebeck coefficient caused by overestimating of temperature difference. Thus, the results of thermopower measurements were interpreted consistently with *I-V* measurements.

5.4. Conclusions

The thermopower of BDT and bipyridine molecular junction have been investigated. Thermopower measurements reveals that conduction orbital of BDT and bipyridine molecular junction is HOMO and LUMO, respectively. The electronic structures of single molecular junction were determined by combining *I-V* measurements and thermopower measurements. The validity of the thermopower measurements were insured by agreement with *I-V* measurements.

6. Investigation of electronic structure of highly conductive single-molecule junctions via direct π-bonding

In this section, I discuss the *I-V* characteristics of highly conductive molecular junctions directly bonding to electrodes by π-conjugated electron systems. In the previous chapters, I described that the method based on *I-V* characteristic measurements and thermopower measurements to statistically analyze electronic structure of a single-molecule junctions was established.

In order to utilize a single molecular junction as molecular device, it is necessary to form a molecular junction having high conductance. In this chapter, *I-V* measurement was applied to a mesitylene single-molecule junction with high single molecule conductance to investigate the origin of high conductance. *I-V* measurements clarified that mesitylene single-molecule junctions has larger coupling than molecular junctions having typical anchor group such as BDT and BDA. It is concluded that the high conductive characteristics of the molecular junction with the bonding by the π conjugate plane is derived from the coupling.

6.1. Introduction

One of problems in applying molecular junctions as devices is low conductance of molecular junctions. High conductance is desirable for use as device. However, the conductance of the molecular junction of the benzene derivative having two anchor groups, which are benzene backbone is very simple, is at most about 0.01 G_0. As described above, single-molecule conductance is ~ 0.01 G_0 for BDA, and - 0.03 G_0 for BDT[37, 41]. There are some trials of selection of molecular backbone to realize high conductance. Molecular systems that introduce metal ions into the backbone and reduce conductance decreasing with distance have been performed to realize high conductance. However, the conductance of single molecule junctions is not only due to backbone. As written in previous chapters, the way molecules are bonded to the electrode greatly affects the conductance of the molecular junctions[41].

Molecular junctions with bonds via π-conjugated systems have high conductance[89-94]. The direct π-binding technique has been applied for various systems such as benzene derivatives[92, 94], C_{60}[95, 96], ethylene[97] , and pyrazine[90, 98]. Benzene single-molecule junctions without anchoring groups have higher conductance of 0.1 G_0[92]. The origin of high conductance of benzene is considered that the π conjugate plane is directly bonded to the metal electrodes. Pyrazine single-molecule junction has two ways to form the junctions with a conjugate plane or with lone pair of nitrogen atoms[90, 98]. It is known that pyrazine single-molecule junction exhibits high conductance as the distance between two electrodes decreases. When the distance between the electrodes is small, the conductance is 0.3 G_0, and the conductance when it is large is approximately 1.0 G_0[98]. This is because if the distance between the electrodes is large, single-molecule junctions are formed by coordination bonding of nitrogen atoms. The distance between the electrodes is getting smaller, pyrazine is considered to be bonded by a π conjugate plane. These examples show that conductance increases when directly bonded by a π conjugate plane in a single-molecule junction. However, the origin of large conductance when bonded on the π conjugate plane has not been clarified.

Asfari *et al.* reported that mesitylene single molecular junction were formed with STM-BJ, and the mesitylene single-molecule junction exhibits high conductance[89]. It is considered that the high conductance of mesitylene single molecular junction is originated in bonding with the electrodes by a π conjugate plane like benzene-Pt junctions[92]. Therefore, I choose the mesitylene single molecule junction as a system having a direct bond by a π conjugate plane to measure its electronic structure in the ambient condition with STM. The origin of high

conductance of the molecular junction bonded to the electrode by the π conjugate electron system were investigated.

6.2. Experimental

6.2.1. Conductance measurements and *I-V* measurements

Conductance measurements were performed with STM-BJ. The setup was STM (Nanoscope V, Bruker, Santa Barbara, CA) with DAQ (National Instruments, USB-6363). Au(111) / mica substrate was used for the measurements. The substrate was fixed in a Teflon liquid cell with Viton O-ring after flame annealing. The STM-BJ experiments were performed in mesitylene solution. STM-BJ experiments were performed as reported previously. The *I-V* measurements were performed as described in Chapter 4.

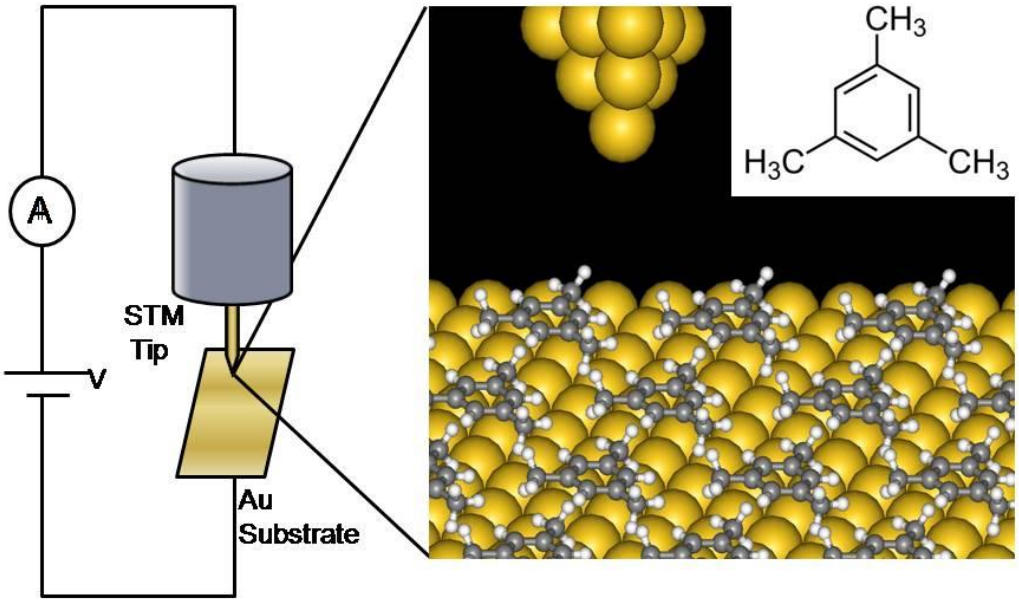

Fig.6-1 Schematic view of this measurement. Inset shows molecular structure of mesitylene.

6.3. Results and Discussion

6.3.1. Conductance measurements

STM-BJ methods were used for investigation of conductance and electronic structure of single-molecule junction of mesitylene[99]. In previous report, it is reported that mesitylene single-molecule junction has conductance of 0.1 G_0[89]. First, I performed STM-BJ conductance measurements in liquid condition to reproduce single-molecule conductance of mesitylene junctions. Fig.6-2 shows examples of the conductance traces during stretching processes. Black lines are the conductance traces in the mesitylene and red lines are the conductance traces measured in the air. These conductance traces display at 1 G_0. These plateaus indicate a Au single atomic junction formed before breaking metallic junctions. In the conductance histograms (Fig.6-3), the significant peak appeared at 1 G_0 corresponding to plateau in the conductance traces. This peak means Au single atomic junctions formed statistically in rupture processes. Focused on the conductance range below 1 G_0, some conductance traces show plateaus at 0.1 G_0 and 0.03 G_0. The conductance histogram in mesitylene also shows peaks at 0.1 G_0 and 0.03 G_0. In blank case, no conductance plateaus in the conductance traces and no peaks in the histogram were observed. I observed two distinct high (H) and low (L) conductance states for mesitylene single-molecule junctions. The main peak at 0.1 G_0 in the histogram is corresponding to previous report. It is considered that this 0.1 G_0 is due to single-molecule junctions where π plane of mesitylene directly binds to Au electrodes to form the structure where molecular plane is perpendicular to Au electrodes. In generally, molecular conductance also appears at integer multiple of a single molecule conductance. In the histogram in Fig.6-3, a shoulder peak at the 0.2 G_0 is observed. This peak indicates formation of double molecule junction. It is a proof that the peak at 0.1 G_0 is due to single-molecule junctions. The peak at 0.03 G_0 is also observed. This peak also represents the single-molecule conductance of mesitylene. In previous report, this peak was not observed[89]. The peak of low state can be hidden in background tunneling currents because of its small frequency.

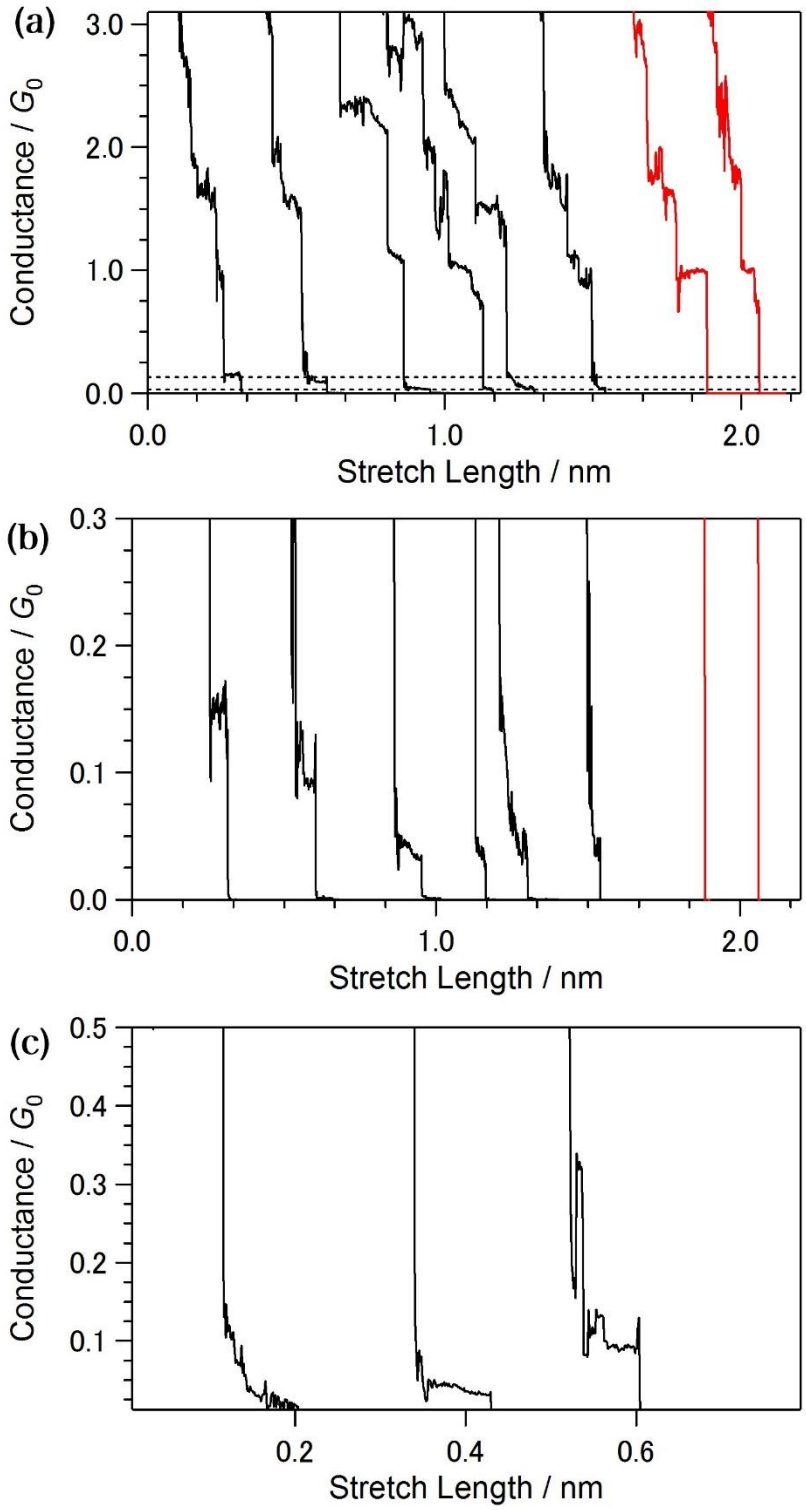

Fig.6-2 Typical conductance traces during STM-BJ rupture process with (black) and without (red) adding mesitylene solution. The bias voltage was set to 20 mV. Conductance windows are 0 – 3 G_0 for (a) and 0 – 0.3 G_0 for (b,c).

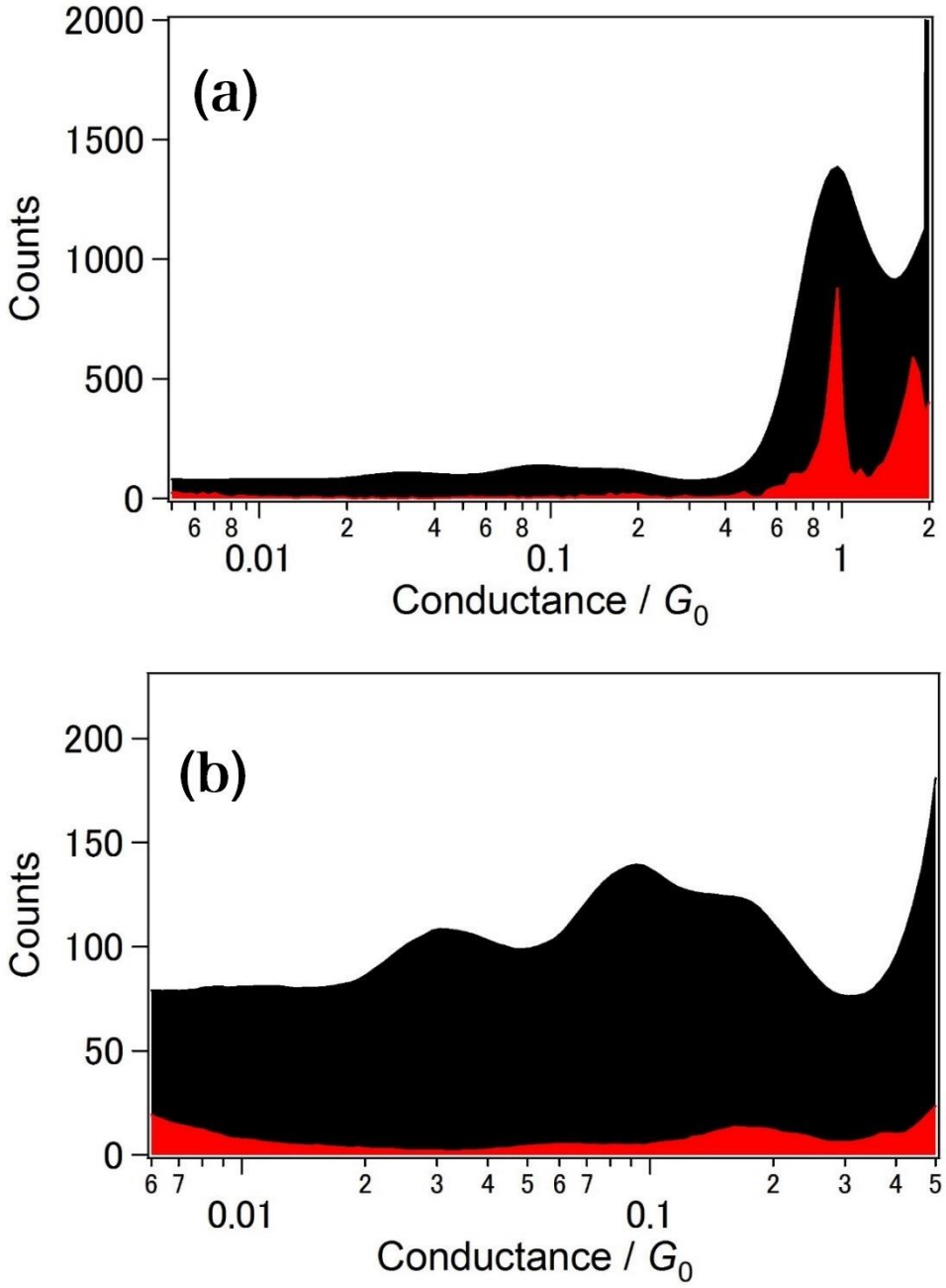

Fig.6-3 Semi-logarithmic conductance histograms during STM-BJ rupture process with (black) and without (red) adding mesitylene solution. The bias voltage was set to 20 mV. Histograms in (a) and (b) are constructed from a choice of 200 conductance traces. A bin size of $\Delta\log(G/G_0) = 0.02$ is used.

To estimate the gap distance between two Au electrodes during H state or L state

single-molecule junction forming, the electrodes stretch length in the conductance traces were analyzed. Fig.6-4 represents stretch length histograms for conductance plateaus of high and low conductance states. Here, the plateau length is defined as length of conductance plateau within the conductance range from 0.02 G_0 to 0.7 G_0 for the low-conductance state and from 0.07 G_0 to 0.7 G_0 for the high-conductance state. the origin of the length is defined as the point just after breakage of Au metallic junctions. Each length distribution was fitted with gaussian to determine effective gap distance of the state. the average length is 0.044 and 0.079 nm for H and L conductance states, respectively. This gap distance does not real distance of the single molecule junctions because the electrodes are retracted just after the breakage of Au atomic junctions. Typically, the gap which width is 0.4 nm is formed[100]. However, the stretch length indicates relative gap distance between two conductance states. The average gap distance of the high conductance state is shorter than the low conductance state. According to the stretch length, it is interpreted that the high conductance states are perpendicular structure and the low conductance state is due to tilted orientation of mesitylene junction.

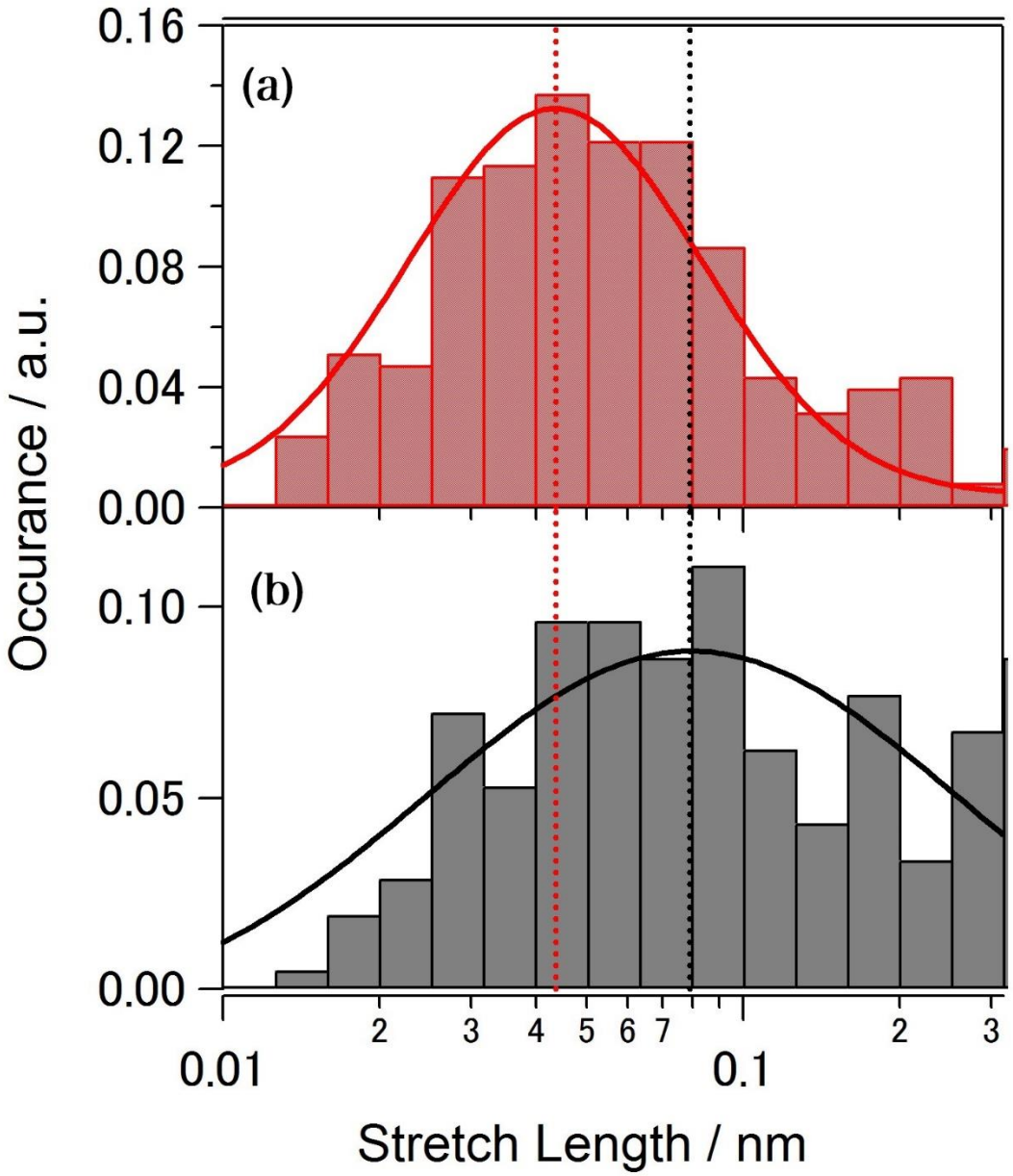

Fig.6-4 Stretch length histograms on a semi-log scale constructed from 2000 of all conductance traces taken at the bias voltage of 20 mV for (a) high and (b) low conductance states (For a detail see main text). The bin size is log (stretch length/nm) = 0.1. Solid curves are results of Gaussian fits. Peak center positions are indicated by dotted lines ((a) 0.044 nm and (b) 0.079 nm).

6.3.2. *I-V* measurements

I-V measurements were performed to investigate the electronic structure of single-molecule

junction of mesitylene. In previous report, the current bias voltage relationship of mesitylene junctions has been reported by single-molecule conductance with STM-BJ method at fixed bias voltages below 0.3 V. It has been reported that the single-molecule conductance is constant, the current increase linearly within the range below 0.3 V. In this study, I obtained *I-V* characteristics in wide range of ±1 V of mesitylene single-molecule junctions to determine the electronic structures. Fig.6-5 represents a typical *I-V* curves of mesitylene molecular junction for high conductance state and low conductance state, respectively. Typical *I-V* curves represents quasi-linear behavior in low bias voltage range as reported previously. In high bias voltage range, non-linear increase is observed due to changing of electron transport mechanism from non-resonant to resonant tunneling process. It is possible to determine electronic structure with fitting these non-linear *I-V* curves.

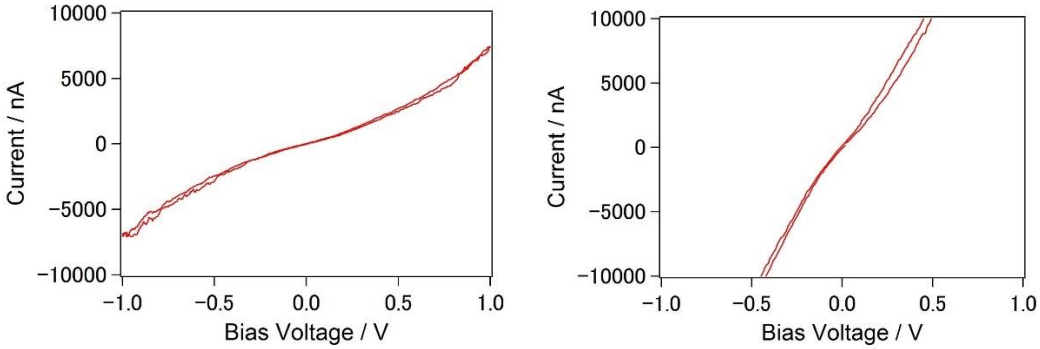

Fig.6-5 Typical *I-V* curves of the mesitylene molecular junctions .

To analyze statistically, 2D *I-V* characteristics histogram are shown in Fig.6-6. Two clear distributions appear in the 2D histogram. It agrees with the existence of two conductance states in the conductance measurements of STM-BJ at fixed bias voltage of 20 mV. I extracted averaged *I-V* characteristic for each state. The average *I-V* curves of high and low conductance state are defined average *I-V* curvet which current at 0.3 V is in range of above 2400 nA (above 0.1 G_0) and 700–1500 nA (0.03–0.065 G_0), respectively. The conductance windows are chosen to separate the *I-V* curve into two states with the two single-molecule conductance state observed in STM-BJ conductance measurement.

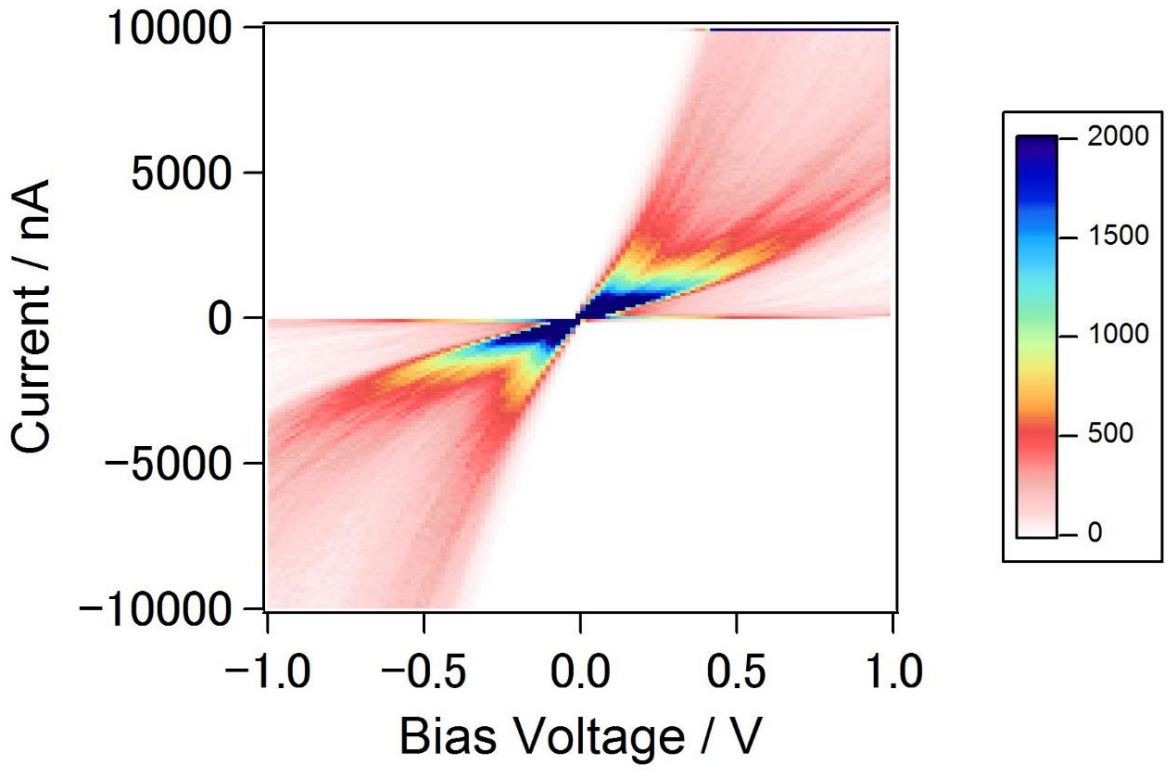

Fig.6-6 2D histogram of *I-V* curves of the mesitylene molecular junctions. The histogram is constituted from more than 1000 *I-V* curves. The bin size is 16 mV × 100 nA.

I adopted Breig-Wigner model (Eq.31) for electron transport through single-molecule junction[55]. Here, the current is described in Eq.43 with considering the number of bridging molecules. The parameter of electronic structure, energy alignment ε_0 and coupling Γ, are determined by fitting each averaged *I-V* curve with Eq.43. The fitting results are Γ_H = 0.15 eV, ε_{0_H} = 0.31 eV for the high conductance state using bias window ±0.4 V and Γ_L = 0.16 eV, ε_{0_L} = 0.72 eV for the low conductance state using bias window ±1.0 V (Γ_L = 0.10 eV, ε_0_L = 0.49 eV for the bias window ±0.4 V). Asymmetric factor of coupling α is 0.5 for both conductance state. To eliminate the possibility of the multiple molecule junction of high conductance state, the averaged *I-V* curve of high conductance curves are fitted with setting the number of molecule bridging *n*. The fitting results are Γ= 0.098 eV, ε_0 = 0.32 eV for *n* = 3, Γ = 0.076 eV, ε_0 = 0.37 eV for *n* = 4. the energy alignment ε_0 of high conductance state for *n* =3 or 4 are much less than ε_{0_L}. the mismatch represents that high conductance state cannot explained by multiple molecule junction. High conductance state is originated different orientation from low conductance state. It is able to distinguish to conductance state which has different electronic

structures with the *I-V* measurements. Compared to BDT junctions with the anchoring groups[68, 56], the coupling of mesitylene junction (Γ = 0.15 eV) is substantially larger than BDT (Γ is less than 0.13eV) and the conduction level of mesitylene junction is closer than BDT. Larger coupling supports the assumption that the mesitylene directly binds to Au electrode via π electron plane with a strong interaction.

6.3.3. Possible model of mesitylene junctions

In this subsection, I propose possibly model of mesitylene junctions for two conductance states observed in the experiment of conductance measurements and *I-V* measurements. In some conductance traces, the low conductance state appeared after the plateau of high conductance state appeared (Fig.6-2). The results of gap distance analysis (Fig.6-4) indicates the high conductance state has shorter gap distance than low conductance state. Proposed possible two structural model for each conductance state are shown in Fig.6-7 based on the experimental results. In high conductance state, the plane of mesitylene molecule is perpendicular to two metal electrodes direction as proposed previously. In low conductance state, tilted structured formed caused stretching after high conductance state appeared in analogy with benzene single-molecule junctions[89, 92].

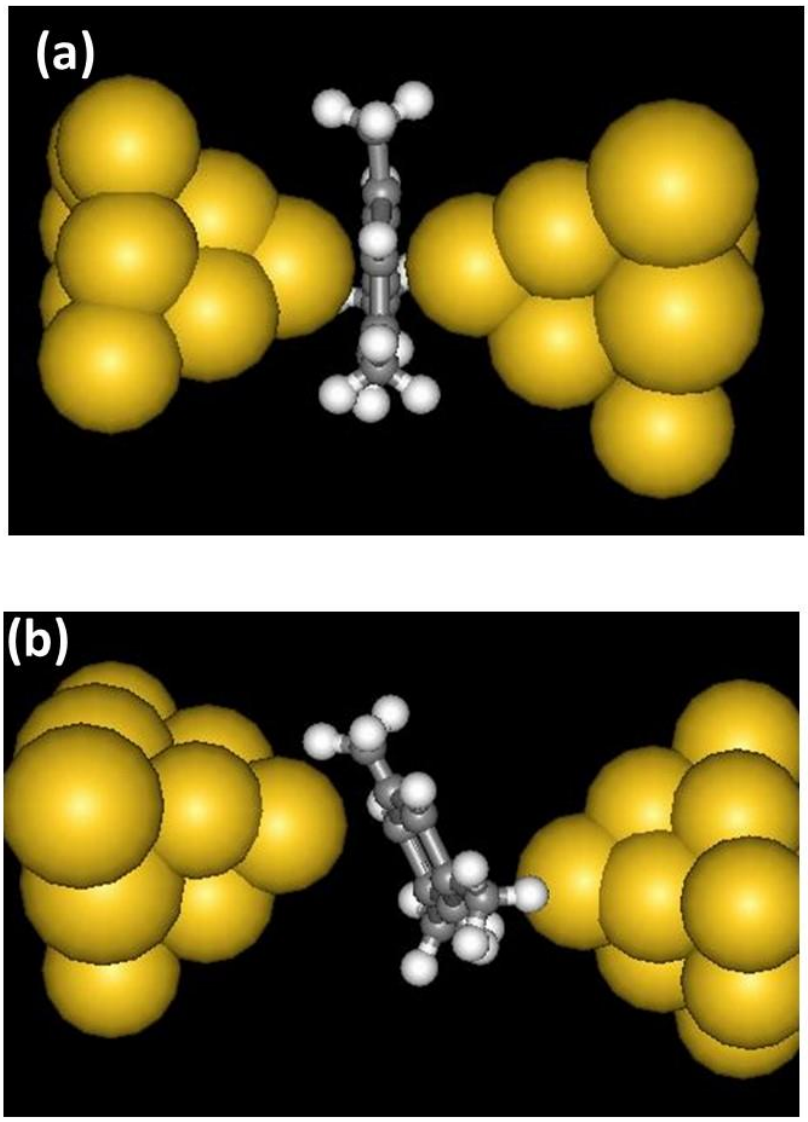

Fig.6-7 Proposed structural models of the mesitylene molecular junctions for (a) high-conductance and (b) low-conductance states. Mesitylene is oriented perpendicular to the charge transport direction in (a). In (b) stretching of the junction leads to a tilted orientation of the mesitylene molecule.

6.4. Conclusions

In this chapter, I fabricated single molecular junctions of mesitylene with the STM-BJ method and performed conductance and *I-V* measurements. In the conductance measurement and *I-V* measurement, two conductance states were observed around 0.1 G_0 as previous reported. The energy level of conduction orbital and the couplings of mesitylene to Au electrodes were determined by fitting of statistically averaged *I-V* curves with Breit-Wigner model. The origin of

the high conductance for the direct π-bonded molecular junctions was ascribed to the experimentally obtained large electronic couplings of *ca.* 0.15 eV for the two states. Based on the stretch length of the conductance trace and the large electronic coupling obtained from the *I-V* analysis, I proposed two possible structural models.

7. Current-Voltage characteristics of asymmetric junctions

In previous chapters, I have reported *I-V* characteristics of symmetric molecular junctions. In this chapter, I discuss the *I-V* characteristics of molecular junctions with asymmetric anchoring groups. Molecular devices have the oldest history in molecular diode research. Some reports on molecular junctions with rectifying properties have been reported. These concepts of molecular junctions with rectifying nature have asymmetry in the molecular backbones. In this chapter, I investigated the *I-V* characteristics of molecular junctions when the anchor groups are asymmetric. *I-V* measurements of 4-aminobenzenethiol with asymmetric anchoring groups and molecules with three binding sites on only one side (C_{60}-tripod) were performed. The statistical rectification was not observed for ABT single-molecule junctions. It is suggested that one coupling affects the other in small conjugated molecules such as ABT. Weak rectification was observed with respect to the three-legged molecule. For three-legged molecule C_{60}-tripod molecules, it can be regarded as asymmetry due to the influence of the backbone. I obtained an asymmetric *I-V* curves depending on the different binding sites.

7.1. Introduction

First research of molecular device is theoretical proposal of molecular diode by Aviram and Ratner in 1974[6]. After establishment of measurement of single-molecule conductance using BJ methods[10, 12, 13, 15], much attention has been focused on realization of molecular diodes[23, 24, 101-103]. The concept of most of molecular diodes including first theoretical proposal reported Aviram and Ratner is introduction of asymmetric molecular backbones. These asymmetric molecular backbones imitate practical diodes with PN junctions. The molecular backbones have donor and accepter parts[23, 24, 101-103].. In Aviram and Ratner model[6], the current increase through molecule as the Fermi level of electrode gets close to accepter level, and *vice versa*. In experimental, some molecular diode with asymmetric backbone have been reported.

Rectification *I-V* character is also expected by introduction of asymmetric molecule-electrode interface structure even with symmetric molecular backbones. Controlling the rectification has advantage in the aspect of design of molecules for use in devices. Some molecular diodes with asymmetric contact parts and symmetric molecular backbone have been reported previously[104-106]. Venkataraman's group have reported the single-molecule rectifier with Au-C bond and Au-S bond. 1,4-aminobenzenthiol (ABT) has both of the most typical anchoring groups, thiol and amino group[40-44, 105]. Wang *et al*. has reported asymmetric *I-V* curves of ABT single-molecule junctions[105]. However, the conductance of single-molecule junction is easily affected by shape of electrodes, the geometries between molecules and metal electrodes, and external noise[39, 44]. The properties of single-molecule junction such as conductance and rectification ratio should be determined by statistical measurement because only one conductance trace is insufficient to determine single molecule conductance. As mentioned in previous chapters, the conductance of the molecule with thiol anchoring groups varies in broad conductance range due to different metal-molecule interface structures[39, 44, 63, 68]. Moreover, BJ methods have a destructive process of metal atomic contacts. This destructive form and rupture process prevents the precise control of the structures of metal-molecule contact parts[70]. The origin of asymmetric *I-V* characteristics of the single-molecule junction of symmetric molecule was assigned as difference of shape of electrodes between tip and substrate in a previous report[107]. Rectification of ABT is not clear because single *I-V* curves cannot exclude the possibility of different electrode structures or conductance change during bias sweep. In this chapter, the statistical *I-V* measurement of ABT and C_{60}-tripod junction as

asymmetric molecular junction is reported. I fabricate single-molecule junctions of ABT and C_{60}-tripod and obtain *I-V* curves more than 1000 times to clarify the rectification property of Au-ABT and Au-C_{60}-tripod junctions.

7.2. Experimental

I performed conductance measurements and *I-V* measurements of ABT and C_{60}-tripod with STM-BJ method. The molecules are shown in Fig.7-1.

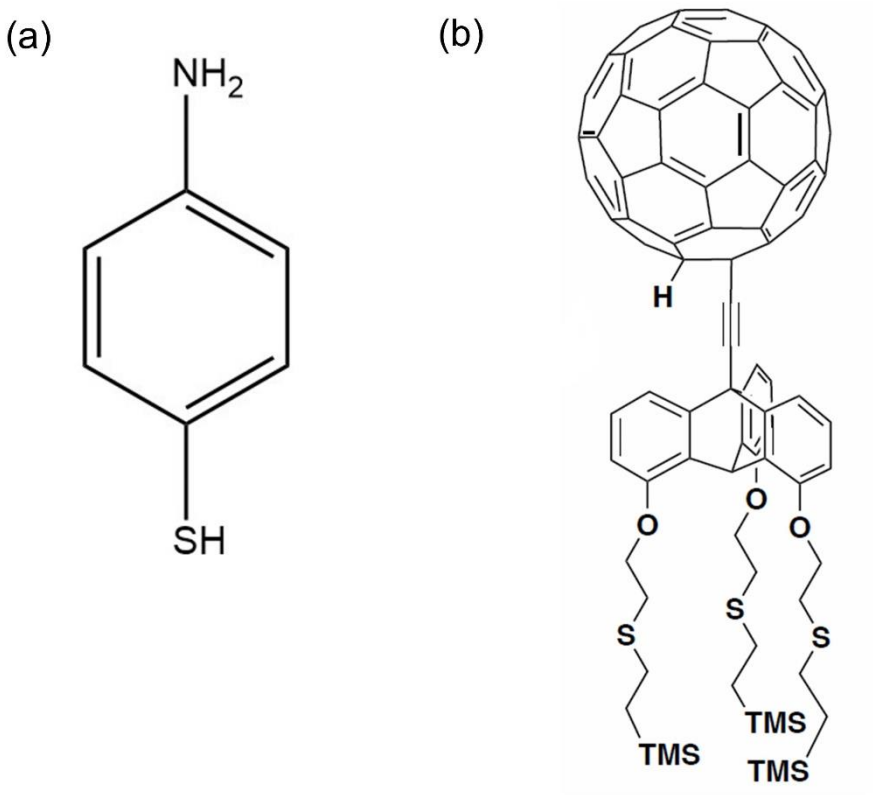

Fig.7-1 molecular formula of (a) ABT and (b) C_{60}-tripod.

7.2.1. Sample preparation

Au(111) on mica substrate were prepared as described in Chapter 4.

ABT

The substrate was dipped into 1mM ethanol solution of ABT after flame annealing. After evaporation of the solution, the substrate was rinsed with ethanol to clean physiosorbed molecules.

C_{60}-tripod

C_{60}-tripod molecule was synthesized by Fukushima Lab.,Tokyo Institute of Technology. The substrate was dipped into 1mM tetrahydrofuran (THF) solution of ABT after flame annealing. The substrate was immersed overnight after tetra-n-butylammonium fluoride is added into the solution. After evaporation of the solution, the substrate was rinsed with THF.

7.2.2. Conductance and *I-V* measurements

Conductance and *I-V* measurements were performed as described in Chapter 4.

7.3. Results and discussions

7.3.1. Conductance and *I-V* measurement of ABT junctions

Fig.7-2 shows the results of single-molecule conductance measured using the STM-BJ method. Typical conductance traces are shown in Fig.7-2 (a). the conductance traces show plateaus at 5 mG_0 and 13 mG_0. These conductance plateaus indicate the conductance of single molecular junctions. Conductance histogram constituted of 300 conductance traces of Au-ABT junctions is shown in Fig.7-2 (b). The conductance histogram also shows two peaks near the 5 mG_0 and 13 mG_0 corresponding to conductance of plateaus observed in conductance traces. The conductance of ABT single-molecule junction are determined be 5 and 13 mG_0. These two conductance peaks agree with previous results reported[108, 105]. There are two possible origin of two single-molecule conductance. One is difference of direction of ABT molecule between two metal electrodes as proposed in a previous report[105]. The other is difference absorption structures. For instance, it is often reported thiol molecule such as BDT has various single-molecule conductance[39-44].

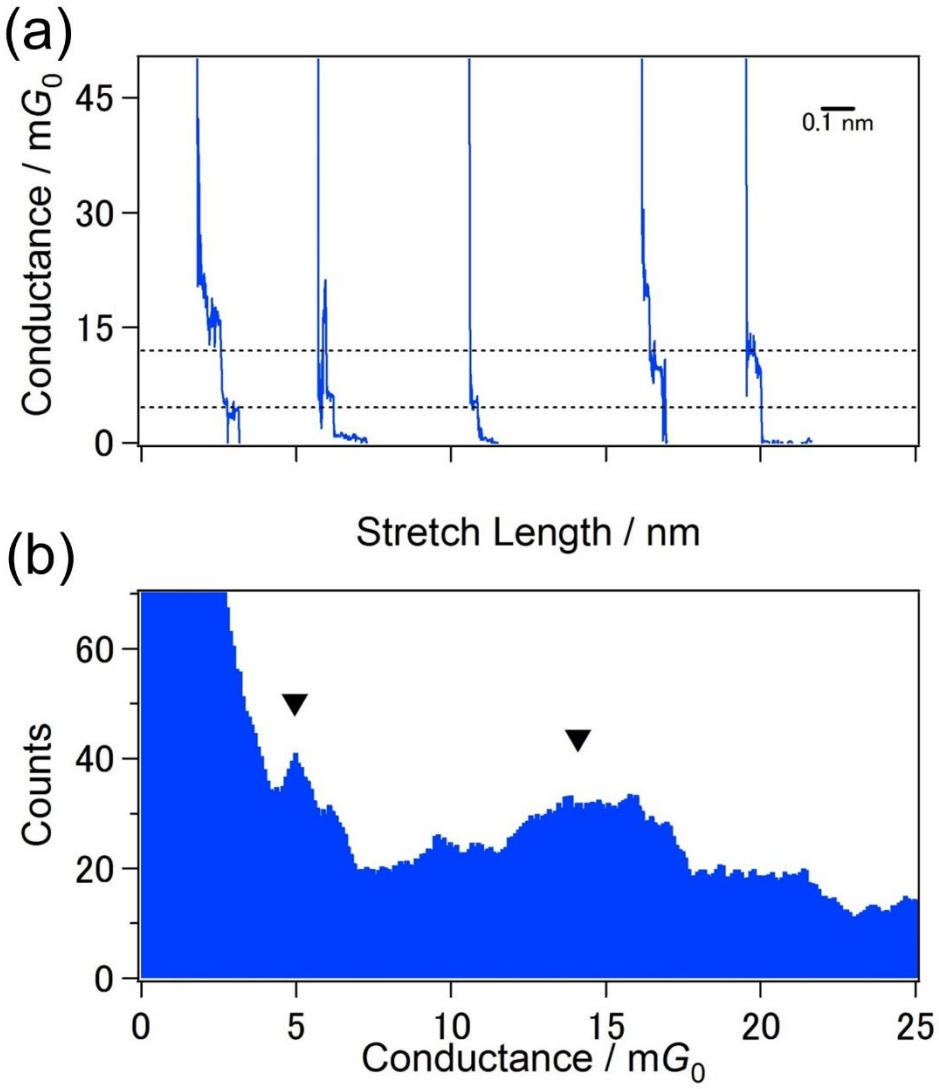

Fig.7-2 (a) Typical conductance trace of the Au-ABT junction. Each dotted line represents the single-molecule conductance of Au-ABT. (b) Conductance histogram of Au-ABT junctions. The histogram consisted of 300 conductance traces. Bias voltage was 20 mV.

Fig.7-3 shows the results of the *I-V* measurement of Au-ABT single-molecule junctions. Fig.7-3 represents the examples of *I-V* curves of Au-ABT junctions. The rectification ratio in Fig.7-3 is 2, 1, and 0.5 for red, black, and blue curve, respectively. Here rectification ratio was defined as ratio of current at ±1V. As reported previously, asymmetric *I-V* curves are observed. Not only asymmetric *I-V* curves but also symmetric curves are also observed. Histogram of

rectification ratio of Au-ABT junctions to clarify rectification of single-molecule junction statistically is shown in Fig.7-4. The most common rectification ratio of ABT single-molecule junctions is 1. Compared to BDT which has same two anchoring groups, rectification of Au-ABT shows no significant difference. It is concluded that the rectification of the averaged Au-ABT junction is 1. Au-ABT junctions do not shows asymmetric *I-V* characteristics due to the two different anchoring groups of ABT molecules against previous report. In Fig.7-3, some *I-V* curves of Au-ABT junctions have asymmetric *I-V* features which rectification ratio is more than 2. However, these asymmetric *I-V* features were also observed for Au-BDT and Au-ABT single-molecule junctions. Therefore, the origin of these rectification observed in ABT junctions is not the different anchoring groups but rather uncontrollable differences such as unexpected geometric asymmetry of contacts between molecule caused to difference of electrode shapes or structural changes during the conductance during bias sweep.

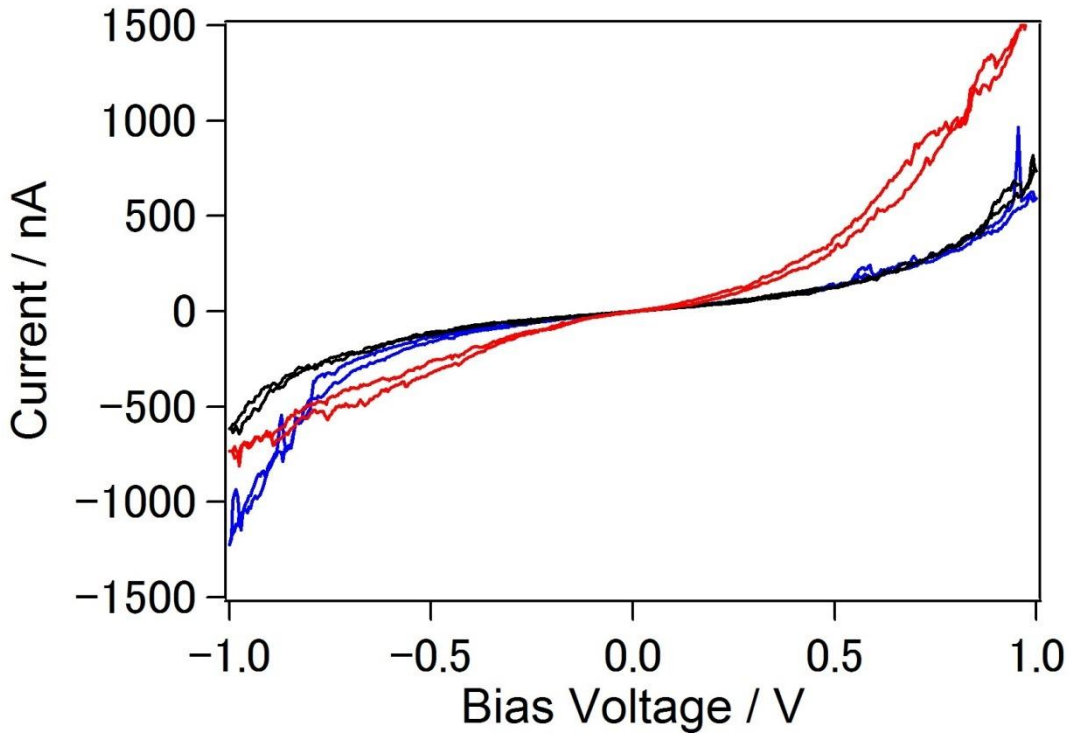

Fig.7-3 Examples of *I-V* curves of Au-ABT single-molecule junction. Scan rate is 100Hz. Bias voltage was swept from +20 mV to +1V, to -1 V, and back to 20 mV.

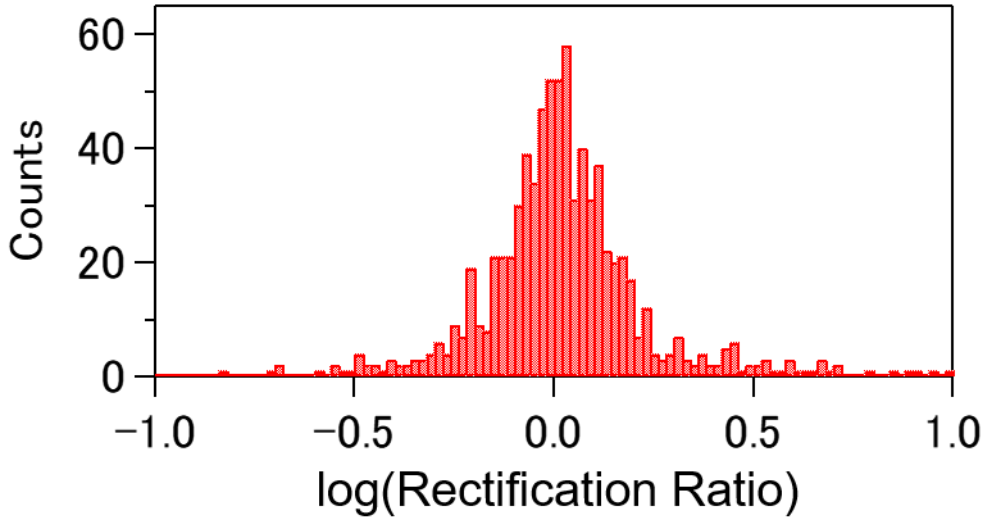

Fig.7-4 Rectification ratio histograms of ABT-Au junctions. Rectification ratio was defined as $|I_{+1\ \mathrm{V}}/I_{-1\ \mathrm{V}}|$. Bin size was calculated as log(rectification ratio) and was 0.02.

Statistical analysis of rectification reveal that no significant rectification features appear for Au-ABT junctions. It means the single-molecule conductance does not depend on molecular direction. Some conductance traces in Fig.7-2(a) also suggest that the origin of two conductance states is not the direction of molecule because some conductance traces has both high and low conductance plateaus in one rupture process. The origin of two conductance states is not direction of molecule but the difference in the adsorption structures of thiol group on the surface of metal electrode as reported in previous report of single molecule conductance of thiol molecule.

Here, I discuss the electronic structures of Au-ABT single-molecule junction with Breit-Wigner model. Here, I assume energy level ε is described in Eq.45 under applying of bias voltage. This assumption is most important for appearance of rectification. This assumption means that the position of the conduction orbital is much affected by a change in the bias voltage of the electrode coupled strongly with the molecule. Using Eq.31 and Eq.45, current through molecular junctions are described in Eq.43. In this model, asymmetric coupling cause rectification because energy difference between Au Fermi levels and molecular level is different between the positive and negative bias. Symmetric coupling does not show any rectification properties. Experimental *I*-*V* curves are fitted with Eq.43 , Histograms of fitting results is shown in Fig.7-5. In Fig.7-5, High and low conductance is defined as the conductance at 0.3V is in

range between 6 mG_0 and 19 mG_0 and in range between 3.3mG_0 and 5.8mG_0, respectively. From Fig.7-5, the coupling is 83meV for high conductance state and 56 meV for low conductance state. The high conductance state had larger coupling. The energy difference between molecular conduction level and Au Fermi level is 0.64 eV and 0.66 eV for high and low conductance state, respectively. This Fitting result suggest that origin of the two conductance states are difference of adsorption structure. Because coupling is mainly influenced by interaction of metal-molecule contacts parts. As mentioned in Chapter 4, the coupling of BDA is 85 meV. BDT has three different coupling for three conductance states. The largest coupling of bridge structure is 129 meV and the second largest coupling of hollow structure is 26meV. The geometrical structure are suspected bridge structure and hollow structure for high and low conductance state, respectively on comparing the coupling values.

The asymmetric factor α, for dual coupling was 0.5 for both states. The coupling of the amino group to the Au electrode equals the coupling of the thiol group. ABT is small and conjugated molecule. Therefore, molecular orbital of ABT is delocalized throughout the molecule. The coupling of one anchoring group could be not independent of the other anchoring group. Hence, Au-ABT single-molecule junction does not show any rectification statistically, in spite of the presence of asymmetric anchoring groups.

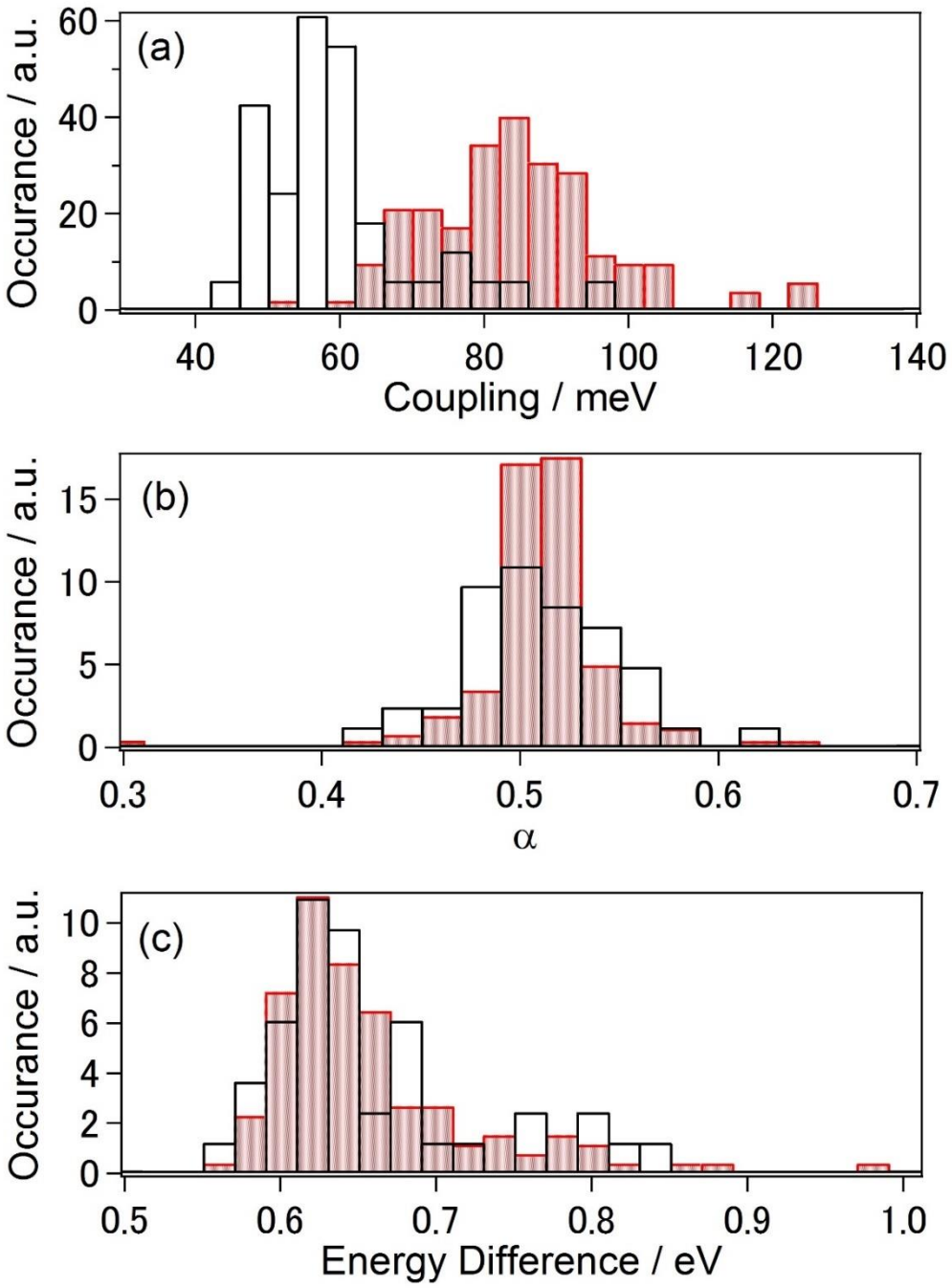

Fig.7-5 Fitting results of observed *I-V* curves. Each *I-V* curve was fitted with single channel Breit–Wigner model after the classified H (red) or L (black) conductance states. *I-V* curves were judged as high state when the conductance at 0.3 V was over 6 mG_0
and under 19 mG_0, and low state when the conductance was over 3.3 mG0 and under 5.8 mG_0. (a) Histogram of coupling. Bin size was 4 meV. (b) Histogram of asymmetric factor α. Bin size was 0.02. (c) Histogram of energy difference. Bin size was 0.02 eV.

7.3.2. Conductance and *I-V* measurement of C_{60}-tripod

I also investigated the conductance and rectification rate of C_{60}-tripod molecule. Fig.7-6, Fig.7-7, and Fig.7-8 shows the conductance traces, conductance histogram and conductance-stretch length 2D histogram of C_{60}-tripod. In typical conductance traces in Fig.7-6 , the conductance plateau was observed. In the histogram, the conductance peak corresponding with conductance plateau is observed at 8 μG_0. The histogram indicates other conductance peak at $10^{-4}G_0$. However, this peak is not reproduceable. Conductance-stretch length 2D histogram displays some conductance traces show plateaus at 8 μG_0. From BJ measurement of C_{60}-tripod molecule, the conductance of most probable single-molecule junction is determined to be 8 μG_0.

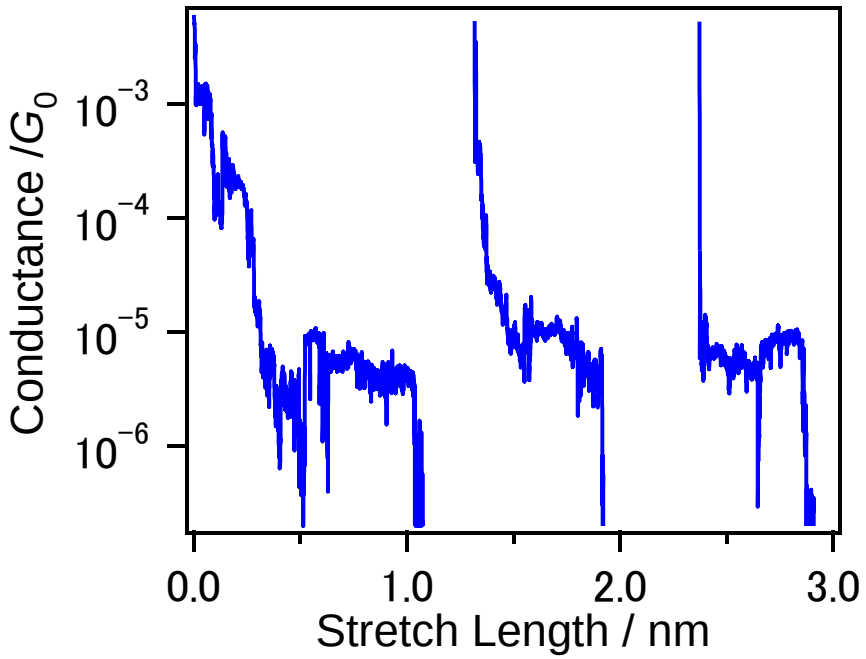

Fig.7-6 The typical conductance traces of Au-C_{60}-tripod junctions. STM-BJ measurement was performed under bias voltage was +200mV.

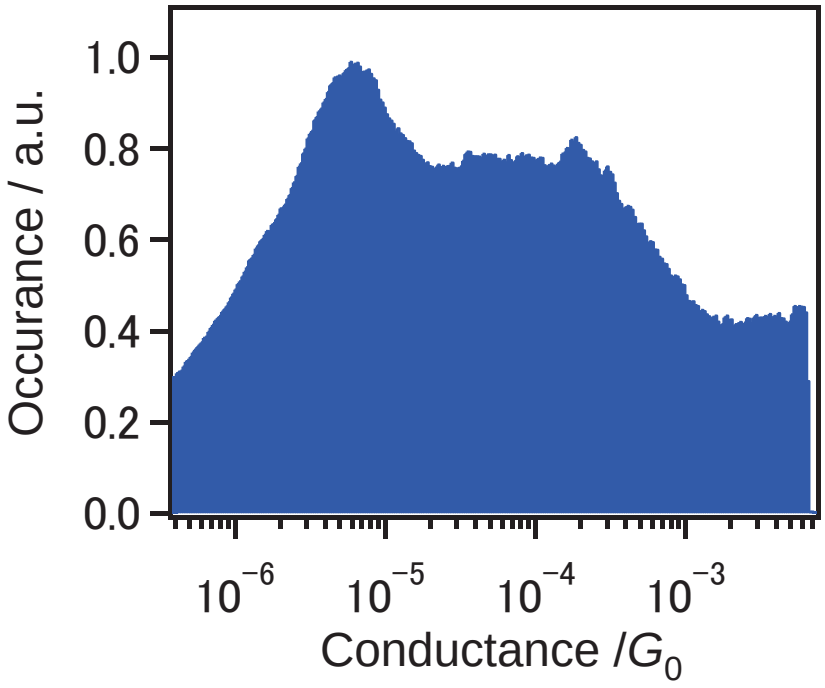

Fig.7-7 The conductance histogram of Au-C_{60}-tripod junctions. Bin size isΔlog(conductance)=0.015. This histogram is consisted from more than 1000 traces.

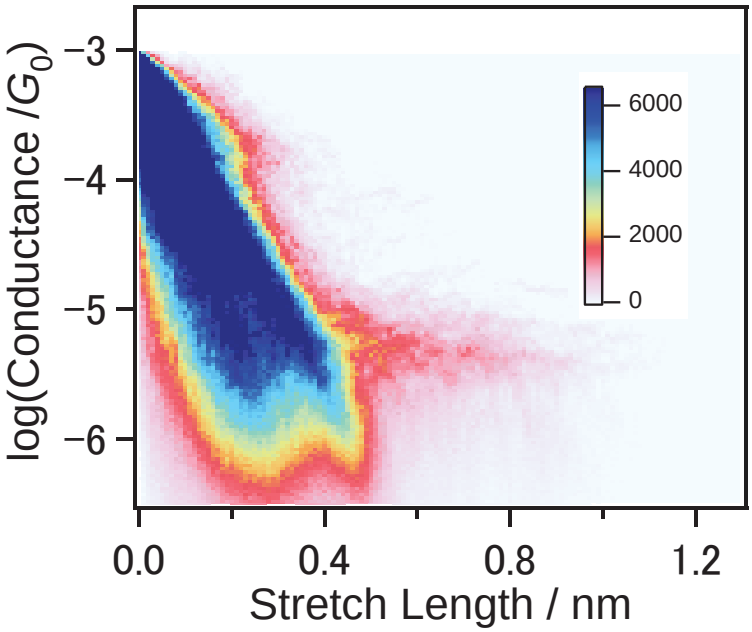

Fig.7-8 The conductance-Stretch length 2D histogram of Au-C_{60}-tripod junctions. The bin size of (stretch length, Δlog(conductance)) is (0.01nm, 0.025).

I-V 2D histogram of C_{60}-tripod is shown in Fig.7-9 . *I-V* curves with small conductance are obtained. However, this conductance is larger than the conductance of most probable single-molecule junction of C_{60}-tripod. The reason of disagreement is difference of bridging structure of C_{60} group. C_{60} binds directly with π conjugation plane and do not have anchoring group[95, 96]. The single-molecule junction with C_{60} group will be changed its contact geometry continuously[78, 109-111]. Many conductance is reported as C_{60} single-molecule conductance[95, 109-111]. The conductance histogram in Fig.7-7 support the C_{60}-tripod single-molecule junction also shows continuous conductance change. The conductance below 10^{-4} G_0 appeared in histogram. However, the histograms display any peak between 10^{-5} – 10^{-4} G_0. The structure which conductance is 8 μG_0 is formed just before breaking junctions.

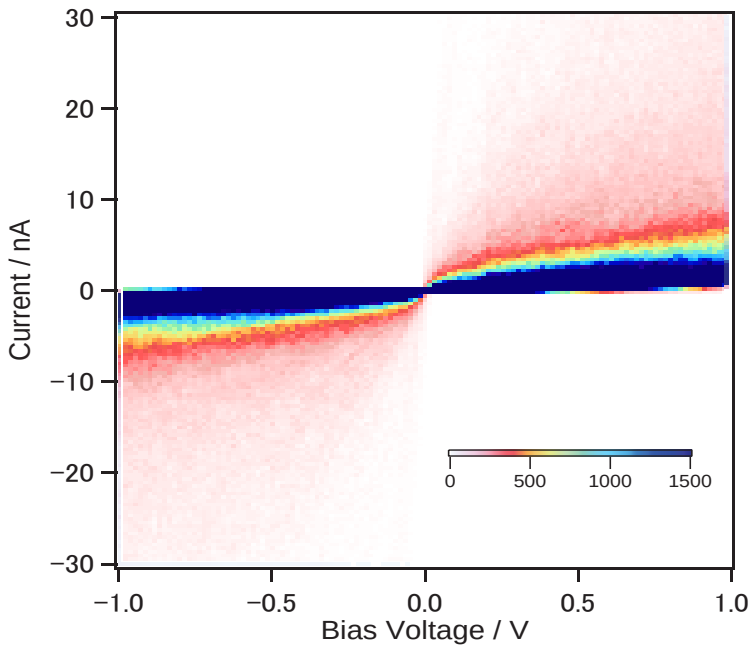

Fig.7-9 *I-V* 2D histogram of Au-C_{60}-tripod junctions. Bias voltage is swept with the direction from +200mV to +1V, to -1V, and to 200mV. The bin size is 0.0125V x 0.4 nA. The histogram is consisted more than 2000 *I-V* curves

Fig.7-10 represents typical *I-V* curves of C_{60}-tripod. Some *I-V* curves of C_{60} are asymmetric curves. The current at positive bias voltage is larger than at negative voltage. As mentioned above, the rectification of molecular junctions is not determined by only single *I-V* curve because the current through single-molecule junction is easily affected with the change of structures during sweep, external noise, and uncontrollable difference of two electrodes. Hence,

statistical analysis is necessary for rectification of single-molecule junctions.

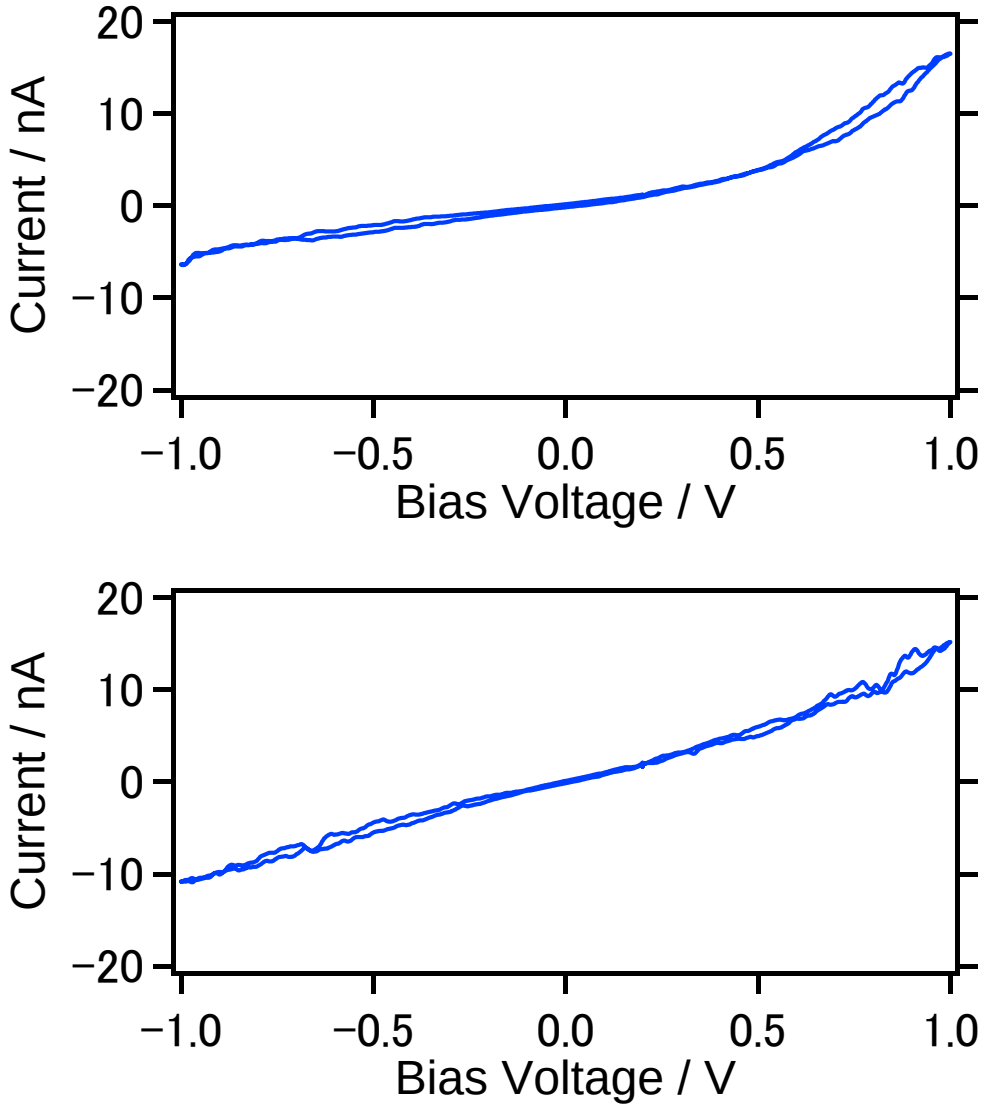

Fig.7-10 typical *I-V* curves of C_{60}-tripod junctions. Bias voltage is swept with the direction of +200 mV to +1 V, -1 V to 200 mV.

Fig.7-11 shows rectification histogram of C_{60}-tripod. The histograms of ABT and BDT are also shown in Fig.7-11 to compare the rectification ratio[112]. Here the rectification is defined as the ratio of current at ± 1 V. The peak tops of rectification ratio of small conjugation molecule, ABT and BDT, are one, that is, the *I-V* curve of ABT and BDT do not show rectification statistically. However, the distribution of C_{60}-tripod (blue) is obviously shifted from rectification ratio = 1. The averaged rectification is determined by gaussian fitting of rectification rage

histogram in Fig.7-11(blue). The rectification ratio in Fig.7-11 is determined to be 1.3. For averaging 9 datasets, the average rectification ratio of C_{60}-tripod is 1.14 ± 0.09. The error is determined by standard deviations. The averaged rectification is small. However, the datasets include dataset which show no significant molecule features. The datasets include many *I-V* curve of vacuum gap. But, the all dataset indicates positive rectification ratio. To conclude the molecular junctions of C_{60}-tripod shows rectification, I have to eliminate the possibility of conductance change during bias sweep. Even if the molecular junctions of C_{60}-tripod do not show rectification, if conductance decrease during bias sweep, the positive rectification is observed in the rectification histogram. To distinguish decreasing of conductance and real rectification, I performed *I-V* measurement with opposite direction bias sweep. Fig.7-12 shows rectification histogram of C_{60}-tripod when bias voltage was swept with opposite direction of Fig.7-11 (from 20mV to -1V, to 1V, and back to 20mV) The histogram also shows the peak center at rectification is positive. According to this measurement, the observed rectification is not due to conductance decreasing during bias sweep. Therefore, I conclude that molecular junction of C_{60}-tripod shows weak rectification. Furthermore, the direction of molecule in the junction is controlled by binding to substrate with chemical reaction.

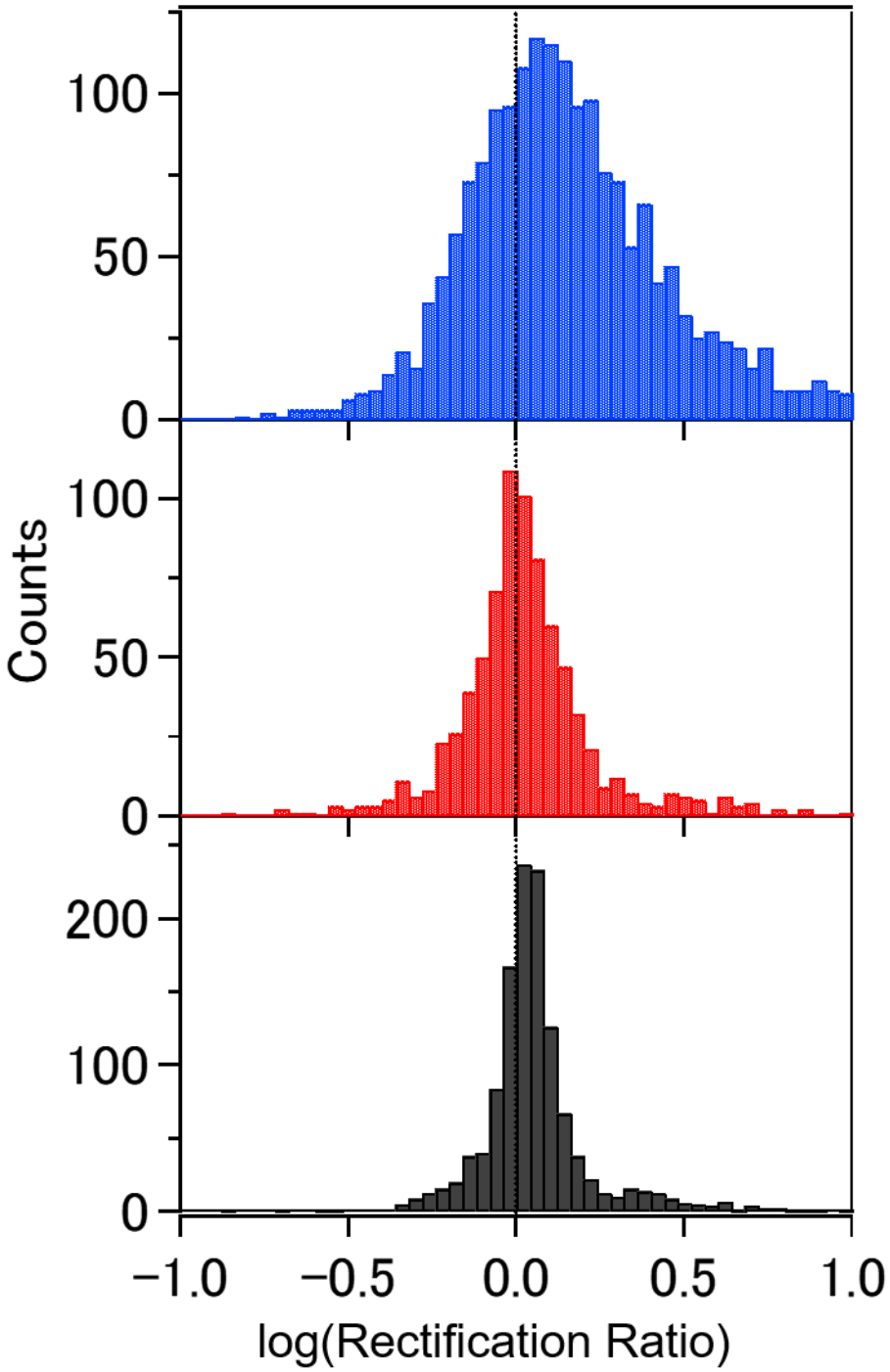

Fig.7-11 Rectification ratio histogram of (blue) C_{60}-tripod, (red) ABT, and (black) BDT. The peak center position determined by gaussian fit is (blue)1.26, (red) 1.02, and (black) 1.08. The bin size is Δlog(Rectification Rate)=0.04. The histogram is consisted from more than (blue) 2000, (red, black) 1000 *I-V* curves. The rectification ratio is defined as the ratio of current at ±1V. Black dotted line indicates rectification ratio = 1.

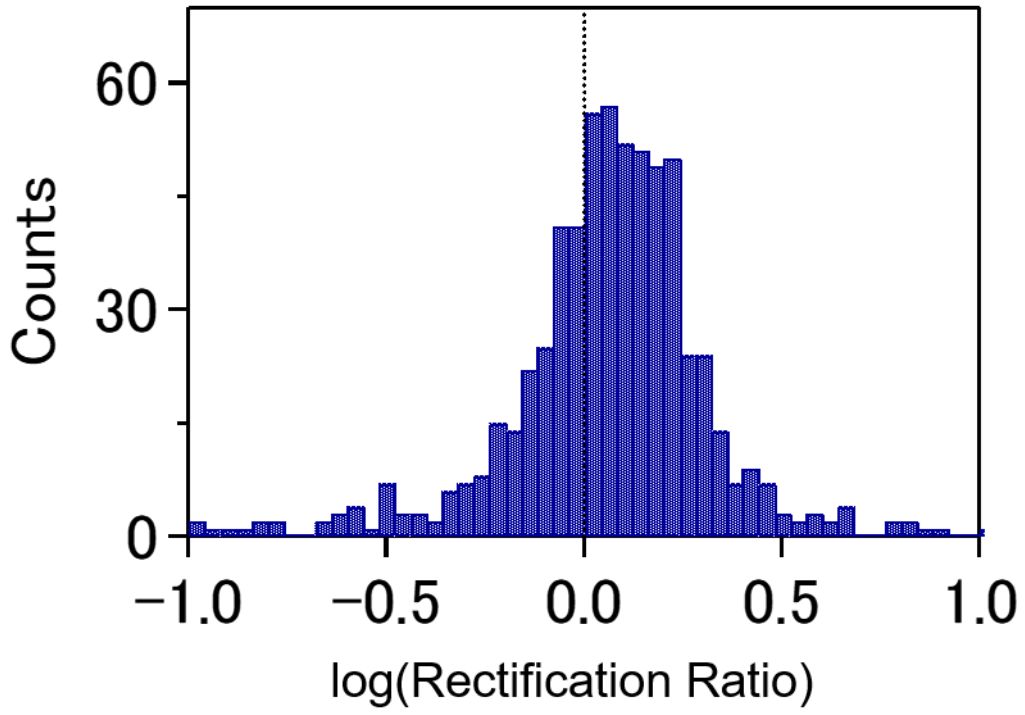

Fig.7-12 Rectification ratio histogram of C_{60}-tripod obtained with different direction bias sweep (from 20mV to -1V, to 1V, and back to 20mV).

I discuss the origin of the weak rectification of C_{60}-tripod. ABT has no significant rectification in spite of binding with different anchoring groups. The difference between C_{60}-tripod and ABT is existence of saturated carbon between two contact parts. The molecular orbital shift depends on bias voltage direction, as described in Eq.45. It can be interpreted the coupling difference cause rectification. However, the molecular orbital shift depending with bias voltage direction is not necessary. This observed rectification is also interpreted by Aviram and Ratner model[6]. The mechanism of the rectification of C_{60}-tripod is not clear. But, the molecular rectifier caused by contact part is developed. To realize rectification with different contact parts, discontinuity of orbital delocalization will be necessary.

7.4. Conclusions

In this chapter, I statistically measured the single molecule conductance and *I-V* characteristics of Au-ABT junctions with STM-BJ method. Two conductance states were observed. Some *I-V*

curves shows rectification. However, no significant rectification appear for Au-ABT single-molecule junction statistically. The origin of two different conductance state is uncontrollable difference of adsorption structure not molecular direction. It is suggested that coupling of one anchoring group is influenced by the other anchoring group in small conjugated molecule such as ABT. This study emphasizes that statistically measurements, not single bias sweep, are necessary for discussing of single molecular rectification.

For C_{60}-tripod, the weak rectification is observed. The direction of rectifier is also controlled by binding to substrate with chemical reaction. The mechanism of the rectification is not confirmed. However, the development of single-molecule rectifier caused by different contact parts is succeeded.

8. General conclusions

In this thesis, I have clarified the contact geometries of single-molecule junctions and established the measurement method of electronic structures of single-molecule junctions with the *I-V* measurement and the thermopower measurement.

It has been well-known that thiol group which is often utilize as anchoring group form single-molecule junction with several contact geometries, and the conductance is affected by the contact conformations. However, determination of bridging structures was not highly reliable because only the conductance at fixed bias is compared to theoretical calculation. In this thesis, the contact geometries of single-molecule junctions are assigned by comparison between experimental and theoretical transmissions.

The conductive properties of single-molecule junctions depend on electronic structures of single-molecule junction. However, previous studies have not clarified the electronic structures quantitatively and statistically. I have developed the quantitative and statistical method to determine the electronic structures of single-molecule junctions. The conductance of single-molecule junctions is easily affected by slightly structural changes, difference configuration of contact parts, and external noise. In this thesis, the importance of statistical approach is elucidated for valid measurement of single-molecule junctions. The Breit-Wigner model analysis of statistically corrected *I-V* curves reveals the electronic structure quantitatively. In addition to *I-V* measurement, the most contributable molecular orbitals to charge transport through single-molecule junctions were determined with thermopower measurement. Combination of *I-V* measurement and thermopower measurement are established as precise measurement method of single-molecule junctions. From the electronic structures of small conjugated single-molecule junctions determined with *I-V* characteristics, conduction through single-molecule junctions is much influenced by the coupling. This result emphasizes the importance of contact parts of single-molecule junctions. This insight will be lead to a better strategy of functional molecular junctions to develop molecular devices.

I-V measurement and thermopower measurement reveals the details of single-molecule junction which are unclear only due to conductance measurement. The establishment of measurement method of the electronic structures of single-molecule junctions will be a basis of the development of future single molecule devices and single-molecule analysis.

However, it is difficult to say that analysis of ‘real single-molecule behaviors’ have been achieved. Although single-molecule junction is system where not ensemble but single molecule behavior is observable, we have not investigated valid single molecule behaviors enough. The statistical measurement and analysis is necessary to avoid the influence of slightly changes of junctions. The some single-molecule features are lost averaging of data. Further investigation is essential for single-molecule analysis.

9. Acknowledgement

I am grateful to Prof. Manabu Kiguchi (Tokyo Institute of Technology, (Tokyo Tech)) for his great supervision. I would like to appreciate Assoc. Prof. Tomoaki Nishino (Tokyo Tech) for meaningful discussions, Assoc. Prof. Shintaro Fujii (Tokyo Tech) who gave me grateful advice and taught me know-how of experiments.

I'm grateful to collaborators, Dr. Hisao Nakamura (National Institute of Advanced Industrial Science and Technology) and Assoc. Prof. Tomofumi Tada (Tokyo Tech) who calculated the transmission of BDT, Prof. Takanori Fukushima (Tokyo Tech) and Assist. Prof. Fumitaka Ishiwari (Tokyo Tech) who synthesized the C_{60}-tripod molecule, Prof. Osamu Ishitani (Tokyo Tech) and Assist. Prof. Yusuke Tamaki (Tokyo Tech) who synthesized the sample.

I would like to thank Assist. Prof. Satoshi Kaneko (Tokyo Tech) and Prof. Toshiaki Enoki (Tokyo Tech) for meaningful discussions. I gratefully acknowledge all members of Kiguchi-Nishino Lab.

I have great experience while I stayed at Leiden Univ. I appreciate Prof. Jan van Ruitenbeek (Leiden University), Dr. Carlos Sabater (Weizmann Institute of Science) and members of AMC group.

I also appreciate discussion of single-molecule junction with Prof. Masateru Taniguchi, Assoc. Prof. Takahito Oshiro, Assoc. Prof. Makusu Tsutsui, and Assis. Prof. Akihide Arima (Osaka univ.).

This work was supported by Grant-in-Aid for JSPS Fellows (15J11830).

10. Reference

[1] Scheer E 2010 *Molecular electronics: an introduction to theory and experiment* vol 1: World Scientific)

[2] Ratner M 2013 A brief history of molecular electronics *Nat. Nanotechnol.* . **8** 378

[3] Kiguchi M and Kaneko S 2012 Electron Transport through Single π-Conjugated Molecules Bridging between Metal Electrodes *Chem.Phys.Chem.* **13** 1116

[4] Aradhya S V and Venkataraman L 2013 Single-molecule junctions beyond electronic transport *Nat. Nanotechnol.* **8** 399

[5] Tsutsui M and Taniguchi M 2012 Single molecule electronics and devices *Sensors* **12** 7259

[6] Aviram A and Ratner M A 1974 Molecular rectifiers *Chem. Phys. Lett.* **29** 277

[7] Di Ventra M and Taniguchi M 2016 Decoding DNA, RNA and peptides with quantum tunnelling *Nat. Nanotechnol.* **11** 117

[8] Ohshiro T, Matsubara K, Tsutsui M, Furuhashi M, Taniguchi M and Kawai T 2012 Single-molecule electrical random resequencing of DNA and RNA *Sci. Rep.* **2** 00501

[9] Tsutsui M, Matsubara K, Ohshiro T, Furuhashi M, Taniguchi M and Kawai T 2011 Electrical detection of single methylcytosines in a DNA oligomer *J. Am. Chem. Soc.*. **133** 9124

[10] Moreland J and Ekin J W 1985 Electron tunneling experiments using Nb-Sn "break" junctions *J. Appl. Phys.* **58** 3888

[11] Smit R, Noat Y, Untiedt C, Lang N, van Hemert M v and Van Ruitenbeek J 2002 Measurement of the conductance of a hydrogen molecule *Nature* **419** 906

[12] van Ruitenbeek J M, Alvarez A, Piñeyro I, Grahmann C, Joyez P, Devoret M H, Esteve D and Urbina C 1996 Adjustable nanofabricated atomic size contacts *Rev. Sci. Inst.* **67** 108

[13] Reed M A, Zhou C, Muller C, Burgin T and Tour J 1997 Conductance of a molecular junction *Science* **278** 252

[14] Martin C A, Ding D, van der Zant H S J and Ruitenbeek J M v 2008 Lithographic mechanical break junctions for single-molecule measurements in vacuum: possibilities and limitations *New J. Phys.* **10** 065008

[15] Xu B and Tao N J 2003 Measurement of Single-Molecule Resistance by Repeated Formation of Molecular Junctions *Science* **301** 1221

[16] Kotiuga M, Darancet P, Arroyo C R, Venkataraman L and Neaton J B 2015 Adsorption-induced solvent-based electrostatic gating of charge transport through molecular junctions *Nano lett.* **15** 4498

[17] Liu Z-F, Wei S, Yoon H, Adak O, Ponce I, Jiang Y, Jang W-D, Campos L M, Venkataraman L and Neaton J B 2014 Control of single-molecule junction conductance of porphyrins via a transition-metal center *Nano lett.* **14** 5365

[18] Marqués-González S, Yufit D S, Howard J A, Martín S, Osorio H M, García-Suárez V M, Nichols R J, Higgins S J, Cea P and Low P J 2013 Simplifying the conductance profiles of molecular junctions: the use of the trimethylsilylethynyl moiety as a molecule–gold contact *Dalton Trans.* **42** 338

[19] Tian J H, Yang Y, Zhou X S, Schöllhorn B, Maisonhaute E, Chen Z B, Yang F Z, Chen Y, Amatore C and Mao B W 2010 Electrochemically Assisted Fabrication of Metal Atomic Wires and Molecular Junctions by MCBJ and STM-BJ Methods *Chem. Phys. Chem.* **11** 2745

[20] Venkataraman L, Klare J E, Nuckolls C, Hybertsen M S and Steigerwald M L 2006 Dependence of single-molecule junction conductance on molecular conformation *Nature* **442** 904

[21] Capozzi B, Dell E J, Berkelbach T C, Reichman D R, Venkataraman L and Campos L M 2014 Length-dependent conductance of oligothiophenes *J. Am. Chem. Soc.*. **136** 10486

[22] Toher C and Sanvito S 2007 Efficient atomic self-interaction correction scheme for nonequilibrium quantum transport *Phys. Rev. Lett.* . **99** 056801

[23] Fu X X, Zhang R Q, Zhang G P and Li Z L 2014 Rectifying properties of oligo(phenylene ethynylene) heterometallic molecular junctions: molecular length and side group effects *Sci. Rep.* **4** 6357

[24] Diez-Perez I, Hihath J, Lee Y, Yu L, Adamska L, Kozhushner M A, Oleynik, II and Tao N 2009 Rectification and stability of a single molecular diode with controlled orientation *Nat. Chem.*. **1** 635

[25] Fujii S, Tada T, Komoto Y, Osuga T, Murase T, Fujita M and Kiguchi M 2015 Rectifying Electron-Transport Properties through Stacks of Aromatic Molecules Inserted into a Self-Assembled Cage *J. Am. Chem. Soc.*. **137** 5939

[26] Wang K, Zhou J, Hamill J M and Xu B 2014 Measurement and understanding of single-molecule break junction rectification caused by asymmetric contacts *J. Chem. Phys.* **141** 054712

[27] Lörtscher E, Gotsmann B, Lee Y, Yu L, Rettner C and Riel H 2012 Transport properties of a single-molecule diode *ACS nano* **6** 4931

[28] Capozzi B, Xia J, Adak O, Dell E J, Liu Z-F, Taylor J C, Neaton J B, Campos L M and Venkataraman L 2015 Single-molecule diodes with high rectification ratios through environmental control *Nat. Nanotechnol.* **10** 522

[29] Elbing M, Ochs R, Koentopp M, Fischer M, von Hänisch C, Weigend F, Evers F, Weber H B and Mayor M 2005 A single-molecule diode *Proc. Natl. Acad. Sci. U.S.A.* **102** 8815

[30] Batra A, Darancet P, Chen Q, Meisner J S, Widawsky J R, Neaton J B, Nuckolls C and Venkataraman L 2013 Tuning rectification in single-molecular diodes *Nano lett.* **13** 6233

[31] Xiang D, Jeong H, Kim D, Lee T, Cheng Y, Wang Q and Mayer D 2013 Three-terminal single-molecule junctions formed by mechanically controllable break junctions with side gating

Nano lett. **13** 2809

[32] Xu B, Xiao X, Yang X, Zang L and Tao N 2005 Large gate modulation in the current of a room temperature single molecule transistor *J. Am. Chem. Soc.*. **127** 2386

[33] Kiguchi M, Ohto T, Fujii S, Sugiyasu K, Nakajima S, Takeuchi M and Nakamura H 2014 Single molecular resistive switch obtained via sliding multiple anchoring points and varying effective wire length *J. Am. Chem. Soc.* **136** 7327

[34] Dulic D, van der Molen S J, Kudernac T, Jonkman H T, de Jong J J, Bowden T N, van Esch J, Feringa B L and van Wees B J 2003 One-way optoelectronic switching of photochromic molecules on gold *Phys. Rev. Lett.* **91** 207402

[35] Jia C, Migliore A, Xin N, Huang S, Wang J, Yang Q, Wang S, Chen H, Wang D and Feng B 2016 Covalently bonded single-molecule junctions with stable and reversible photoswitched conductivity *Science* **352** 1443

[36] Gerhard L, Edelmann K, Homberg J, Valášek M, Bahoosh S G, Lukas M, Pauly F, Mayor M and Wulfhekel W 2017 An electrically actuated molecular toggle switch *Nat. Commun.* **8** 14672

[37] Xu B and Tao N J 2003 Measurement of Single-Molecule Resistance by Repeated Formation of Molecular Junctions *Science* **301** 1221

[38] Huang C, Rudnev A V, Hong W and Wandlowski T 2015 Break junction under electrochemical gating: testbed for single-molecule electronics *Chem. Soc. Rev.* **44** 889

[39] Guo S, Hihath J, Diez-Perez I and Tao N 2011 Measurement and statistical analysis of single-molecule current-voltage characteristics, transition voltage spectroscopy, and tunneling barrier height *J. Am. Chem. Soc.* **133** 19189

[40] Li X, He J, Hihath J, Xu B, Lindsay S M and Tao N 2006 Conductance of single alkanedithiols: conduction mechanism and effect of molecule− electrode contacts *J. Am. Chem. Soc.*. **128** 2135

[41] Venkataraman L, Klare J E, Tam I W, Nuckolls C, Hybertsen M S and Steigerwald M L 2006 Single-molecule circuits with well-defined molecular conductance *Nano lett.* **6** 458

[42] Xiao X, Xu B and Tao N J 2004 Measurement of single molecule conductance: Benzenedithiol and benzenedimethanethiol *Nano Lett.* **4** 267

[43] Kim Y, Hellmuth T J, Burkle M, Pauly F and Scheer E 2011 Characteristics of amine-ended and thiol-ended alkane single-molecule junctions revealed by inelastic electron tunneling spectroscopy *ACS nano* **5** 4104

[44] Kim Y, Pietsch T, Erbe A, Belzig W and Scheer E 2011 Benzenedithiol: a broad-range single-channel molecular conductor *Nano lett.* **11** 3734

[45] Quek S Y, Venkataraman L, Choi H J, Louie S G, Hybertsen M S and Neaton J B 2007 Amine−Gold Linked Single-Molecule Circuits: Experiment and Theory *Nano Lett.* **7** 3477

[46] Koga J, Tsuji Y and Yoshizawa K 2012 Orbital control of single-molecule conductance perturbed by π-accepting anchor groups: cyanide and isocyanide *J. Phys. Chem. C* **116** 20607

[47] Komoto Y, Fujii S, Hara K and Kiguchi M 2013 Single Molecular Bridging of Au Nanogap Using Aryl Halide Molecules *J. Phys. Chem. C* **117** 24277

[48] Hakkinen H 2012 The gold-sulfur interface at the nanoscale *Nat. Chem.* **4** 443

[49] Fujihira M, Suzuki M, Fujii S and Nishikawa A 2006 Currents through single molecular junction of Au/hexanedithiolate/Au measured by repeated formation of break junction in STM under UHV: Effects of conformational change in an alkylene chain from gauche to trans and binding sites of thiolates on gold *Phys. Chem. Chem. Phys.* **8** 3876

[50] Landauer R 1970 Electrical resistance of disordered one-dimensional lattices *Philosophical magazine* **21** 863

[51] Simmons J G 1963 Generalized formula for the electric tunnel effect between similar electrodes separated by a thin insulating film *J. Appl. Phys.* **34** 1793

[52] Beebe J M, Kim B, Gadzuk J W, Frisbie C D and Kushmerick J G 2006 Transition from direct tunneling to field emission in metal-molecule-metal junctions *Phys. Rev. Lett.* . **97** 026801

[53] Bruot C, Hihath J and Tao N 2011 Mechanically controlled molecular orbital alignment in single molecule junctions *Nat. Nanotechnol.* **7** 35

[54] Huisman E H, Guédon C M, van Wees B J and van der Molen S J 2009 Interpretation of transition voltage spectroscopy *Nano lett.* **9** 3909

[55] Breit G and Wigner E 1936 Capture of Slow Neutrons *Phys. Rev.* **49** 519

[56] Matsuhita R, Horikawa M, Naitoh Y, Nakamura H and Kiguchi M 2013 Conductance and SERS Measurement of Benzenedithiol Molecules Bridging Between Au Electrodes *J. Phys. Chem. C* **117** 1791

[57] Frisenda R, Perrin M L, Valkenier H, Hummelen J C and van der Zant H S J 2013 Statistical analysis of single-molecule breaking traces *Phys. Status Solidi B* **250** 2431

[58] Paulsson M and Datta S 2003 Thermoelectric effect in molecular electronics *Phys. Rev. B* **67** 241403

[59] Kim Y, Pietsch T, Erbe A, Belzig W and Scheer E 2011 Benzenedithiol: a broad-range single-channel molecular conductor *Nano Lett.* **11** 3734

[60] Bruot C, Hihath J and Tao N 2012 Mechanically controlled molecular orbital alignment in single molecule junctions *Nat. Nanotechnol.* **7** 35

[61] Widawsky J R, Kamenetska M, Klare J, Nuckolls C, Steigerwald M L, Hybertsen M S and Venkataraman L 2009 Measurement of voltage-dependent electronic transport across amine-linked single-molecular-wire junctions *Nanotechnology* **20** 434009

[62] Lörtscher E, Weber H B and Riel H 2007 Statistical Approach to Investigating Transport through Single Molecules *Phys. Rev. Letters* **98**

[63] Li C, Pobelov I, Wandlowski T, Bagrets A, Arnold A and Evers F 2008 Charge transport in single Au| alkanedithiol| Au junctions: coordination geometries and conformational degrees of freedom

J. Am. Chem. Soc.. **130** 318

[64] Fujii S, Akiba U and Fujihira M 2002 Geometry for self-assembling of spherical hydrocarbon cages with methane thiolates on Au (111) *J. Am. Chem. Soc.*. **124** 13629

[65] Nakamura H, Yamashita K, Rocha A R and Sanvito S 2008 Efficientab initiomethod for inelastic transport in nanoscale devices: Analysis of inelastic electron tunneling spectroscopy *Phys. Rev. B* **78**

[66] Rocha A R, García-Suárez V M, Bailey S, Lambert C, Ferrer J and Sanvito S 2006 Spin and molecular electronics in atomically generated orbital landscapes *Phys. Rev. B* **73**

[67] Rungger I and Sanvito S 2008 Algorithm for the construction of self-energies for electronic transport calculations based on singularity elimination and singular value decomposition *Phys. Rev. B* **78**

[68] Komoto Y, Fujii S, Nakamura H, Tada T, Nishino T and Kiguchi M 2016 Resolving metal-molecule interfaces at single-molecule junctions *Sci. Rep.* **6** 26606

[69] Haiss W, Wang C, Grace I, Batsanov A S, Schiffrin D J, Higgins S J, Bryce M R, Lambert C J and Nichols R J 2006 Precision control of single-molecule electrical junctions *Nat. Mater.* **5** 995

[70] Frei M, Aradhya S V, Koentopp M, Hybertsen M S and Venkataraman L 2011 Mechanics and chemistry: single molecule bond rupture forces correlate with molecular backbone structure *Nano lett.* **11** 1518

[71] Kamenetska M, Quek S Y, Whalley A, Steigerwald M, Choi H, Louie S G, Nuckolls C, Hybertsen M, Neaton J and Venkataraman L 2010 Conductance and geometry of pyridine-linked single-molecule junctions *J. Am. Chem. Soc.*. **132** 6817

[72] Kim T, Darancet P, Widawsky J R, Kotiuga M, Quek S Y, Neaton J B and Venkataraman L 2014 Determination of energy level alignment and coupling strength in 4,4'-bipyridine single-molecule junctions *Nano Lett.* **14** 794

[73] Paulsson M and Datta S 2003 Thermoelectric effect in molecular electronics *Phys. Rev. B* **67**

[74] Reddy P, Jang S-Y, Segalman R A and Majumdar A 2007 Thermoelectricity in Molecular Junctions *Science* **315** 1568

[75] Widawsky J R, Darancet P, Neaton J B and Venkataraman L 2011 Simultaneous determination of conductance and thermopower of single molecule junctions *Nano lett.* **12** 354

[76] Tsutsui M, Morikawa T, Arima A and Taniguchi M 2013 Thermoelectricity in atom-sized junctions at room temperatures *Sci. Rep.* **3** 3326

[77] Yee S K, Malen J A, Majumdar A and Segalman R A 2011 Thermoelectricity in fullerene–metal heterojunctions *Nano lett.* **11** 4089

[78] Evangeli C, Gillemot K, Leary E, Gonzalez M T, Rubio-Bollinger G, Lambert C J and Agraït N s 2013 Engineering the thermopower of C_{60} molecular junctions *Nano lett.* **13** 2141

[79] Morikawa T, Arima A, Tsutsui M and Taniguchi M 2014 Thermoelectric voltage measurements

of atomic and molecular wires using microheater-embedded mechanically-controllable break junctions *Nanoscale* **6** 8235

[80] Tsutsui M, Morikawa T, He Y, Arima A and Taniguchi M 2015 High thermopower of mechanically stretched single-molecule junctions *Sci. Rep.* **5** 11519

[81] Lee S K, Ohto T, Yamada R and Tada H 2014 Thermopower of benzenedithiol and C_{60} molecular junctions with Ni and Au electrodes *Nano Lett.* **14** 5276

[82] Yee S K, Malen J A, Majumdar A and Segalman R A 2011 Thermoelectricity in fullerene-metal heterojunctions *Nano Lett.* **11** 4089

[83] Bergfield J P, Solis M A and Stafford C A 2010 Giant thermoelectric effect from transmission supernodes *ACS nano* **4** 5314

[84] Kim P, Odom T W, Huang J-L and Lieber C M 1999 Electronic density of states of atomically resolved single-walled carbon nanotubes: Van Hove singularities and end states *Phys. Rev. Lett.* **82** 1225

[85] Van Hove L 1953 The occurrence of singularities in the elastic frequency distribution of a crystal *Phys. Rev.* **89** 1189

[86] Cui L, Jeong W, Hur S, Matt M, Klöckner J C, Pauly F, Nielaba P, Cuevas J C, Meyhofer E and Reddy P 2017 Quantized thermal transport in single-atom junctions *Science* **355** 1192

[87] Lee W, Kim K, Jeong W, Zotti L A, Pauly F, Cuevas J C and Reddy P 2013 Heat dissipation in atomic-scale junctions *Nature* **498** 209

[88] Kim Y, Jeong W, Kim K, Lee W and Reddy P 2014 Electrostatic control of thermoelectricity in molecular junctions *Nat. Nanotechnol.* **9** 881

[89] Afsari S, Li Z and Borguet E 2014 Orientation-controlled single-molecule junctions *Angew. Chem. Int. Ed.* **53** 9771

[90] Kaneko S and Kiguchi M 2013 Investigation on the Pyrazine Molecular Junction Studied by Conductance Measurement and Near Edge X-ray Absorption Fine Structure *Fuller. Nanotub. Car. N.* **22** 166

[91] Kaneko S, Nakazumi T and Kiguchi M 2010 Fabrication of a Well-Defined Single Benzene Molecule Junction Using Ag Electrodes *J. Phys. Chem. Lett.* **1** 3520

[92] Kiguchi M, Tal O, Wohlthat S, Pauly F, Krieger M, Djukic D, Cuevas J C and van Ruitenbeek J M 2008 Highly conductive molecular junctions based on direct binding of benzene to platinum electrodes *Phys. Rev. Lett.* **101** 046801

[93] Schneebeli S T, Kamenetska M, Cheng Z, Skouta R, Friesner R A, Venkataraman L and Breslow R 2011 Single-molecule conductance through multiple pi-pi-stacked benzene rings determined with direct electrode-to-benzene ring connections *J. Am. Chem. Soc.* **133** 2136

[94] Yelin T, Vardimon R, Kuritz N, Korytar R, Bagrets A, Evers F, Kronik L and Tal O 2013 Atomically wired molecular junctions: connecting a single organic molecule by chains of metal

atoms *Nano Lett.* **13** 1956

[95] Kiguchi M and Murakoshi K 2008 Conductance of single C_{60} molecule bridging metal electrodes *J. Phys. Chem. C* **112** 8140

[96] Martin C A, Ding D, Sørensen J K, Bjørnholm T, van Ruitenbeek J M and van der Zant H S J 2008 Fullerene-Based Anchoring Groups for Molecular Electronics *J. Am. Chem. Soc.*. **130** 13198

[97] Nakazumi T, Kaneko S, Matsushita R and Kiguchi M 2012 Electric Conductance of Single Ethylene and Acetylene Molecules Bridging between Pt Electrodes *J. Phys. Chem. C* **116** 18250

[98] Kaneko S, Motta C, Brivio G P and Kiguchi M 2013 Mechanically controllable bi-stable states in a highly conductive single pyrazine molecular junction *Nanotechnology* **24** 315201

[99] Xiao, Xu and Tao N J 2004 Measurement of Single Molecule Conductance: Benzenedithiol and Benzenedimethanethiol *Nano Lett.* **4** 267

[100] Zhao J W, Murakoshi K, Yin X, Kiguchi M, Guo Y, Wang N, Liang S and Liu H 2008 Dynamic Characterization of the Postbreaking Behavior of a Nanowire *J. Phys. Chem. C* **112** 20088

[101] Batra A, Darancet P, Chen Q, Meisner J S, Widawsky J R, Neaton J B, Nuckolls C and Venkataraman L 2013 Tuning rectification in single-molecular diodes *Nano Lett.* **13** 6233

[102] Fujii S, Tada T, Komoto Y, Osuga T, Murase T, Fujita M and Kiguchi M 2015 Rectifying Electron-Transport Properties through Stacks of Aromatic Molecules Inserted into a Self-Assembled Cage *J. Am. Chem. Soc.*. **137** 5939

[103] Zhang N, Lo W-Y, Cai Z, Li L and Yu L 2016 Molecular Rectification Tuned by Through-Space Gating Effect *Nano Lett.*

[104] Kanthasamy K and Pfnur H 2015 Conductance through single biphenyl molecules: symmetric and asymmetric coupling to electrodes *Beilstein J. Nanotechnol.* **6** 1690

[105] Wang K, Zhou J, Hamill J M and Xu B 2014 Measurement and understanding of single-molecule break junction rectification caused by asymmetric contacts *J. Chem. Phys.* **141** 054712

[106] Yuan L, Nerngchamnong N, Cao L, Hamoudi H, del Barco E, Roemer M, Sriramula R K, Thompson D and Nijhuis C A 2015 Controlling the direction of rectification in a molecular diode *Nat. Commun.* **6** 6324

[107] Guo S, Hihath J, Díez-Pérez I and Tao N 2011 Measurement and statistical analysis of single-molecule current–voltage characteristics, transition voltage spectroscopy, and tunneling barrier height *J. Am. Chem. Soc.*. **133** 19189

[108] Tsutsui M, Taniguchi M and Kawai T 2009 Quantitative Evaluation of Metal− Molecule Contact Stability at the Single-Molecule Level *J. Am. Chem. Soc.*. **131** 10552

[109] Komoto Y, Isshiki Y, Fujii S, Nishino T and Kiguchi M 2017 Evaluation of the Electronic Structure of Single-Molecule Junctions Based on Current-Voltage and Thermopower

Measurements: Application to C_{60} Single-Molecule Junction *Chem. Asian J.* **12** 440

[110] Bilan S, Zotti L A, Pauly F and Cuevas J C 2012 Theoretical study of the charge transport through C_{60}-based single-molecule junctions *Phys. Rev. B* **85** 205403

[111] Böhler T, Edtbauer A and Scheer E 2007 Conductance of individualC_{60}molecules measured with controllable gold electrodes *Phys. Rev. B* **76** 125432

[112] Komoto Y, Fujii S and Kiguchi M 2017 Statistical *I-V* measurements of single-molecule junctions with an asymmetric anchoring group 1,4-aminobenzenethiol *Adv. Nat. Sci.: Nanosci. Nanotech.* **8** 025007

11. Achievements

Original papers

[1] **Komoto Y**, Fujii S, Hara K and Kiguchi M 2013 Single Molecular Bridging of Au Nanogap Using Aryl Halide Molecules *J. Phys. Chem. C* 117 24277

[2] Liu C, Kaneko S, **Komoto Y**, Fujii S and Kiguchi M 2014 Fabrication of single linear aromatic molecular junction with high formation probability *Appl. Phys. Express* 7 105201

[3] Murai D, Nakazumi T, Fujii S, **Komoto Y**, Tsukagoshi K, Motta C and Kiguchi M 2014 Highly stable Au atomic contacts covered with benzenedithiol under ambient conditions *Phys. Chem. Chem. Phys.* 16 15662

[4] Terao J, Homma K, Konoshima Y, Taniguchi M, Kiguchi M, **Komoto Y**, Horikawa M, Naito Y, Fujihara T and Tsuji Y 2014 Molecular Wiring Method Based on Polymerization or Copolymerization of an Insulated π-Conjugated Monomer *Bull. Chem. Soc. Jpn.* 87 871

[5] Fujii S, Tada T, **Komoto Y,** Osuga T, Murase T, Fujita M and Kiguchi M 2015 Rectifying Electron-Transport Properties through Stacks of Aromatic Molecules Inserted into a Self-Assembled Cage *J. Am. Chem. Soc.* 137 5939

[6] **Komoto Y,** Fujii S, Nishino T and Kiguchi M 2015 High electronic couplings of single mesitylene molecular junctions *Beilstein J. Nanotechnol.* 6 2431

[7] Liu C, Kaneko S, **Komoto Y**, Fujii S and Kiguchi M 2015 Highly conductive single naphthalene and anthracene molecular junction with well-defined conductance *Appl. Phys. Lett.* 106 103103

[8] Kaneko S, Murai D, Marques-Gonzalez S, Nakamura H, **Komoto Y**, Fujii S, Nishino T, Ikeda K, Tsukagoshi K and Kiguchi M 2016 Site-Selection in Single-Molecule Junction for Highly Reproducible Molecular Electronics *J. Am. Chem. Soc.* 138 1294

[9] **Komoto Y**, Fujii S, Nakamura H, Tada T, Nishino T and Kiguchi M 2016 Resolving metal-molecule interfaces at single-molecule junctions *Sci. Rep.* 6 26606

[10] Li Y, Kaneko S, **Komoto Y**, Fujii S, Nishino T and Kiguchi M 2016 Atomic and Electronic Structures of a Single Oxygen Molecular Junction with Au, Ag, and Cu Electrodes *J. Phys. Chem. C* 120 16254

[11] **Komoto Y**, Fujii S and Kiguchi M 2017 Statistical I–V measurements of single-molecule junctions with an asymmetric anchoring group 1,4-aminobenzenethiol *Adv. Nat. Sci.: Nanosci. Nanotech.* 8 025007

[12] **Komoto Y**, Isshiki Y, Fujii S, Nishino T and Kiguchi M 2017 Evaluation of the Electronic Structure of Single-Molecule Junctions Based on Current-Voltage and Thermopower Measurements:

Application to C60 Single-Molecule Junction *Chem Asian J* 12 440

[13] **Komoto Y**, Yamazaki Y, Tamaki Y, Iwane M, Nishino T, Ishitani O, Kiguchi M and Fujii S 2018 Single Ruthenium Tris Bipyridine Molecular Junction having Multiple Joint Configurations *Chem. Asian J. 13, 1297*

Review articles

[1] **Komoto Y**, Fujii S, Iwane M and Kiguchi M 2016 Single-molecule junctions for molecular electronics *J. Mater. Chem. C* 4 8842

[2] **Komoto Y,** Fujii S and Kiguchi M 2018 Single-molecule junctions of π molecules *Mater. Chem. Front.* 2 214

Conferences

International Conferences

1. " Single-molecule conductance measurement of Ru(bpy)3 derivative"

Y. Komoto, S. Fujii, T. Nishino, M. Kiguch, Y. Tamaki, O. Ishitani, ECOSS33, Szeged (Hungary) 2017/8/31

2." Thermopower and current-voltage measurement of1,4-benzenedithiol-single molecular junctions "

Y. Komoto, S. Fujii, H. Nakamura,T. Tada, M. Kiguchi, ECOSS32, Grenoble (France) 2016/8/29

3.“Metal-Molecule Interface of the Single Molecular Junction studied with Current-Voltage Characteristics”

Y. Komoto, Shintaro Fujii, Tomofumi Tada, Manabu Kiguchi, ECOSS31, Barcelona (Spain) 2015/9/3

Domestic Conferences

Oral presentation

1." 非対称な分子ー電極界面構造を有する単分子接合の電流-電圧特性 "

小本 祐貴, 藤井 慎太郎, 木口 学, 分子科学討論会 神戸 2016/9/14

2. " ベンゼンジチオール単分子接合の電流-電圧特性計測及び熱起電力計測 "

小本祐貴、藤井慎太郎、中村恒夫、多田朋史、木口学, 日本化学会 京都 2016/3/24

3. " 電流-電圧特性計測による単分子接合の電子状態解明 "

小本祐貴, 藤井慎太郎, 木口学, 分子科学討論会 広島 2014/9/24

4 “STM-BJ 法による 1,4-ジヨードベンゼンの電気伝導度計測 "

小本祐貴, 木口学 日本化学会 滋賀 2013/3/24

Poster presentation

“Thermopower and current-voltage characteristics of 1,4-benzenedithiol-single-molecule junction”

小本　祐貴, 表面・界面スペクトロスコピー 仙台 2016/11/25

3. “Au-BDT 単分子接合の電子状態計測による界面構造決定”

小本 祐貴, 藤井 慎太郎, 中村 恒夫, 多田 朋史, 木口 学, 第 6 回分子アーキテクトニクス研究会, 大阪 2015/10/23

4." 電流-電圧特性計測による単分子接合の電子状態解明 "

小本祐貴，藤井慎太郎，木口学，第 5 回分子アーキテクトニクス研究会，大阪 2014/11/25

Award

第 6 回分子アーキテクトニクス研究会　若手奨励賞 2015/10/24